Numerical Modeling of Whiplash Injury

by

Jason Bradley Fice

A thesis

presented to the University of Waterloo

in fulfillment of the

thesis requirement for the degree of

Master of Applied Science

in

Mechanical Engineering

Waterloo, Ontario, Canada, 2010

AUTHOR'S DECLARATION

I hereby declare that I am the sole author of this thesis. This is a true copy of the thesis, including any required final revisions, as accepted by my examiners.

I understand that my thesis may be made electronically available to the public.

Abstract

Soft tissue cervical spine (neck) injuries, known as 'whiplash', are a leading cause of injury in motor vehicle collisions. A detailed finite element (FE) model of the cervical spine that is able to predict local tissue injury is a vital tool to improve safety systems in cars, through understanding of injury mechanisms at the tissue level and evaluation of new safety systems. This is the motivation for the formation of the Global Human Body Models Consortium, which is a collective of major automotive manufacturers with the goal of producing a detailed FE human body model to predict occupant response in crash. This work builds on an existing detailed cervical spine model, with a focus on improved validation in terms of kinematics and tissue level response.

The neck model used in this research represents a 50th percentile male and was developed at the University of Waterloo. The model includes both passive and active musculature, detailed nucleus and annulus models of the discs, rate dependent non-linear ligaments, facet capsules with a squeeze film model of the synovial fluid, and rigid vertebrae with the geometry derived from CT scans. The material properties were determined from published experimental testing and were not calibrated to improve the model response.

The model was previously validated at the segment level. In this study, the model was validated for tension loading, local tissue response during both frontal and rear impacts, and head kinematic response during frontal and rear impact. The whole neck model without musculature was exposed to a tensile load up to 300N and the predicted response was within the experimental corridors throughout. The ligament strains and disc shear strains predicted by the model were compared to bench-top cadaver tests. In frontal impact, the ligament and disc strains were within a standard deviation of the experiments 26/30 and 12/15 times respectively. In rear impact, the strains were within a standard deviation of the experiments 9/10 and 12/15 times for the ligaments and discs respectively. All of the ligament strains were within two standard deviation of the experimental average and the disc strains were all within three standard deviations. The global kinematic response of the head for 4g and 7g rear impacts and 7g and 15g frontal impacts was generally a good fit to the experimental corridors. These impact loads are relevant to the low speed impacts that generally cause whiplash. In the global kinematic validation, the model was shown to oscillate more, which is likely due to the lack of soft-tissues such as the skin and fat or the lack of high-rate material data for the intervertebral discs. In rear impact, the head over extended by 17° and 6° for 4g and 7g impacts respectively; this is likely

due to difficulties defining the facet gap or lack of uncovertebral joints. Even with these limitations the model response for these varied modes of loading was considered excellent.

A review of organic causes of whiplash revealed the most likely sources of whiplash include the capsular ligament, other ligaments, and the vertebral discs. The model was exposed to frontal and rear impacts with increasing severities until the soft tissue strains reached damage thresholds. In frontal impact, these strains started to reach damage values at a 15g impact. The disc annulus fibres were likely injured at 10g in a rear impact, and the ligaments were likely injured at 14g in a rear impact. These impact severities agree with findings from real-life accidents where long term consequences were found in rear impacts from 9g to 15g. The model was used to show that bench-top cadaver impacts under predict strain because they lack active musculature.

A number of recommendations have been proposed to improve the biofidelity of the model including perform in-vivo measurement of human facet gaps, incorporate the uncovertebral joints, measure rate-dependent properties for the annulus fibrosus of the disc, include non-structural soft tissues for increased damping, determine a muscle activation strategy that can maintain head posture in a gravity field, and continue to develop relationships between prolonged painful injury and strain in structures of the neck other than the capsular ligaments. Furthermore, it was recommended that the model should be developed further for whiplash injury prediction with out of position occupants.

Acknowledgements

I would like to thank my supervisor Professor Duane Cronin for his guidance, optimism, and long hours helping me with the research that constitutes this thesis. I am pleased that his heart continues to hold up, despite the intake of energy drinks. I wish him all the best for his future research projects.

The model I use for this work was developed by Matthew B. Panzer and Professor Cronin. Without Matt's attention to detail the model would not have performed as well as it has. I thank you for providing the frame work for my masters.

For supporting me financially during my masters, I would like to thank the Global Human Body Models Consortium, the Ontario Graduate Scholarship Program, and the University of Waterloo. Without this support, I would not have been able to produce this thesis.

I am happy to thank my lovely wife Amanda for her inspiration and motivation in completing this work. For housing and support, I would like to thank Amanda's family, Gill, Tracy, Steve, and Andrew. I would like to thank my parents, Randy and Mary-Lynn, and my brother, Chris, for shaping the person that I am today.

Finally, I would like to thank my office mates, others in my research group, and my friends. Thanks for putting up with me all this time!

Table of Contents

List of Figures

xi

List of Tables

Chapter 1

Introduction

1.1 Motivation for Research

Whiplash or soft tissue cervical spine sprains/strains are the most common injury in motor vehicle collisions, with 27.8-53% of victims sustaining this type of injury (Quinlan et al., 2004, Galasko et al., 1993). The annual societal costs of whiplash in the United States are estimated to be between 4.5 and 29 billion dollars (Keinberger, 2000; Freeman, 1997). Whiplash can reduce the victim's quality of life for a significant amount of time, as up to 33% of patients continued to seek treatment for whiplash 33 months after sustaining the injury (Freeman, 1997). Radanov et al., (1995) reported that 24% of whiplash victims had their symptoms remain for one year after the accident, and 18% after two years.

Rear impacts and frontal impacts are the most common source of MVC whiplash cases. Rear impacts account for between 38.1-51.9% of reported whiplash cases and frontal impacts account for between 22.6-27.2% of cases (Galasko et al., 1993; Berglund et al., 2003). Many researchers focus solely on rear-impacts as the source of whiplash injury, but this research will focus on both frontal and rear impacts as frontal impacts have been shown to cause a significant amount of whiplash injuries.

Automotive safety researchers often use finite element (FE) models of crash test dummies to assess the injury potential of occupants during motor vehicle collisions. However, these dummies and their FE representations lack the biofidelity required to predict local tissue injury, and instead rely on global kinematic indicators that have been correlated to occupant injury. Due to their interest in predicting these local tissue injuries, many of the major automotive companies have formed the Global Human Body Models Consortium (www.ghbmc.com), with the goal to produce finite element models of the human body.

1.2 Objectives and Approach

The first objective of this thesis is to validate the existing University of Waterloo (UW) human neck model. The model was previously validated at the segment level (Panzer & Cronin, 2009) and the whole neck in frontal impact (Panzer, 2006). In this research, the head and neck excluding musculature was validated in tension, the local tissue response was validated against a bench-top cadaver spine model, and the global kinematics of the head were validated against post mortem

human subjects (PMHS) and volunteer sled tests in both frontal and rear impact scenarios. The other objective of this research was to identify which structures in the neck are likely sources of whiplash symptoms, and at what impact severities these injuries are likely to occur.

The neck model used in this thesis was developed at the University of Waterloo by Mathew B. Panzer and Professor Duane Cronin (Panzer, 2006; Panzer & Cronin, 2009). The neck model is a finite element model representing a 50th percentile male, including both passive and active musculature, detailed nucleus and annulus models of the discs, rate dependent non-linear ligaments, facet capsules with a squeeze film model of the synovial fluid, and rigid vertebrae derived from CT scans. All of the material properties were determined from independent experimental testing in the literature, and implemented using appropriate constitutive models. It should be noted that the properties were not adjusted to improve the model response.

The model was previously validated at the segment level under nine loading conditions including but not limited to: flexion, extension, posterior and anterior shear, tension, and compression (Panzer, 2006; Panzer & Cronin, 2009). Also the full model was validated in frontal impact at 15g against volunteer experimental corridors (Panzer, 2006).

In this thesis, the model validation was continued with the neck in tension and frontal and rear impact for both global head kinematics and local tissue validation. The tensile response of the model was validated by removing the musculature, constraining the head as per the experiment and then applying a downwards displacement of the first thoracic vertebra. The load-displacement curve of the model was then compared to the experimental results. Frontal and rear impact validations were carried out by applying experimental acceleration traces to the first thoracic vertebrae of the model and measuring the response. To measure the local kinematic response, the tissue strains predicted by the model were compared to experimental results from bench-top sled tests of whole cadaver cervical spines. For global kinematic response, the response of the head and vertebrae were compared to experimental corridors from human volunteer and post mortem human subjects (PMHS).

Material thresholds were used to determine if the structures in the neck were damaged during an impact scenario. These thresholds include distraction limits for nociceptive pain receptor activation or tissue strain at the ultimate force. The material thresholds were derived from published experimental uniaxial testing of cadaver tissue, or in-vivo animal studies. The model was exposed to incremental severity levels until these damage threshold holds were met. When possible, the predicted tissue

damage sites were compared to published data showing the prevalence of whiplash symptoms in that structure, which established the likelihood of whiplash symptoms in that site.

1.3 Outline

The second chapter of this thesis provides a brief description of the anatomy and physiology of the neck. It also provides a description of biomechanical terms that are used throughout this thesis. This information provides a knowledge basis required to continue with the neck model validation and injury prediction.

An understanding of the neck anatomy and biomechanical terms helps the reader follow the model description, which is presented in chapter three. This chapter describes the geometry and material model used for each part of the neck as well as outlining how the different components were attached. Chapter three also describes the enhancements that were made to the model to address responses to rear impact and tension.

Chapter four presents a literature review of whiplash symptoms and possible causes. To begin the chapter, the reader is given an introduction to the current knowledge of pain, including how it is produced, perceived, and the different forms it can take. The review of sources of whiplash pain focuses on the organic causes of whiplash. For example, rather than measuring the acceleration of the head and using established correlations with injury, this research investigated thresholds of individual tissue for the mode of loading to which they are exposed.

The fifth chapter continues the full neck validation started by Mathew Panzer. This includes results and discussion from the three types of validation carried out. These include the ligamentous spine under tension, soft tissue response of the whole spine with passive musculature compared to cadaveric bench-top sled tests, and the global response of the head compared to PMHS and volunteer sled tests.

Soft tissue strains, including ligament and disc fibre strains, for increasing severities of both frontal and rear impact are presented in chapter six. These strains were compared to published injury criteria in order to determine at what impact severity the various tissues are likely to be injured. This chapter also includes a discussion of the soft tissue strain results. The final chapter of this thesis provides conclusions and recommendations that follow from the results and discussion from the preceding chapters.

Chapter 2

Anatomy and Physiology of the Cervical Spine

2.1 Biomechanics Terms

The anatomy of the human body is normally described relative to three planes; the transverse (or axial) plane splits the upper and lower portions of the body; the frontal plane splits the front and back of the body; the sagittal plane splits the left and right portions of the body and is called the median plane when it goes down the centre (Figure 2-1). When referencing the forwards and backwards directions for a body the correct terminology is the anterior and posterior directions respectively (Figure 2-1). The terms left and right can be confused depending on the observer's frame of reference, so anatomists use the medial and lateral directions, which refer to getting closer and further away from the median plane respectively (Figure 2-1). The final important directions for the human body are the superior and inferior directions, which refer to up and down respectively (Figure 2-1). The term in-vivo applies to anything in an alive being without any changes to its natural environment and in-vitro means that the test sample is removed from either an alive or deceased being and it is no longer in its natural environment.
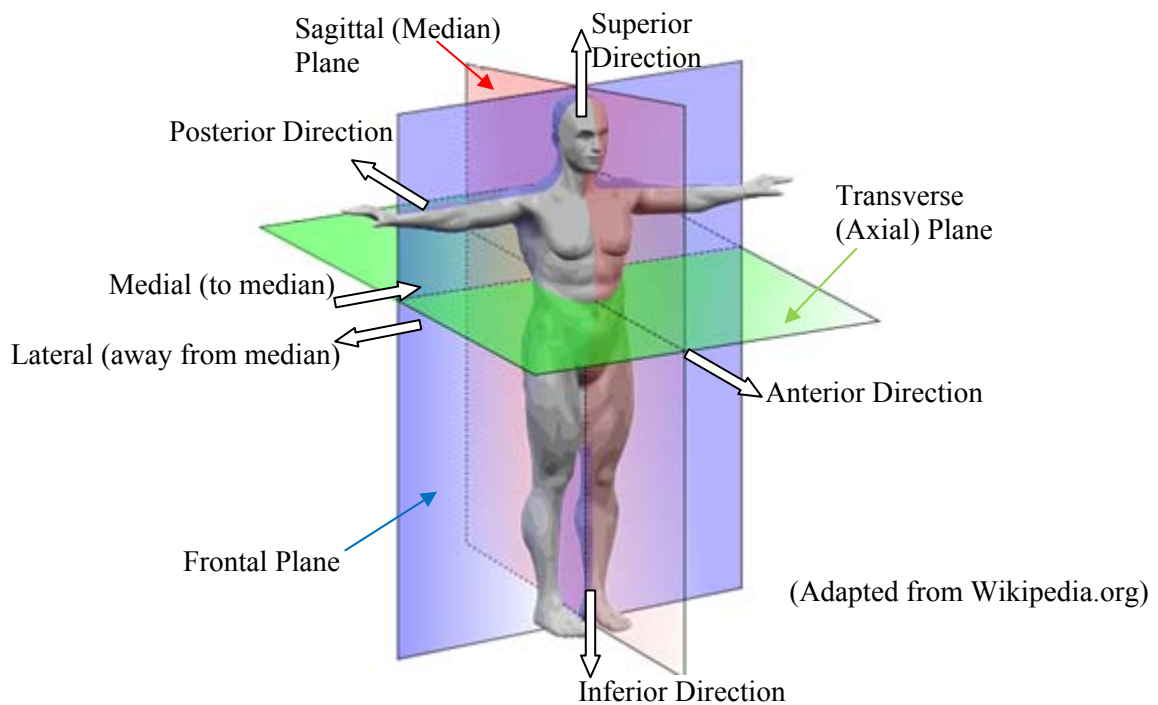
Figure 2-1: Anatomical reference frames and directions.

4

The motions of the cervical spine can be described by extension, flexion, lateral bending, and axial rotation (Figure 2-2). Extension is the motion resulting from looking up, and is nominally the motion the neck experiences during a rear impact. The opposite of extension is flexion, which results from looking down or frontal impacts. Lateral bending is the tilting of the head trying to touch one's ear to their shoulder, and this motion nominally occurs during side impacts. Finally, axial rotation is the 'no' motion of the head.

a)   b)   c)   d)
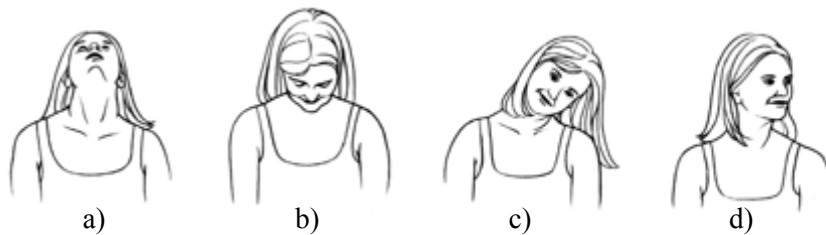
(Adapted from the American Academy of Family Physicians)

Figure 2-2: Terms used to describe head rotation.

a) Extension (looking up), b) flexion (looking down), c) lateral bending, and d) Axial rotation.

2.2 Vertebrae

The human spinal column is composed of 26 bones, which are called vertebrae, and these vertebrae are classified in three groups (cervical, thoracic, and lumbar) depending on their position in the body (Figure 2-3). The vertebrae of the neck are part of the cervical spine; these are labeled C1 to C7, and the upper two vertebrae are also referred to as the atlas and axis. The next twelve vertebrae are part of the thoracic spine. Inferiorly to the thoracic spine are the five vertebrae of the lumbar spine.

1st Cervical (Atlas)
2nd Cervical (Axis)
1st Thoracic
1st Lumbar
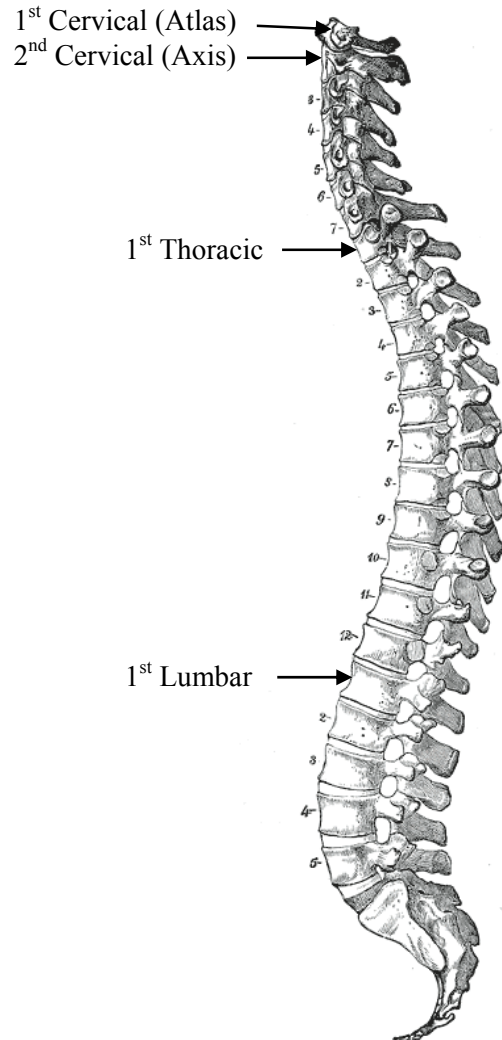
(Adapted from Gray, 1918)

Figure 2-3: Spinal column.

The third through seventh cervical vertebrae are similar in shape and function to the vertebrae of the thoracic and lumbar region (Figure 2-4). The body is the largest portion of each vertebra and is the main load bearing structure, serving as a pivot point for intervertebral motion (White & Panjabi, 1990). The average height of the vertebral bodies is 14mm, and they have an elliptical cross-section of approximately 15 mm depth and 30 mm width (Gilad & Nissan, 1986; Pooni et al., 1986; Panjabi et al., 2001). The superior and inferior surfaces of the articular pillars from adjacent vertebra form a joint called the facet joint, which guides intervertebral motion. The vertebral foramen is the open space created by the posterior surface of the body, the pedicles, and the lamina. The function of this

6

foramen is to protect the spinal cord. The posterior portion of the vertebrae is called the spinous process, which acts as a ligament and muscle attachment point.
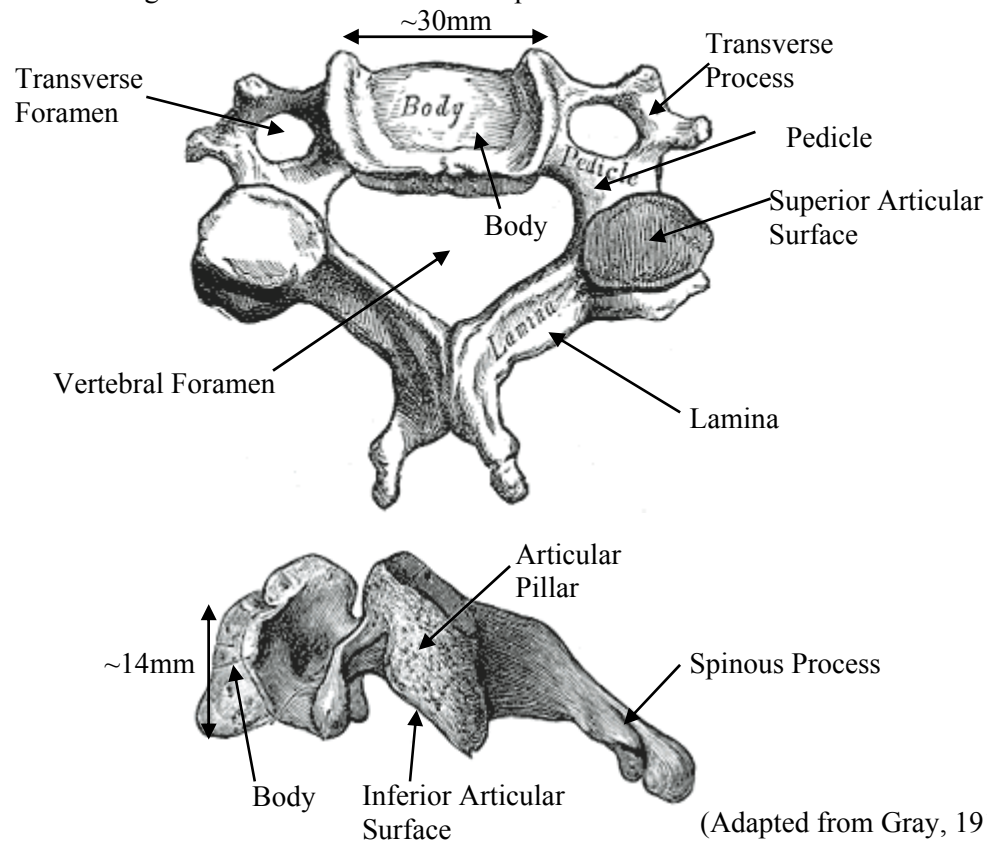
Figure 2-4: Anatomical details of the C3 to C7 vertebrae.

The second cervical vertebra (C2) is called the axis (Figure 2-5). The C2 is similar in shape and function to the C3 to C7 vertebrae except for the odontoid process (or dens) attached to the superior surface of the body. The first cervical vertebra (C1 or atlas) has a dramatically different shape than the other vertebrae in the human body (Figure 2-6). The atlas consists of an anterior and posterior arc that connects two lateral masses. The inferior articular surface on the C1 forms a conventional facet joint with the superior articular surface of the C2. A unique joint exists between the anterior surface of the dens with the posterior surface of the anterior arch. This joint is stabilized by the transverse ligament that attaches to the C1 and runs along the posterior surface of the dens. This joint allows the skull and C1 to rotate axially around the dens, which is responsible for the majority of axial head rotation. The lateral masses of the C1 support the weight of the head and a facet joint is formed between the superior articular surface and the occipital condyles of the skull. The facet joint between

7

the skull and C1 allows the most relative rotation in flexion and extension, and is responsible for much of the 'yes' motion of the head. The assembled atlas and axis can be seen in Figure 2-7.

Odontoid
Process (Dens)

Superior Articular
Surface

Odontoid
Process (Dens)

Groove for the
Transverse Ligament

Articular Surface
(for contact with
the Atlas)
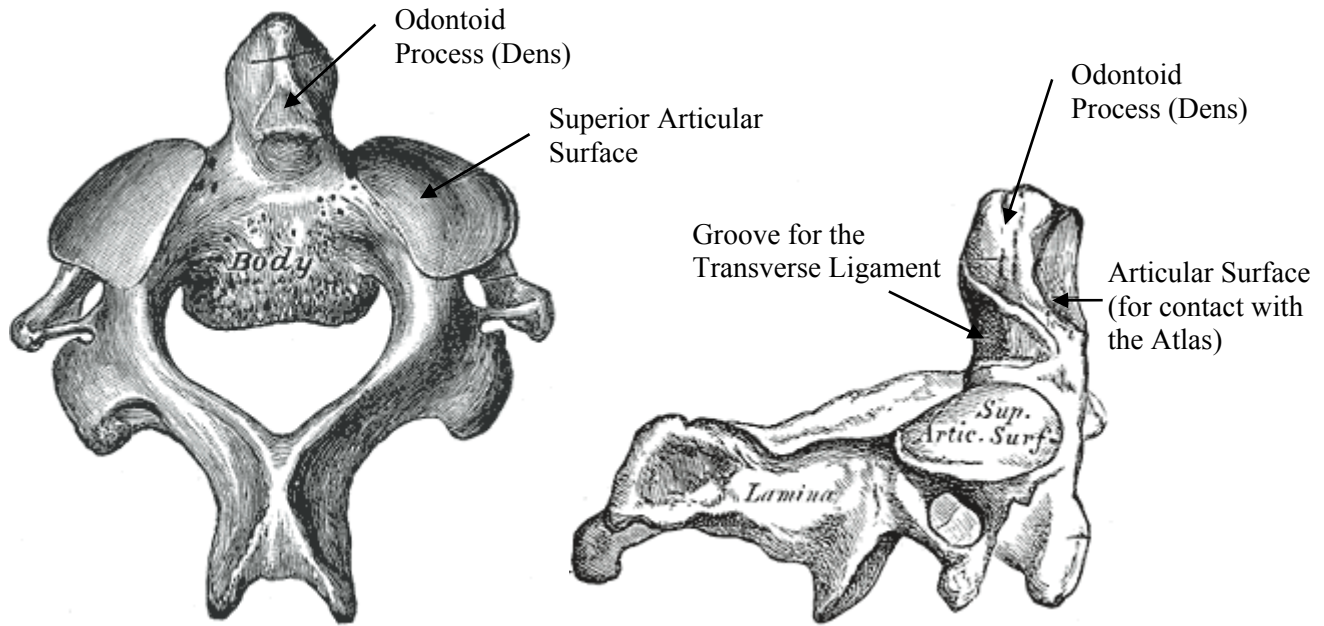
(Adapted from Gray, 1918)

Figure 2-5: The second cervical vertebra (C2 or Axis).

Superior Articular
Surface

Anterior Arch

Articular Surface
(for contact with
the Dens)

Lateral Masses

Posterior Arch
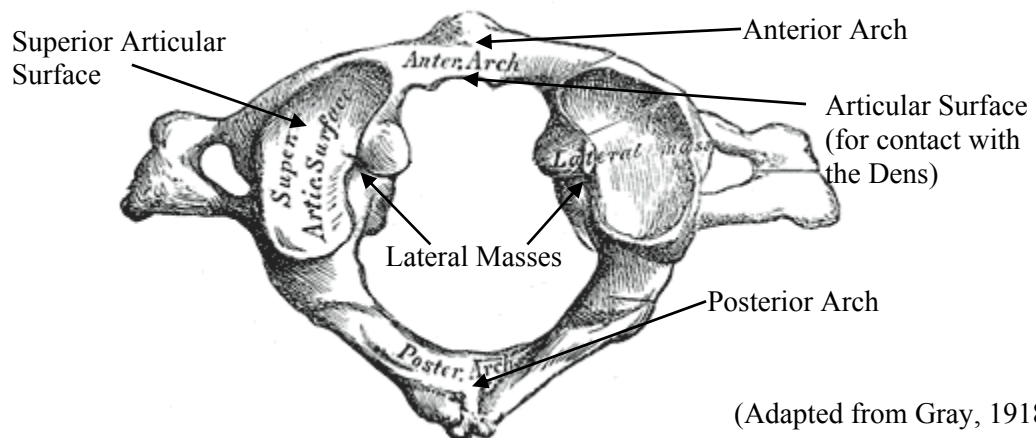
(Adapted from Gray, 1918)

Figure 2-6: The first cervical vertebra (C1 or Atlas).

Atlas (C1)

Axis (C2)

C3

C4
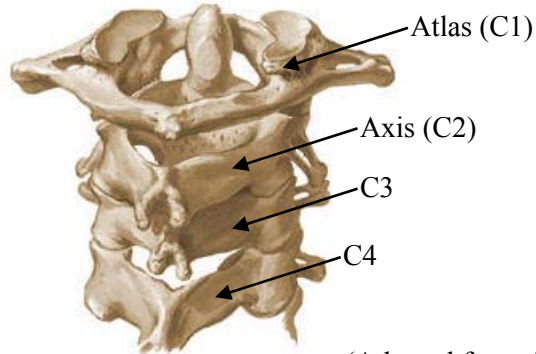
(Adapted from Agur & Dalley, 2004)

Figure 2-7: Upper cervical vertebrae assembled along with C3 and C4.

2.3 Intervertebral Discs

The intervertebral discs are a soft material that connect the vertebral bodies of two adjacent vertebrae, and they form the most important joint at all spinal levels except the C1 (Figure 2-8). The discs in the cervical spine are elliptical in shape, with a height between 4.8 to 5.5mm on the anterior edge and 3.0 to 4.3mm on the posterior edge (Gilad & Nissan, 1986; Przybylski et al., 1998). At the centre of the disc is a pocket of entrapped fluid called the nucleus pulposus, and around that is a fibrous annulus that is suitably called the annulus fibrosus (Figure 2-9). The annulus is composed of several layers of fibres embedded in a soft ground substance, and the angles of the fibres change from ±25° in the outer layers to ±45° in the inner layers, measured from the transverse plane (Cassidy et al., 1989; Marchand & Ahmed, 1990; Wagner & Lotz, 2004; White & Panjabi, 1990).

The main purpose of the disc is to support vertical loads in the spinal column, which is achieved by fluid flowing into the nucleus pulposus creating a positive pressure that can support loads. When the nucleus swells the annulus fibres bulge outwards and the fibres go into tension, which supports the hydrostatic pressure. The annulus fibres are also stretched when the neck goes into tension, extension, flexion, lateral bending, or axial rotation. For example, when the neck goes into flexion, the vertebrae will rotate about the nucleus and the posterior annulus fibres will go into tension. The opposite is true when the neck goes into extension. The disc is stiffer in compression compared to tension, because the annulus fibres are angled closer to the axial plane and the nucleus and ground substance are essentially fluid and do not support tensile load. Due to the alternating orientation of the annulus fibres, during axial rotation only half of the fibres go into tension to support the load and the disc is relatively weak in this mode of loading. Therefore, the physiology of the disc is heavily dependent on

9

the layered composite structure of the annulus fibrosus and the fluid like response of the nucleus pulposus.

(Adapted from purehealthyback.com)
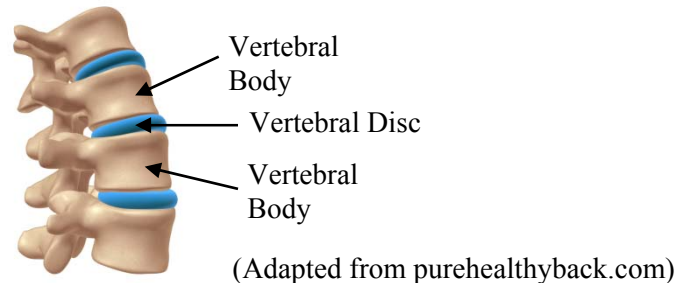
Figure 2-8: The vertebral discs, present at every spinal level except C1-C2.

(Adapted from White & Panjabi, 1990)
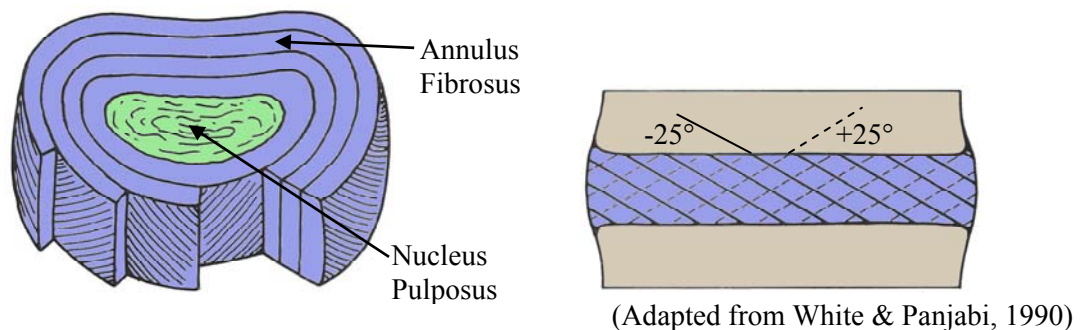
Figure 2-9: Vertebral disc is comprised of the nucleus pulposus and annulus fibrosus.

2.4 Facet Joints

The facet joint is a synovial joint that connects the articular pillar of adjacent vertebrae at every level of the human spine (Figure 2-10). The facet joint consists of an inferior and superior layer of articular cartilage sandwiching synovial fluid, which is encased around the circumference by the synovial membrane (Figure 2-11). The synovial joints in the neck are different from other areas in the body because the synovial membrane is surrounded by the capsular ligament, which provides tensile resistance to the joint. The purpose of the articular cartilage and synovial fluid is to create a low friction joint and protect the bone from wear.

The purpose of the facet joints is to support a portion of the compressive load on the spine (Goel & Clausen, 1998) and control the primary and secondary motions of the spine (Bogduk & Mercer, 2000). The facet joints support 6% of the compressive load in an erect posture and up to 51% when extension is included (Goel & Clausen, 1998). Due to the orientation of the facet joints, 30 to 60deg in the sagittal plane from the superior direction (Panjabi et al., 1993; Pal et al., 2001) (Figure 2-10),

the only motion that is uncoupled is flexion-extension (Bogduk & Mercer, 2000). For example, when the vertebrae axially rotate, one of the superior articular surfaces will slide up its inferior surface and the other will slide down creating lateral bending. In the same manner, lateral bending of the spine will be coupled with axial rotation.

30 - 65°
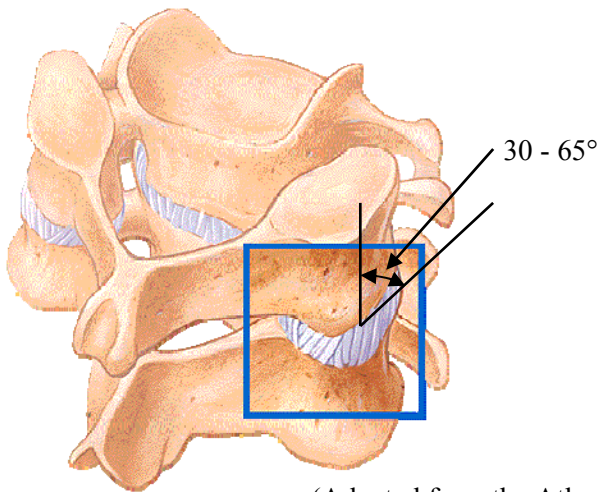
(Adapted from the Atlanta Spine Institute)

Figure 2-10: The facet joint, showing the orientation.

Synovial Fluid

Articular Cartilage

Articular Pillar of the Superior Vertebra

Articular Pillar of the Inferior Vertebra

Synovial Membrane

Capsular Ligament
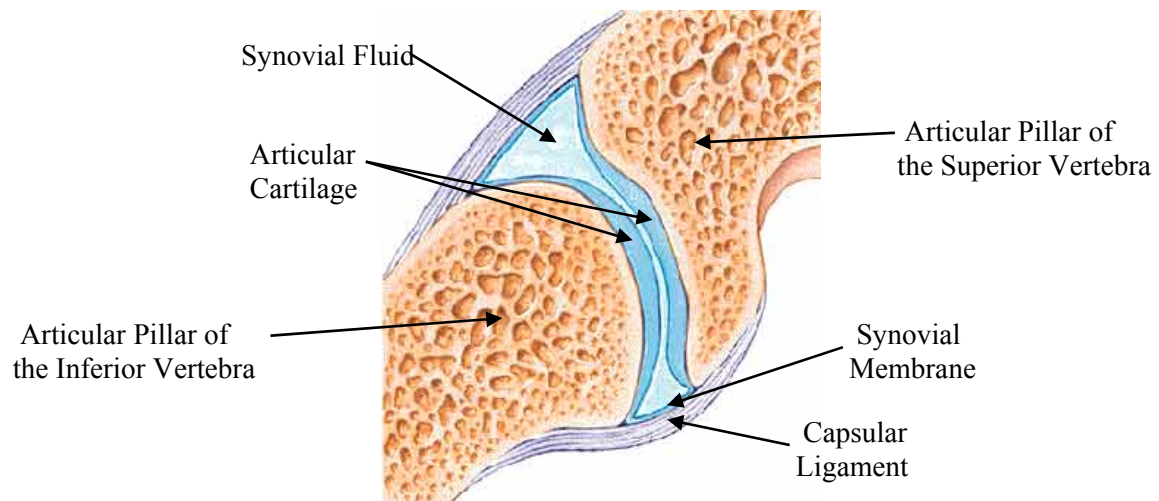
(Adapted from Spine University)

Figure 2-11: Anatomy of the facet joints.

2.5 Ligaments

Ligaments are fibrous cords that attach bone segments to form all of the joints in the human body. In the spinal column the ligaments essentially take the same form from the lumbar spine all the way up to the third cervical vertebrae (Figure 2-12, Figure 2-13). The anterior longitudinal ligament (ALL) is a continuous band that runs along the anterior surface of the vertebral bodies. The posterior longitudinal ligament (PLL) connects each vertebral body along the posterior surface. Around the circumference of every facet joint, including the upper cervical spine, lays the capsular ligament (CL), which provides those joints a resistance to tension. Connecting the lamina of adjacent vertebrae is the ligamentum flavum (LF). Finally, the interspinous ligament (ISL) connects the spinous process of each vertebra.

Ligamentum Flavum (LF)

Capsular Ligament (CL)

Interspinous Ligament
(ISL)

Posterior Longitudinal
Ligament (PLL)

Anterior Longitudinal
Ligament (ALL)

(Adapted from Spine Universe)
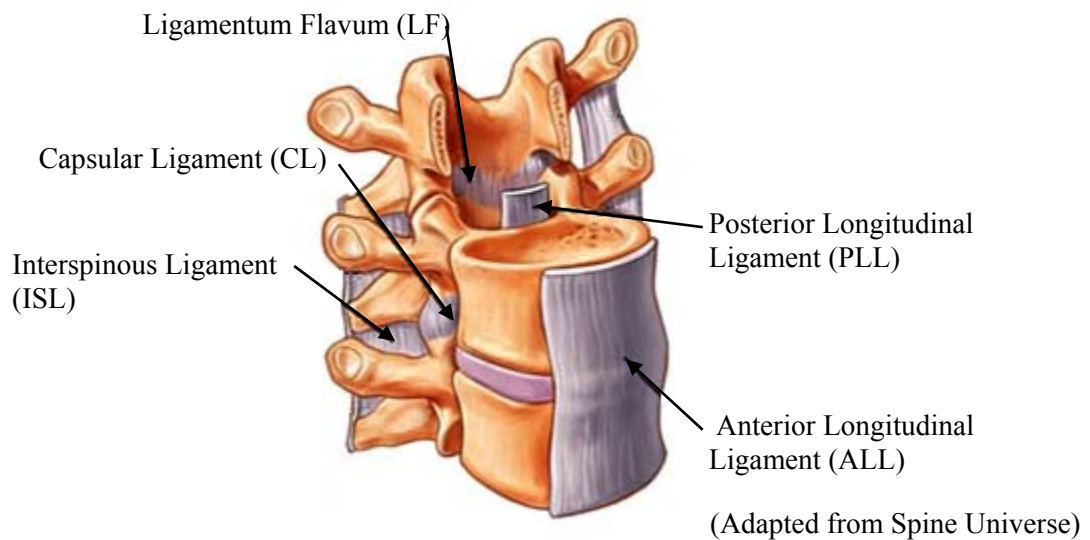
Figure 2-12: The spinal ligaments of the lower and middle cervical spine (C3-C7).

Posterior Longitudinal Ligament (PLL)

Anterior Longitudinal Ligament (ALL)

Ligamentum Flavum (LF)

Interspinous Ligament (ISL)

Capsular Ligament (CL)

(Adapted from Gray, 1918)
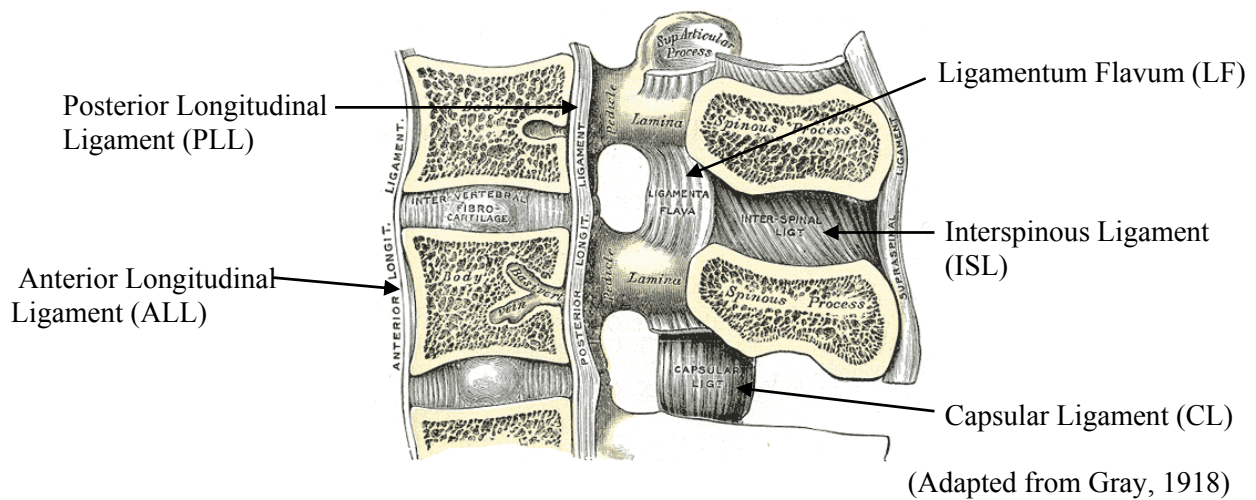
Figure 2-13: Sagittal plane slice of the cervical spine showing the ligament attachments.
Note that the inferior ligamentum flavum was dissected to expose the capsular ligament
beneath.

The upper cervical spine contains some continuations of ligaments from the lower spine, including the ALL, PLL, CL, and LF, but it also contains some unique ligaments that attach the odontoid process of the atlas to the axis and occipital bone of the skull (Figure 2-14). The continuation of the ALL connecting the atlas and axis is the anterior atlanto-axis membrane (AAAM), and connecting the axis and occipital bone is the anterior atlanto-occipital membrane (AAOM). The LF is continued by the posterior atlanto-axis membrane (PAAM) and the posterior atlanto-occipital membrane (PAOM). The tectorial membrane (TM) that attaches from the skull down to the posterior surface of atlas' body can be considered a continuation of the PLL.

13
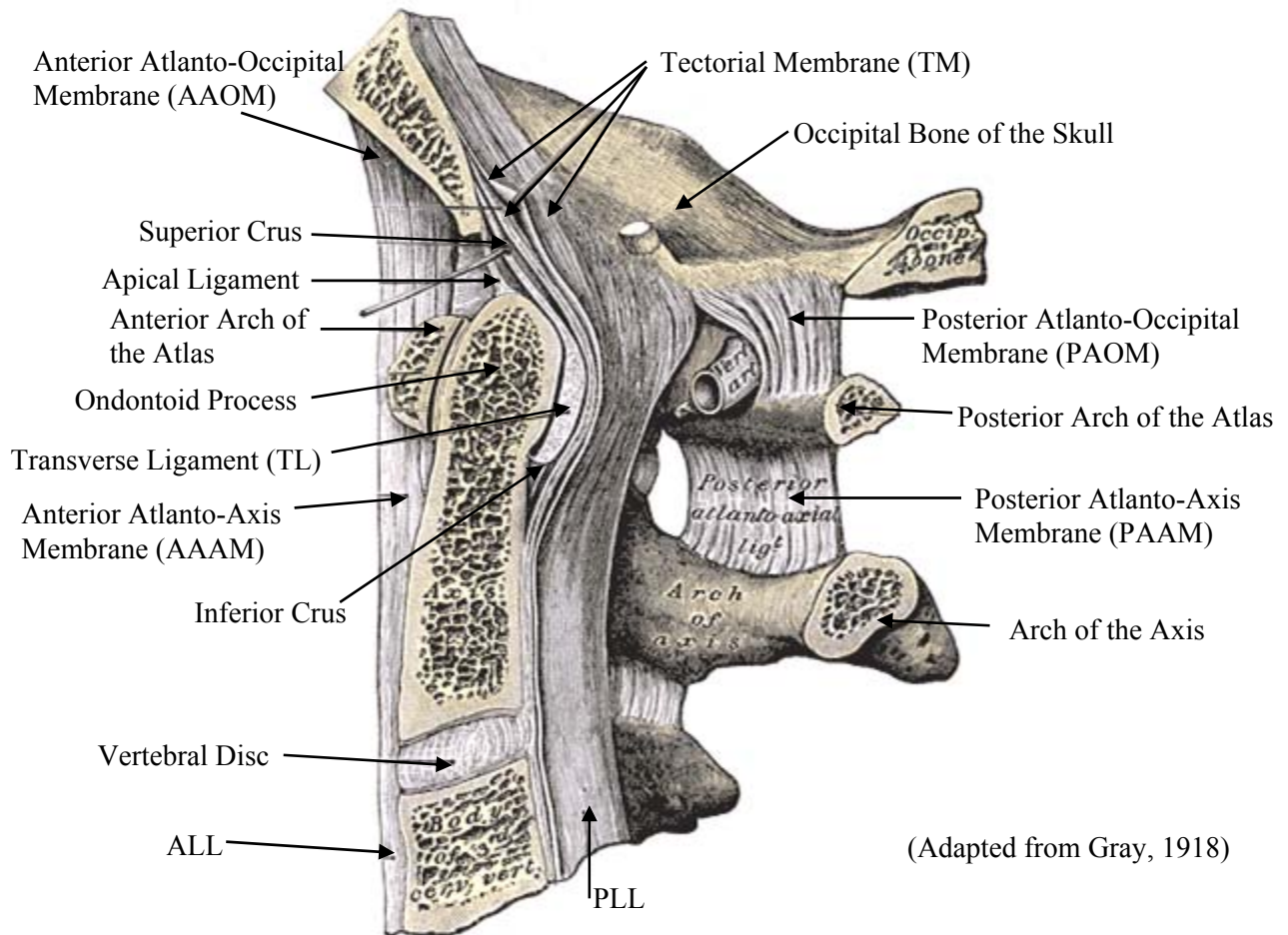
Figure 2-14: Sagittal plane slice of the occipital bone (skull), atlas, and axis.
Shows the upper cervical spine ligament attachments.

Ligaments that are unique to the upper cervical spine include the transverse ligament (TL), superior and inferior crus, alar ligaments, and apical ligament (Figure 2-14, Figure 2-15). The transverse ligament forms a joint between the odontoid process of the atlas with the anterior arch of the axis (Figure 2-16). To maintain the axial position of the transverse ligament, the superior crus inserts into its superior edge and attaches to the occipital bone of the skull and the inferior crus inserts into its inferior edge and attaches to the posterior surface of the atlas' body. These three ligaments form a cross shape and therefore the group is called the cruciate ligament. The apical ligament runs beside the superior crus and inserts between the superior tip of the odontoid process and the occipital bone. Two distinct pairs of ligaments are referred to as the alar ligaments; one of the pairs inserts between

14

the occipital bone and superior/lateral surface of the odontoid process and the other pair insert between the inferior/lateral surface of the odontoid process and the posterior surface of the anterior arch of the axis.
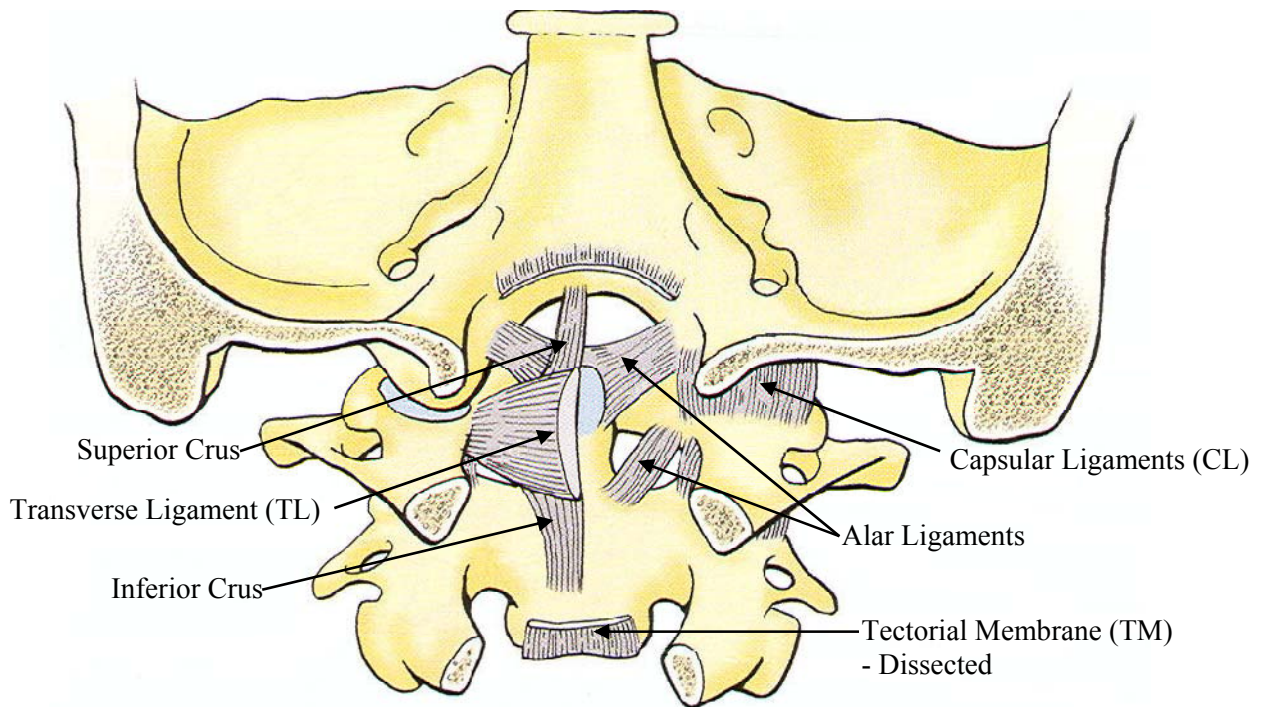
(Adapted from Agur and Dalley, 2005)

Figure 2-15: Sectioned posterior view of the upper cervical spine ligaments.
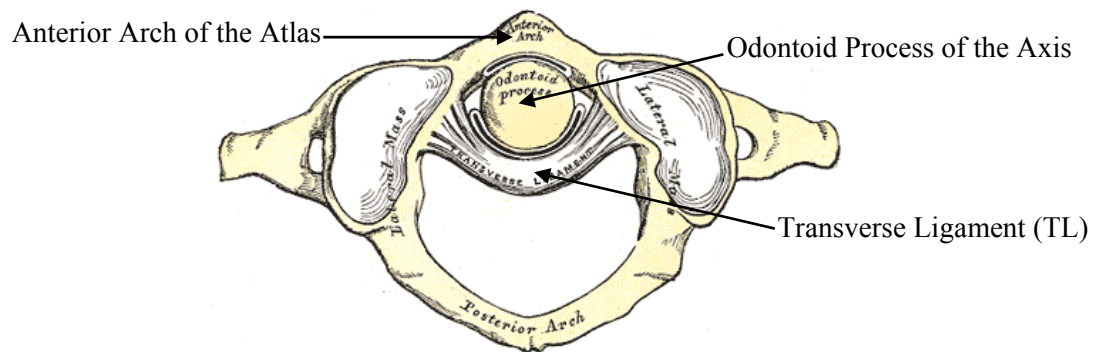
(Adapted from Gray, 1918)

Figure 2-16: Superior view of the atlas and axis Joint.

Ligaments are fibrous cords with all of the fibres running parallel to the orientation of the ligament; as such they are only able to support a tensile load in the direction of fibre orientation. A typical force-displacement curve of a ligament is shown in Figure 2-17. The toe region of the curve occurs because

15

in the resting state, the fibres of an in-vitro ligament will be crimped and as load is applied the fibres will straighten and begin to take load (Bartel et al., 2006). The linear region of curve is when all the fibres are straightened and they stretch in a linear fashion. The slope of the curve drops off in the sub-traumatic region likely because individual fibres are starting to fail. The ligaments of the neck in-vivo are preloaded in the neutral posture to prevent joint laxity caused by the toe region of the ligament (Heuer et al., 2007; Nachemson & Evans, 1968; Viejo-Fuertes et al., 1998).
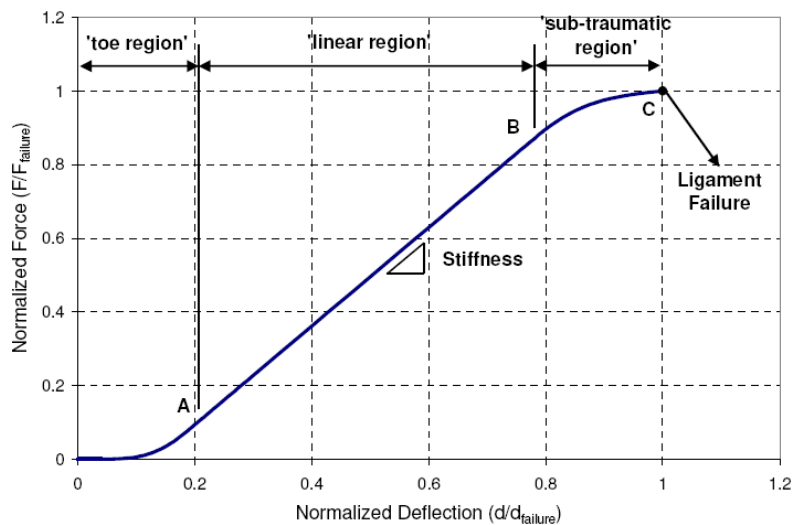
(Adapted from Panzer, 2006)

Figure 2-17: Normalized force vs. normalized deflection for a typical ligament.

2.6 Muscles

There are 31 pairs of muscle in the human neck (Knaub & Myers, 1998), which can be divided into six groups: hyoid muscles, lateral muscles, anterior muscles, suboccipital muscles, back muscles, and vertebral column muscles (Gray, 1918). These muscles are symmetric about the sagittal plane, meaning that the muscles on the left and right hand side of the neck are the same. The muscles in the neck attach to bone via tendons and the attachment points of muscles are referred to as the origin and insertion. The origin of a muscle is on the bone that remains stationary when the muscle is activated and the insertion point is on the bone that moves due to muscle contraction.

The hyoid muscles are a group of muscles that attach to the hyoid bone and they can be broken into two sections the suprahyoids and infrahyoids (Figure 2-18, Figure 2-19). The suprahyoids are superior of the hyoid bone and attach between the hyoid bone and the mandible or skull, and are used to swallow food (Grey, 1918), so they have little biomechanical relevance for automotive impacts.

16

The infrahyoids (omohyoid, sternothyoid, sternohyoid and thyrohyoid) are a group of muscles inferior to the hyoid bone and connect with the sternum, scapula, or thyroid cartilage. The infrahyoid muscles are used in swallowing and have been shown to contribute to the flexion motion of the neck (Gray, 1918; Chancey et al., 2003).
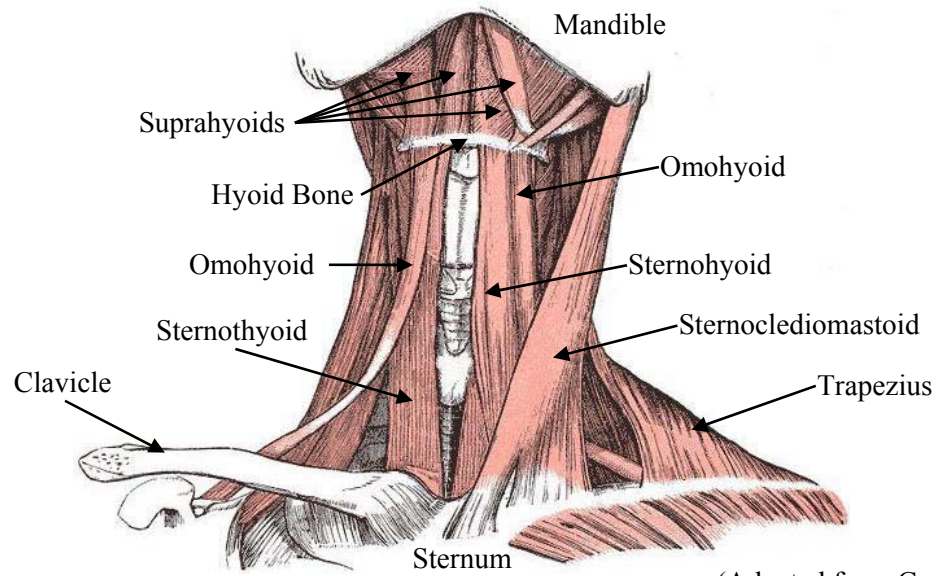
(Adapted from Gray, 1918)

Figure 2-18: Anterior view of the superficial muscles.

The lateral muscle group consists of the sternoclediomastoid and the scalene muscles (anterior, middle, and posterior) (Figure 2-19, Figure 2-20). The sternoclediomastoid is a broad muscle that has its origin at the clavicle and sternum, and it inserts onto the mastoid process of the skull. The scalene muscles have three parts: anterior, middle and posterior, which insert onto the transverse process of the second through seventh cervical vertebrae and their origin is on the first or second rib. The lateral muscle group generates much of the force required for lateral bending.

Sternoclediomastoid

Splenius Capitis

Levator Scapula

Middle Scalene

Anterior Scalene

Trapezius

Stylohyoid

Hyoid Bone

Thyrohyoid

Sternothyoid

Omohyoid

Clavicle

(Adapted from Gray, 1918)
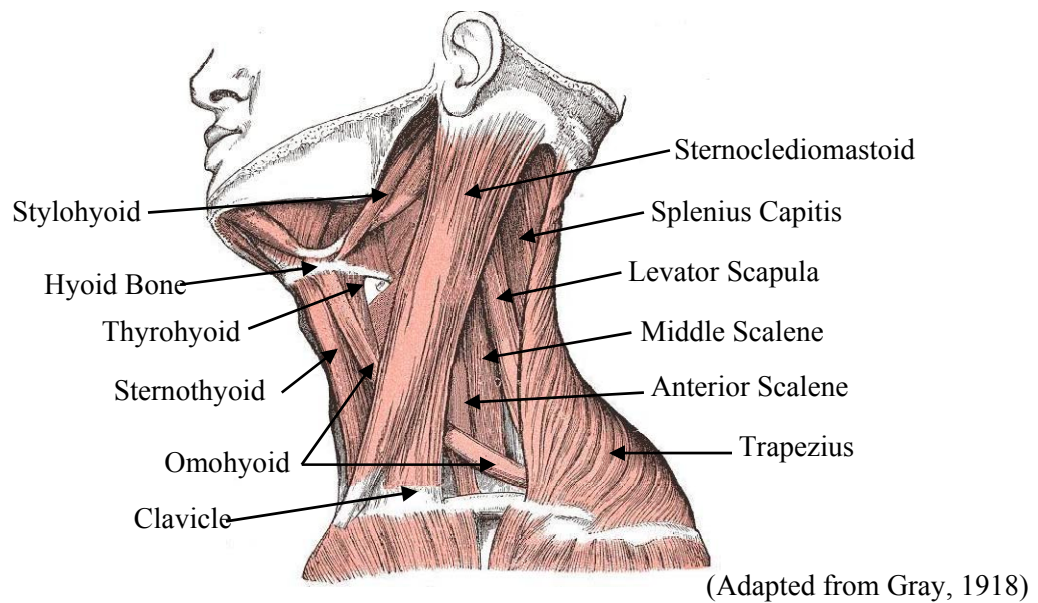
Figure 2-19: Lateral view of the neck muscles.

The muscles that run adjacent to the anterior surface of the vertebral bodies are called the anterior muscle group (Figure 2-20). The anterior muscle group is comprised of the longus capitis, the longus colli (inferior and vertical), and the rectus capitis anterior and lateralis. The longus colli inserts onto the occipital bone and originates on the transverse process of C2 to C5, and is responsible for head flexion. The longus colli is long muscle that starts in the thoracic spine and terminates at the atlas, attaching to each vertebra along the way. The rectus capitis anterior and lateralis attach the atlas to the occipital bone and are responsible for rotation and lateral bending of the head.

Occipital Bone — Rectus Capitis Anterior

Rectus Capitis Lateralis

Longus Capitis

Longus Colli (Superior)

Longus Colli (Vertical)

Middle Scalene

Anterior Scalene

Posterior Scalene

7th Cervical Vertebra

Longus Colli (Inferior)

(Adapted from Gray, 1918)
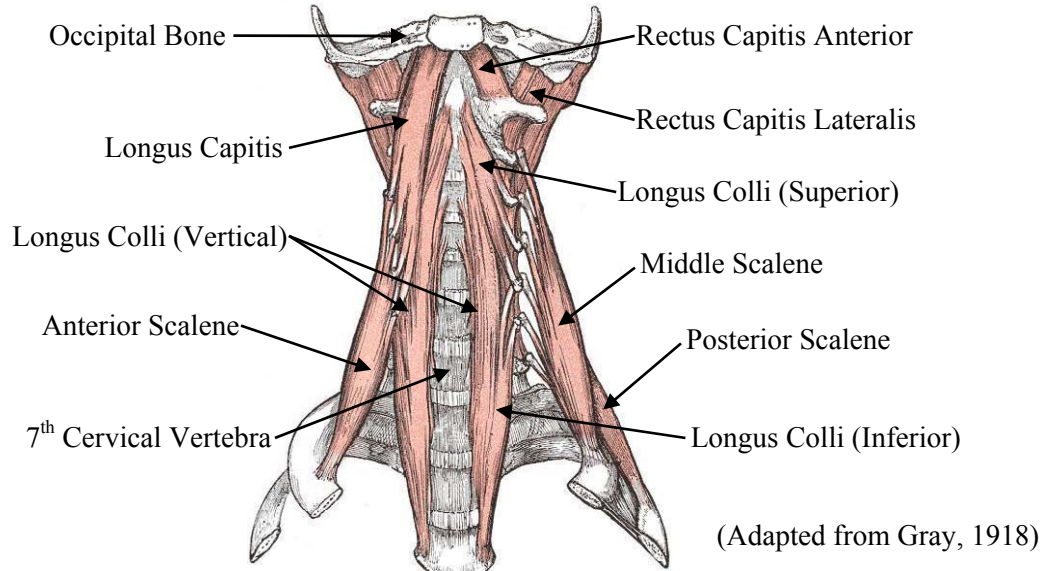
Figure 2-20: Anterior view of the deep neck muscles.

Control of head motion relative to the cervical spine is primarily achieved with the suboccipital muscle group (Figure 2-21). This group consists of the superior and inferior oblique capitis, and the major and minor posterior rectus capitis. Both the rectus capitis posterior minor and the oblique capatis superior originate on the atlas and insert onto the occipital bone of the skull. The rectus capitis posterior major acts between the spinous process of the axis and the occipital bone. Finally, the oblique capatis superior originates on the atlas and inserts onto the occipital bone.

Occipital Bone
Rectus Capitis Posterior Minor
Oblique Capatis Superior
Semispinallis Capitis
Rectus Capitis Posterior Major
Oblique Capatis Inferior
Longissimus Capitis
Multifidus
Semispinalis Cervicis
Longissimus Cervicis
Illocostalis
Longissimus Cervicis
(Adapted from Gray, 1918)
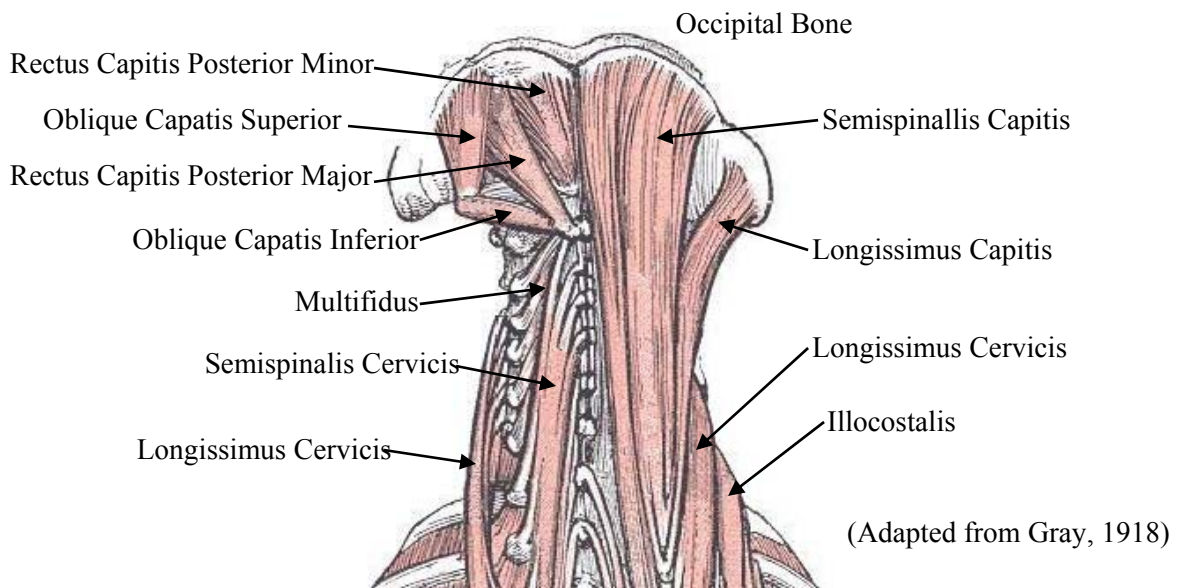
Figure 2-21: Posterior view of the deep neck and back muscles.

The back muscle group is a set of long muscles that run along the posterior of the neck, which consist of the longissimus muscles, the semispinalis muscles, the splenius muscles, the iliocostalis, and the multifidus muscle (Figure 2-21, Figure 2-22). The longissimus capitis, the semispinalis capitis, and the splenius capitis muscles originate in the upper thoracic spine and insert at every vertebral level up to the occipital bone. The longissimus cervicis, the semispinalis cervicis, and the splenius cervicis muscles also originate in the upper thoracic spine, but terminate at the third cervical vertebra. The multifidus muscle originates on the articular process and inserts on the spinous process of the vertebra two levels up, and exists over the entire cervical spine (Gray, 1918). The back muscle group is primarily used to create extension of the neck.

The final group of muscles is called the vertebral column group, and is comprised of the levator scapula, the minor rhomboid, and the trapezius muscle (Figure 2-22). The trapezius muscle is the largest muscle in the neck, and it has a flat triangular shape. It originates at the clavicle and scapula, and it inserts onto the occipital bone and the spinous process of every vertebral level in the thoracic and cervical spine. The levator scapula and minor rhomboid originate at the scapula and insert onto the spinous process of the seventh vertebra and the upper cervical spine respectively. The vertebral column group is primarily responsible for neck extension, but can also be used for lateral bending.
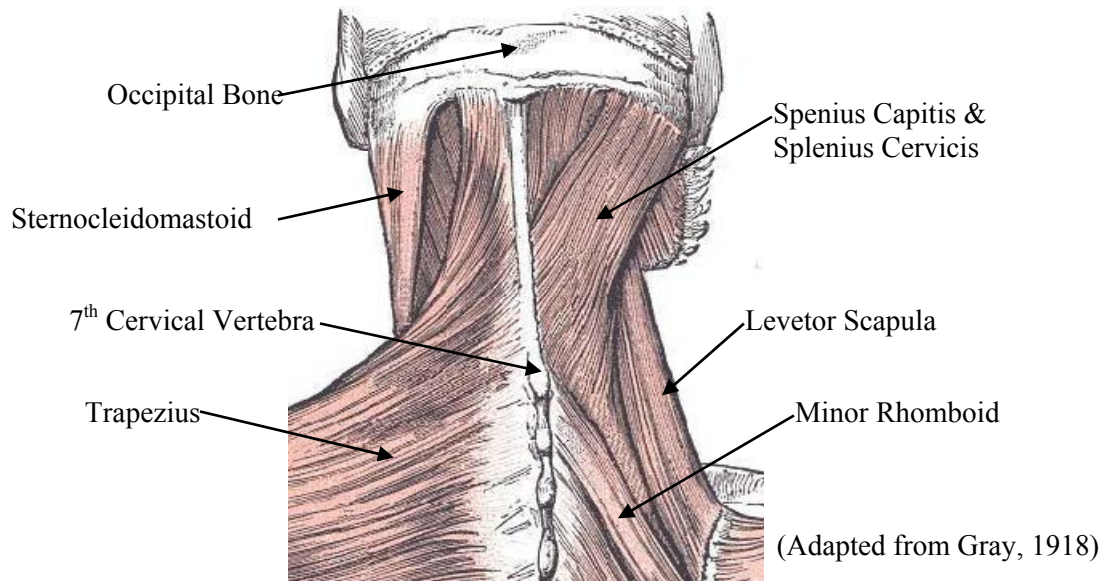
Figure 2-22: Posterior view of superficial neck and back muscles.

Muscles are only able to generate a contractile force causing the muscle to shorten and they need an opposing muscle to lengthen. These opposing muscles are called an antagonistic pair and every muscle in the human body is part of an antagonistic pair.

The neutral length, zero velocity maximum contractile force a muscle can generate is called the peak isometric force. This peak isometric force is a function of the physiological cross sectional area (PCSA) and the resting sacromere length. The PCSA is a function of the muscle's pennation angle (orientation of muscle fibres relative to the line of action) and the muscle's physical cross sectional area, normally measured at the muscle's mid length (Knaub & Myers, 1998; Garrett at al., 1988). Depending on the muscle, the PCSA can vary from $0.6cm^2$ (sternohyoid) to $13.7cm^2$ (trapezius) (Knaub & Myers, 1998). The sacromere length (2.4-3.1µm in the cervical spine) is the length of the basic filaments that are bundled together to form muscle fibres, which are then bundled to create muscle tissue (Knaub & Myers, 1998). The force a muscle is producing at any time is a function the current muscle length, the velocity of contraction/extension, peak isometric force, and the activation level (J. M. Winters & S. L. Woo, 1990).

Chapter 3
Model Description

The model used in this thesis was developed at the University of Waterloo by Matthew B. Panzer and Professor Duane S. Cronin (Panzer, 2006; Panzer & Cronin, 2009). The cervical spine model is an explicit finite element model of a 50th percentile male. The model contains both passive and active musculature, detailed nucleus and annulus models of the discs, rate dependent non-linear ligaments, facet capsules with a squeeze film model of the synovial fluid, and rigid vertebrae derived from CT scans (Figure 3-1). The material properties used in this model were derived from independent experimental testing in the literature, and implemented using appropriate constitutive models. It should be noted that the properties were not adjusted to improve the model response. The model was built for LS-DYNA software (LSTC, Livermore, CA) and solved with version R3_2_1. The model has 40,678 shell elements, 1,696 discrete elements, and 65,980 solid elements. In total, the model has 108,354 elements and 90,465 nodes. What follows is a brief description of the geometry and material properties of the model; for a full description see Panzer (2006).
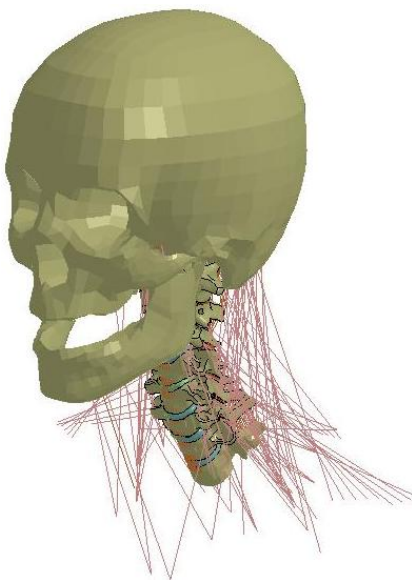
Figure 3-1: Isometric view of the UW cervical spine model.

3.1 Vertebrae

The geometry of the vertebrae was extracted from a model by Y.C. Deng et al (1999), which came from a commercially available dataset of 3D surfaces (Viewpoint DataLab, Orem, UT). These surfaces came from CT scans of a male subject, and were scaled to agree with dimensions from a 50th percentile male (Gilad & Nissan, 1986). The skull and first thoracic vertebra were modeled with a course shell mesh (Figure 3-2). The skull and the T1 are included solely for the application of boundary conditions and inertial effects, so a fine solid mesh is not required. The first though seventh cervical vertebrae are meshed with a fine solid mesh (~1.5mm) in order to predict vertebral fractures in future work (Figure 3-3 & Figure 3-4). The mass properties of the vertebrae and skull were taken from literature and are shown in Table 3-1 (Walker at al., 1973; Robbins, 1983). The bony geometry of the model was modeled as rigid for computational efficiency, which is possible because bony fractures are not expected at the impact loads that cause soft tissue injury.
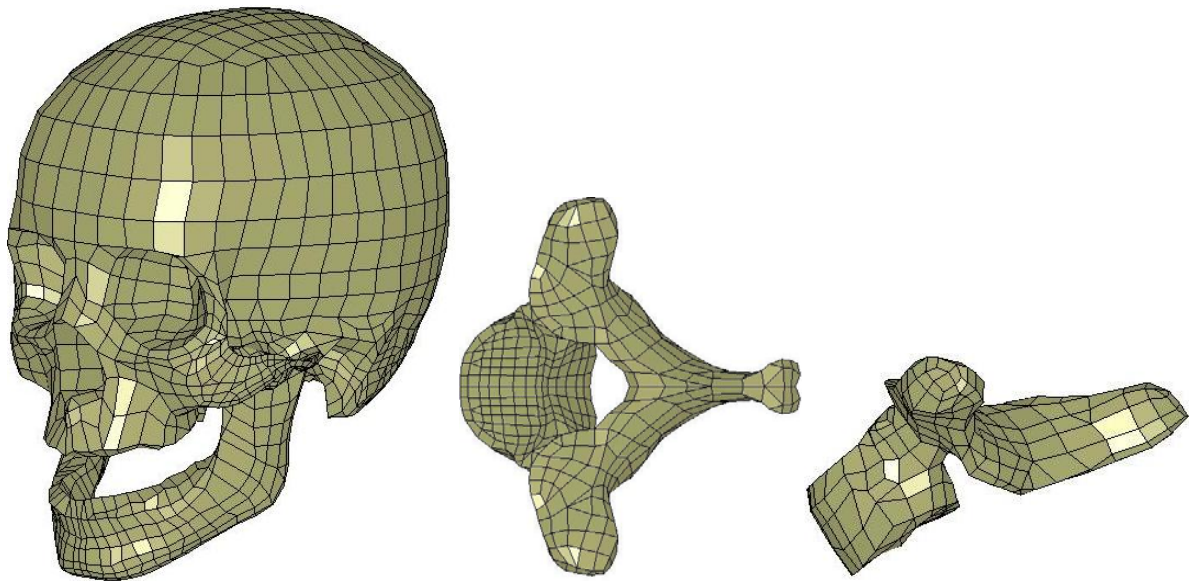
Figure 3-2: From left to right: Isometric view of the skull, T1 superior view and lateral view.
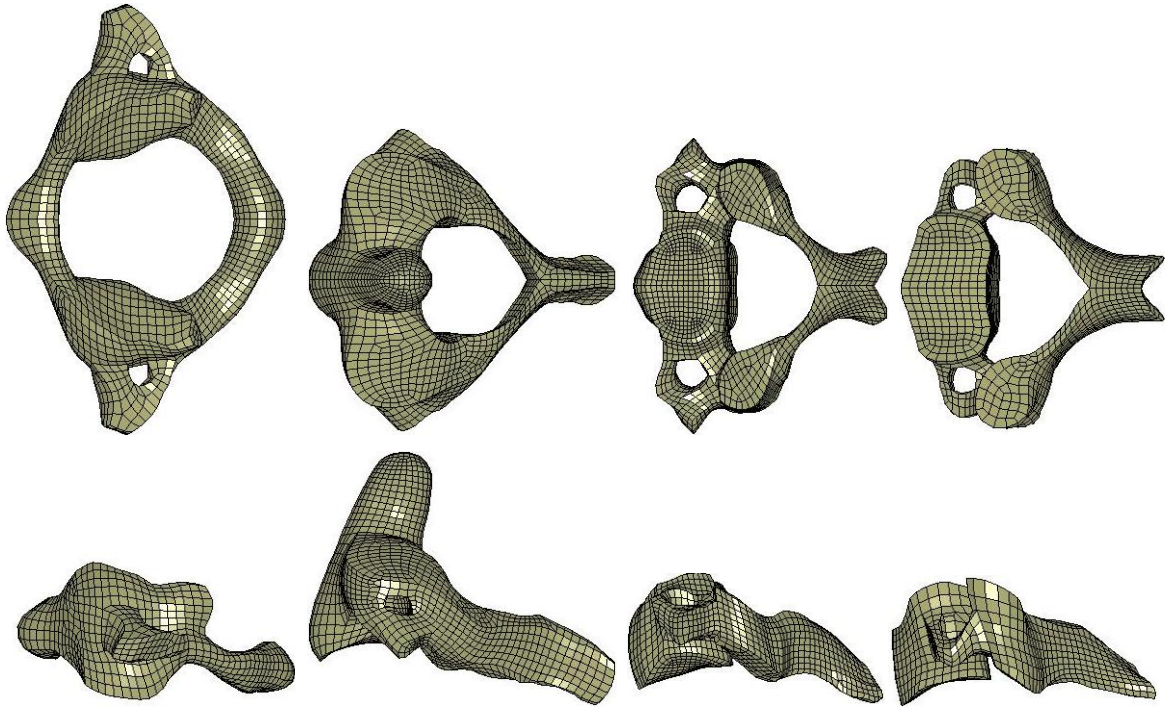
Figure 3-3: The first through fourth cervical vertebrae from left to right.

A superior view (above) and lateral view (below).
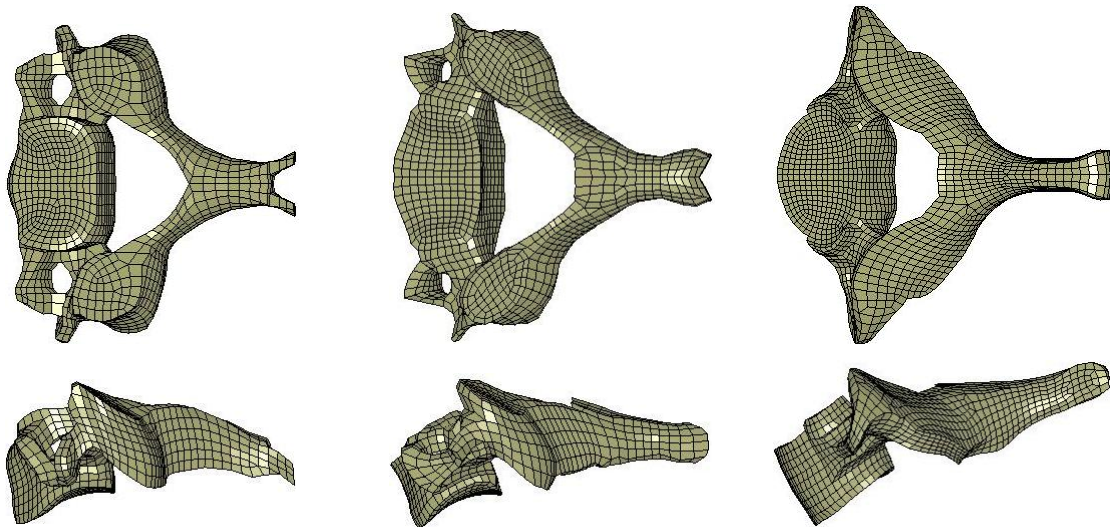
Figure 3-4: The fifth through seventh cervical vertebrae from left to right.

A superior view (above) and lateral view (below).

Table 3-1: Mass properties of the cervical spine bones.

Bone	Mass (g)	Sagittal Plane Moment of Inertia (g mm^2)
Skull	4376	23.3 x 10^6
C1	22.6	3,759
C2	25.4	5,372
C3	16.2	2,166
C4	17.0	2,183
C5	18.8	2,559
C6	19.1	3,260
C7	18.5	3,461

The vertebrae were positioned so that when the model was fully assembled, the curvature and length of the spine agreed with literature. It was also required that the vertebrae were spaced such that the vertebral discs were the desired height as per Gilad & Nissan (1986). The superior and inferior Bezier curve angles were 14.7° and 17.5° respectively, which agrees with the data reported by Klinich et al. (2004) for a 50th percentile male in a seated position (Figure 3-5). The length of the cervical spine was measured as per Robbins (1983) (Figure 3-5). The length of the cervical spine in the model was 121.4mm, compared to 118.8mm reported by Robbins (1983) for a mid size male.
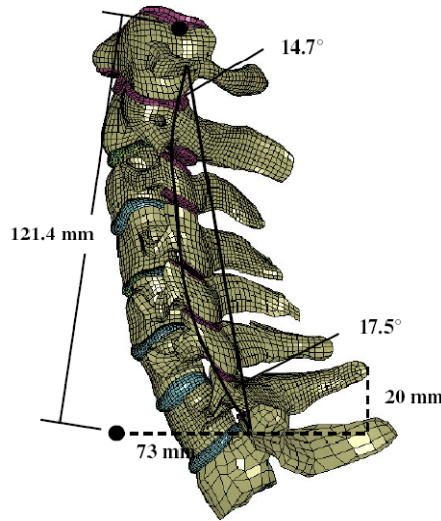
(Adapted from Panzer, 2006)

Figure 3-5: The curvature and length of the UW cervical spine model.

3.2 Intervertebral Discs

The intervertebral discs are located between adjacent vertebral bodies, such that the superior and inferior surfaces of the disc are determined by the geometry of the vertebrae. The soft ground substance and nucleus pulposus are modeled with solid elements and the annulus fibrosus is modeled with five pairs of concentric shell layers (Figure 3-6). The three constituents of the disc transfer loads to one another by sharing nodes and the discs attach to the vertebrae with a tied contact interface to allow for dissimilar meshes. The area of the nucleus pulposus in the transverse plane is approximately half of the area of the entire disk for each vertebral level (43.2% to 56.5%), which is supported by literature (Pooni et al., 1986; Iatridis et al., 1996).
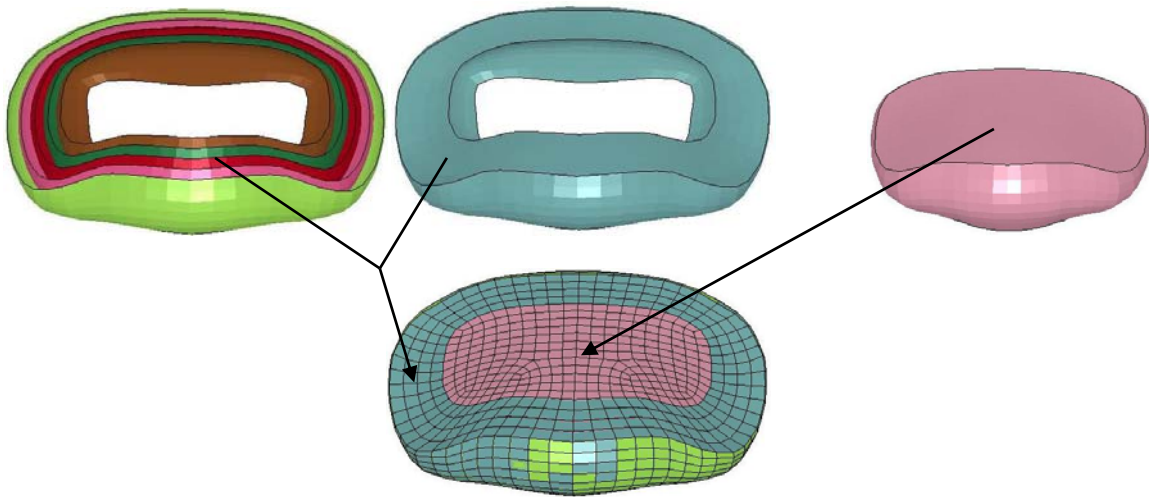
Figure 3-6: Geometry of the intervertebral discs.

The annulus fibrosus and ground substance (upper left) and the nucleus pulposus (upper right) combine to form the intervertebral disc (below).

The nucleus pulposus has fluid like characteristics, and is modeled with a general linear viscoelastic model. The parameters for the model come from a curve fit to data reported by Iatridis et al. (1996), who looked at nucleus stress relaxation (Table 3-2; Panzer, 2006).

Table 3-2: Nucleus pulposus material model parameters.

Parameter	Value
K	1.720GPa
G_1, β_1	5.9300E-4 MPa, 1.4770E-3 1/s
G_2, β_2	6.7630E-4 MPa, 6.1524E-2 1/s
G_3, β_3	9.5160E-4 MPa, 1.018 1/s
G_4, β_4	2.0384E-3 MPa, 13.200 1/s

The material properties for the annulus fibres were taken from single lamina samples extracted from cadavers, and tested along the fibre direction (Holzapfel et al., 2005) (Figure 3-7). Holzapfel et al. (2005) provided averaged curves for the inner and outer lamina, up to 4% strain. The data was extrapolated to higher strain levels using continuity of slope. Then the response of the intermediate fibre layers was interpolated from data for the inner and outer layers. The fibre direction for the outer pair of annulus shells was ±25° from the transverse plane, and increased by five degrees for each layer until it was ±45° at the inner fibres (Cassidy et al., 1989; Marchand & Ahmed, 1990; Wagner & Lotz, 2004; White & Panjabi, 1990).
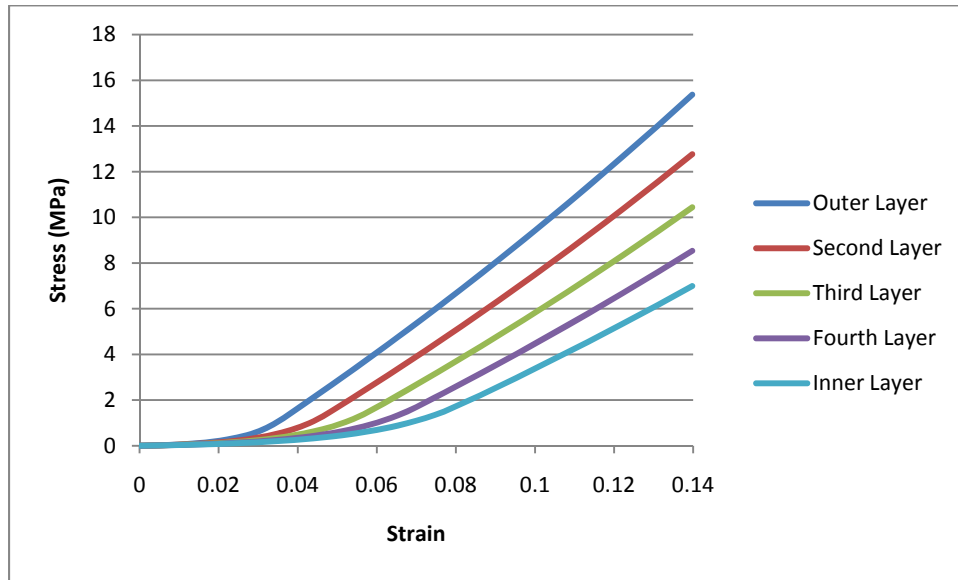
Figure 3-7: The stress-strain response of the annulus fibres along the fibre direction.

To measure the properties of the annulus ground substance, researchers tested samples of cadaver annulus fibrosus perpendicular to their fibre lamina because the fibres have no influence in this direction (Iatridis et al., 1998; Fujita et al., 1997). The experimental data was fit to an Ogden-Rubber

material model using the method of least squares (Figure 3-8; Panzer, 2006). By testing samples of ground substances in different directions, it was shown that the ground substance is isotropic (Iatridis et al., 1998; Klisch & Lotz, 2000). The tensile and compression response of the annulus ground substance was found to be site independent (Fujita et al., 1997; Iatridis et al., 1998). It is know that the ground substance is highly viscoelastic at low strain rates (<10/s), due to fluid-transport mechanisms (Iatridis et al., 1998; Iatridis et al., 1999). At higher strain rates, as experienced in an automotive impact, data is not available for the viscoelastic properties of annulus fibrosus ground substance.
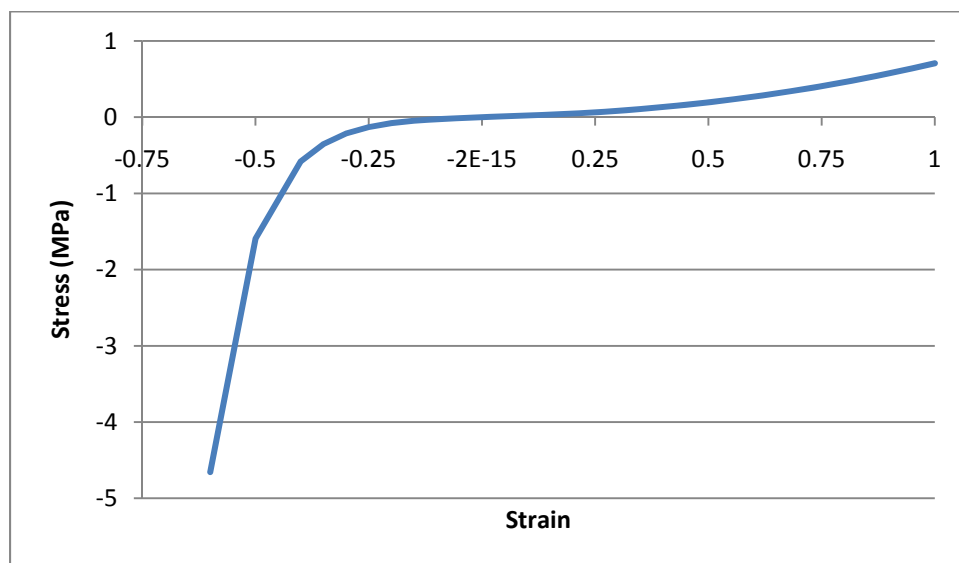
Figure 3-8: The uniaxial stress-strain response of the annulus fibrosus ground substance.

3.3 Facet Joints

The facet joints in the model consist of two layers of solid elements representing articular cartilage sandwiching pressure-volume airbag model of the synovial fluid, and surrounded around the perimeter by beam elements representing the capsular ligaments (Figure 3-9). The geometry and properties of the capsular ligaments will be discussed in a following section. The articular cartilage geometry was created by extruding the inferior and superior surfaces of the articular pillar of the respective vertebrae by 0.5mm for C3 to T1, and 1mm for C2 to skull. These cartilage thicknesses agree with measurements taken from cadavers in experimental studies (Womack et al., 2008; Yoganandan et al., 2003). The synovial fluid air bag segments were defined by the space remaining between the two layers of articular cartilage. It should be noted that the gap between the articular

cartilage plays a role in the response of the model in rear impact, but no data pertaining to this measure could be found. It is possible to match other postural data for the overall spine length and curvature with variations of the facet gaps.
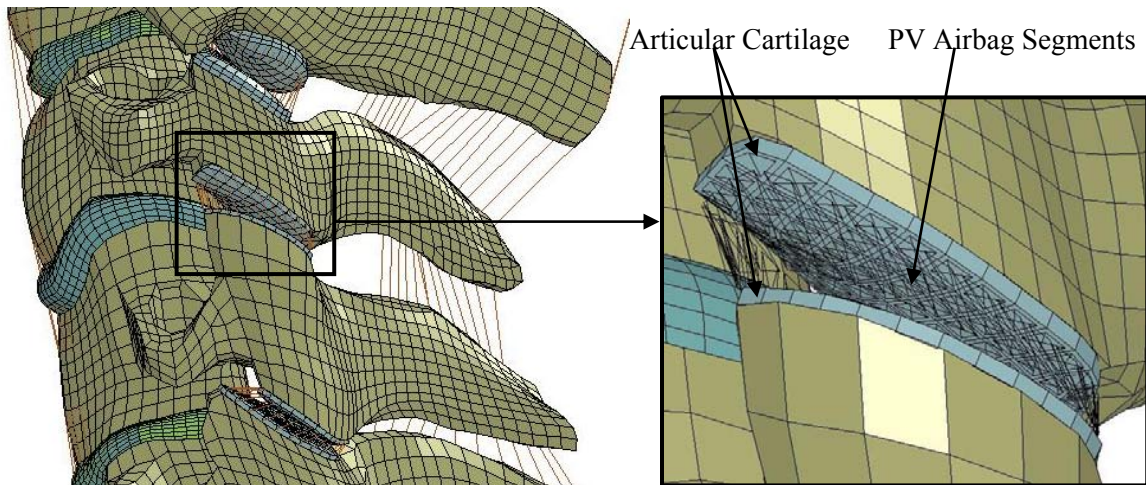
Figure 3-9: Geometry of the facet joints in the model.

The articular cartilage is a poroelastic material that has non-linear mechanical properties with a strong dependency on internal fluid flow at low stain rates, but at the stain rates seen in automotive impact fluid loss is not expected to occur. Therefore, the cartilage can be modeled with a quasi-linear viscoelastic material model. Parameters for this material were found by curve fitting to stress relaxation of bovine cartilage material data reported by DiSilvestro & Suh (2001) (Table 3-3; Panzer, 2006). It should be noted that the strain rates used by DiSlvestro & Suh were 0.001/s, well below the 100/s or higher expected in impact cases, and the model does not predict much stiffening beyond 0.1/s. This may be a limitation of the model and high rate testing of cartilage would be useful.

Table 3-3: Articular cartilage material model parameters.

Parameter	Value
K	2 GPa
G_1, β_1	0.2100 MPa, 0 1/s
G_2, β_2	0.0243 MPa, 0.303E-3 1/s
G_3, β_3	1.0824 MPa, 80.807E-3 1/s
G_4, β_4	1.9984 MPa, 12.927E-3 1/s

The synovial fluid, as the name suggests is a fluid and although LS-DYNA has the ability to model fluid behaviour, this was not used because large deformations in the space between the articular

cartilage would lead to highly distorted elements, small time-step, and an unstable model. Instead, airbag segments were placed in-between the articular cartilage and a pressure-volume relationship was defined using a simple squeeze-film finite element model (Kumaresan et al., 1998; Panzer, 2006) (Figure 3-10). In this model, solid synovial fluid elements (K=2.2 GPa i.e. water) were compressed by two rigid elliptical plates 1mm apart with the average facet dimensions corresponding to each spinal level, and shell elements were used for the synovial membrane (E = 10 MPa, ν = 0.4) around the circumference as per Kumaresan et al. (1998). The force required to compress the plates was recorded and converted to pressure using the area of the plates and the volume was calculated as the area of the plates times the distance between the plates (Figure 3-11). The pressure-volume relationship still allows the articular surfaces to contact one another, as a fluid would, so the coefficient of friction between the articular cartilage was set to zero to model the lubricating nature of synovial fluid.

Elliptical plates

Synovial Fluid

Synovial Membrane

Adapted from Panzer 2006
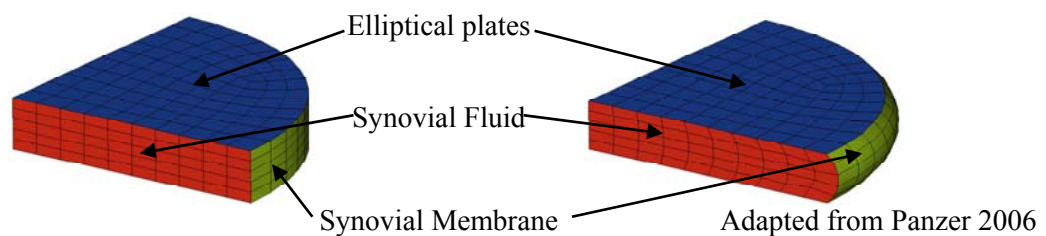
Figure 3-10: Squeeze-film finite element model.

The model is undeformed on the left and compressed on the right.
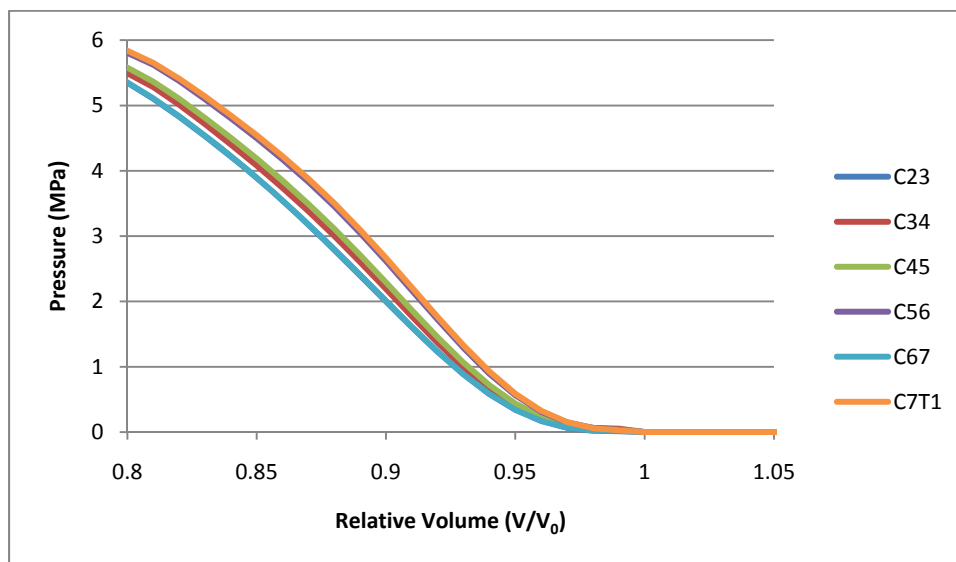
Figure 3-11: Pressure-volume relationship of the synovial fluid model.

3.4 Ligaments

The ligaments in the UW cervical spine model are modeled using 1D discrete elements, which do not support bending or shear, only tension. Discrete elements were used instead of shells because most experimental data reports ligament response in terms of force vs. displacement, which is unsuitable for shell elements, and because the main purpose of a ligament is to transfer tensile loads. Each ligament was broken up into several elements to simulate the force distribution of ligaments in-vivo. The ligaments attach to the vertebrae using a shared node. All of the ligaments in the lower to upper spine were modeled (Figure 3-12 & Figure 3-13).
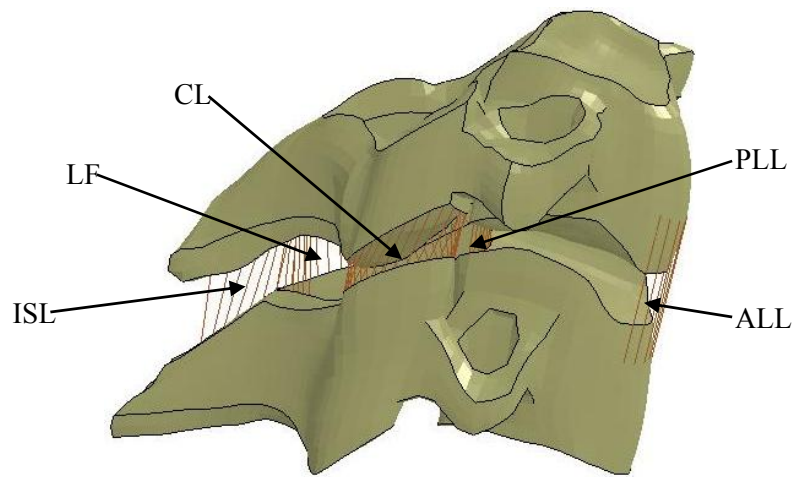
Figure 3-12: Geometry of the lower and middle cervical spine ligaments in the model.
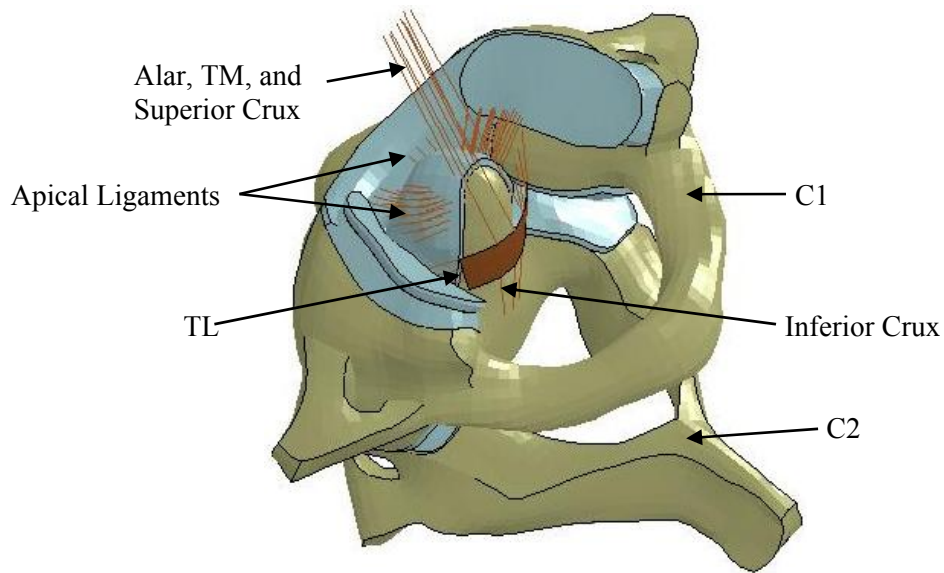
Figure 3-13: Geometry of the upper cervical spine ligaments in the model.

The material model chosen to represent the ligaments in the UW cervical spine model was a discrete nonlinear elastic spring model. This material model determines the force in the element by multiplying the quasi-static force at a given displacement by a dynamic scaling factor that is dependent on the rate of loading. For each ligament, a force-displacement curve was created from various experimental studies that looked at the uniaxial response of the cadaver ligaments under tension (Yoganandan et al., 2001; Myklebust et al., 1988; Dvorak & Panjabi, 1987; Panjabi et al., 1998a; Chazal et al., 1985). The only ligament not discussed in these studies was the hyothroid ligament, which connects the hyoid bone to the thyroid cartilage. Although this ligament is weak compared to the main cervical ligaments, because of its distance from the spinal column it contributes to the rear impact response of the model. Data for the failure of hyothyroid ligament was not available, but the toe region and linear portion of the curve were fit to data by Vilkman & Karma (1989), who vertically distracted a cadaver hyoid bone and recorded the force. The force-displacement curves including preload, which will be discussed below, for the ligaments in the model are shown in Figure 3-14, Figure 3-15, Figure 3-16, and Figure 3-17. The dynamic scale factor for the model was curve fit to experimental tests performed by Yoganandan et al. (1989), who tested the ALL and LF from cadavers at rates of 9, 25, 250, and 2500mm/s (Figure 3-18).
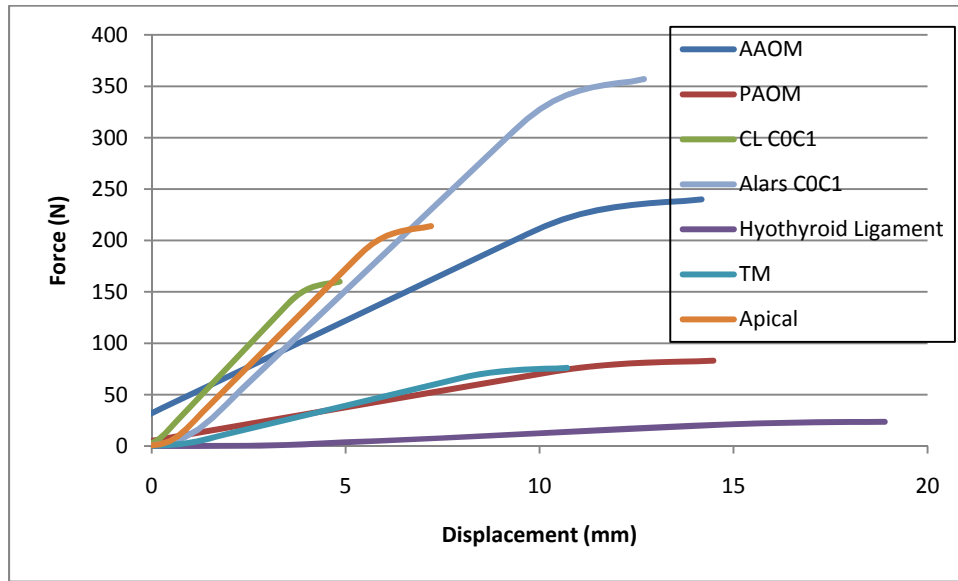
Figure 3-14: Quasi-static force-displacement response of upper cervical spine ligaments in the model, including preload. Part I.
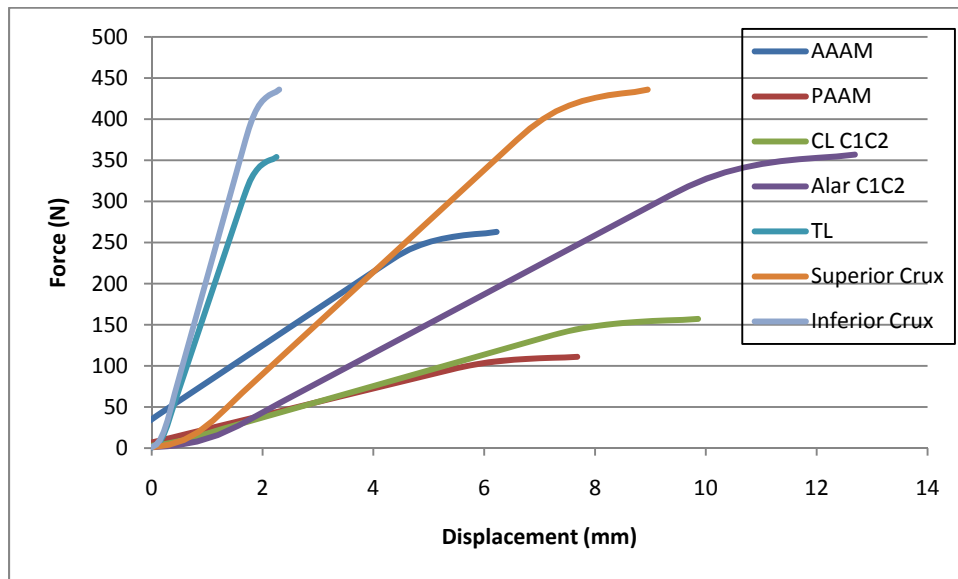
Figure 3-15: Quasi-static force-displacement response of upper cervical spine ligaments in the model, including preload. Part II.
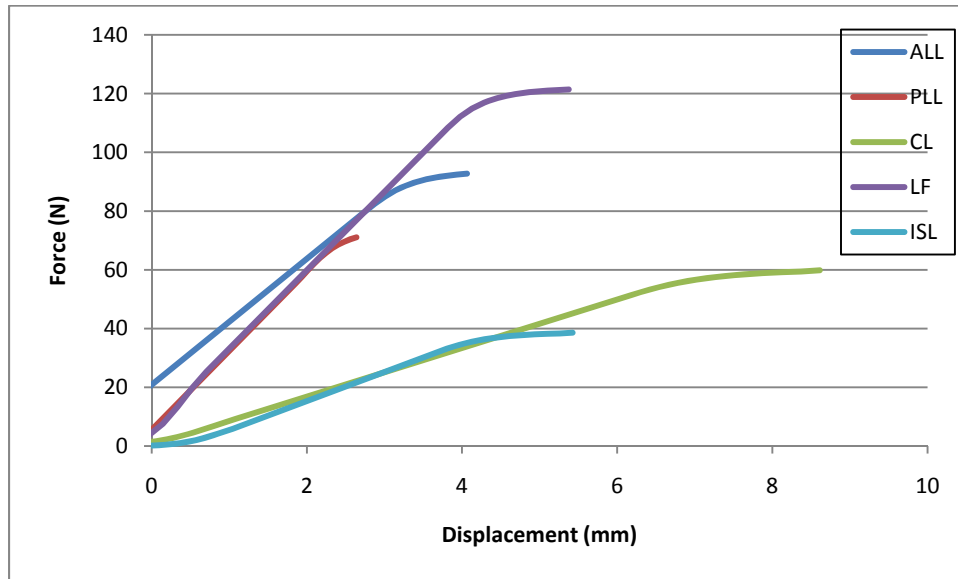
Figure 3-16: Quasi-static force-displacement response of middle cervical spine (C2-C5) ligaments in the model, including preload.
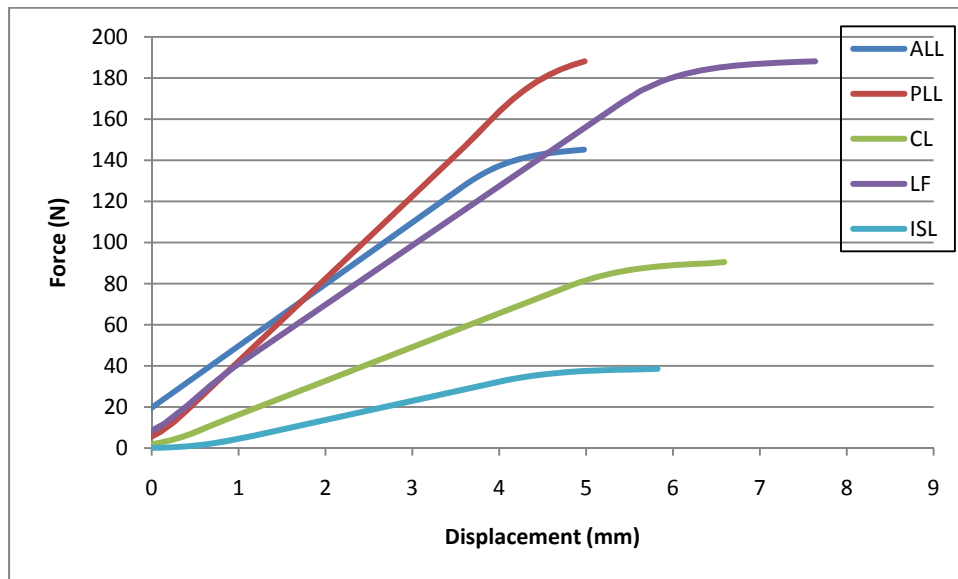
Figure 3-17: Quasi-static force-displacement response of lower cervical spine (C5-T1) ligaments in the model, including preload.
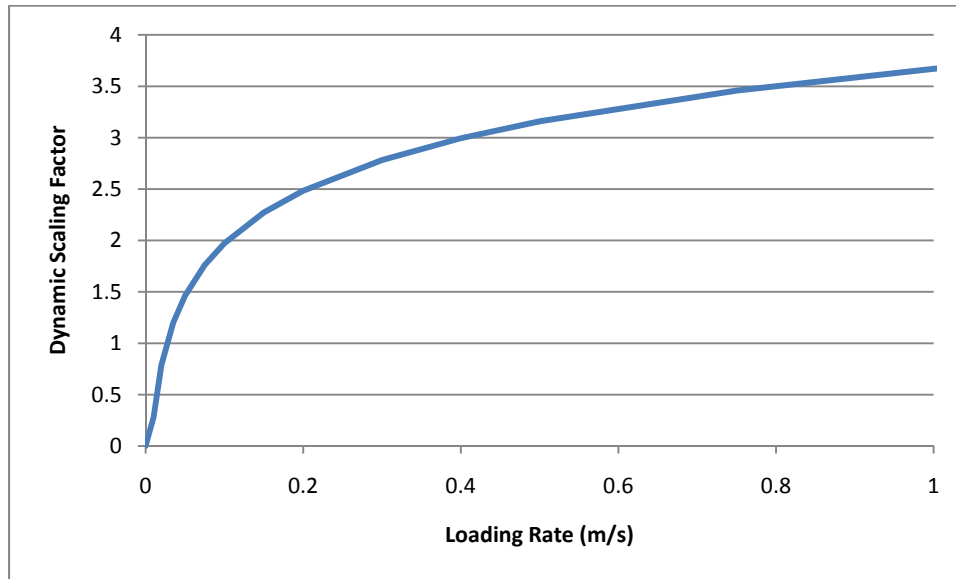
Figure 3-18: Dynamic scaling factor for ligaments in the model.

Heuer et al. (2007) showed that the ligaments in the spinal column are under a preload in-vivo, by extracting vertebral segments from cadavers, fixing the lower vertebra and then sequentially dissecting ligaments. They were able to measure the change in neutral position of the upper vertebra, showing that the ligaments were carrying a force before being dissected. In order to use the data by Heuer, a free-body diagram mimicking their tests was set up (Figure 3-19) and solved using compatibility equations and equilibrium. The compatibility equations relate the change in neutral angle (Δdeg) of the vertebra from Heuer et al. (2007) to the moments (M) being generated by the ligaments (Equation 3-1). The positions of the forces were measured from the model, and the forces were assumed to act downwards. The force in the disc was calculated by multiplying the disc area in the transverse plane by the intrinsic pressure that resides in the disc in the neutral position, 0.1 MPa (Ferguson, 2008). The force of gravity on the vertebra (F_{C4} in the FBD) was measured from the model. In total, there were five unknowns (F-ALL, PLL, CL, LF, ISL), which were solved with three compatibility equations, equilibrium of the vertical forces, and equilibrium of moments. The calculated preloads are shown in Figure 3-14, Figure 3-15, Figure 3-16, Figure 3-17, and Table 3-4.
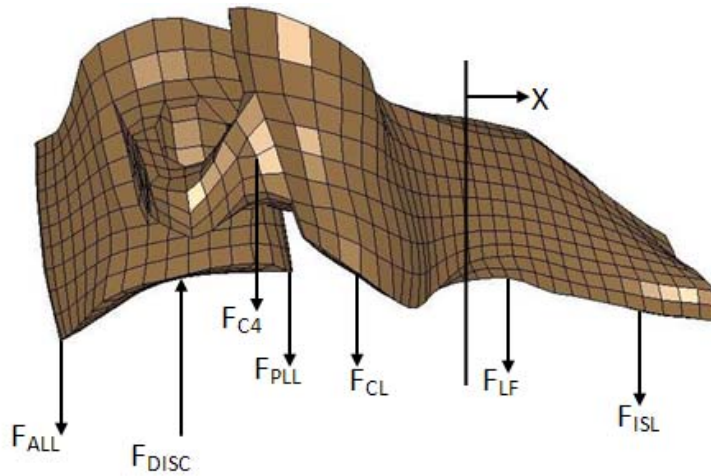
Figure 3-19: Free-body diagram to extract preload data from research by Heuer et al. (2007).

$$\frac{M_{LF}}{M_{ISL}} = \frac{\Delta deg_{LF}}{\Delta deg_{ISL}} \qquad \frac{M_{LF}}{M_{CL}} = \frac{\Delta deg_{LF}}{\Delta deg_{CL}} \qquad \frac{M_{ALL}}{M_{PLL}} = \frac{\Delta deg_{ALL}}{\Delta deg_{PLL}} \qquad \textbf{Equation 3-1}$$

Table 3-4: Ligament preloads used in the model, reported as force(N) (displacement(mm)).

	C2C3	C3C4	C4C5	C5C6	C6C7	C7T1
ALL	20.82	18.76	19.00	19.67	18.35	18.13
	(1.72)	(1.63)	(1.639)	(1.50)	(1.45)	(1.45)
PLL	5.62	6.46	6.64	5.69	7.22	7.40
	(0.81)	(0.84)	(0.85)	(1.12)	(1.19)	(1.19)
LF	2.61	3.12	2.94	3.41	3.10	3.52
	(1.042)	(1.08)	(1.07)	(1.45)	(1.42)	(1.45)
ISL	0.53	0.69	0.62	0.62	0.55	0.56
	(1.13)	(1.19)	(1.17)	(1.25)	(1.22)	(1.23)
CL	1.77	2.41	2.21	2.02	2.17	1.81
	(1.46)	(1.59)	(1.56)	(1.06)	(1.07)	(1.04)

In the upper cervical spine, the geometry of the ligaments does not allow the same approach to calculate preloads, so the preload strains of their equivalent lower cervical spine ligaments were used. The calculated preload displacements of the LF are equivalent to 15.2 to 16.6% strain, which agrees with the value of 15% reported by literature (Nachemson & Evans, 1968; Viejo-Fuertes et al., 1998)

3.5 Muscle

As with the ligaments, the muscles are modeled using 1D discrete elements. The origin and insertion point of each muscle was defined using anatomical landmarks referenced in anatomy textbooks (Gray, 1918; Agur & Dalley, 2004). Each muscle was broken up into segments to properly represent the multiple attachment points common in the neck. This resulted in 90 pairs of muscle segments to represent the 27 muscles of the human neck (Knaub & Myers, 1998). The segments of muscle were broken up into elements along their length, and the ends of the elements were constrained to adjacent vertebrae to allow the neck muscles to curve with the neck (Figure 3-20). Muscles that attach below the 1st thoracic vertebra were positioned anatomically, but they were constrained to the T1. The hyoid bone is not modeled, so muscles that would attach to it are constrained to the skull. This will alter the line of action of these muscles, but their cross section is small and the influence on the kinematics of the head will be small. The use of discrete elements does not include any mass, so the mass elements were added to the end nodes of each muscle element. The amount of mass added was determined using reported neck muscle volumes (Knaub & Myers, 1998) and a reported average muscle density of 1.06g/cm^3 (Ward & Lieber, 2005).
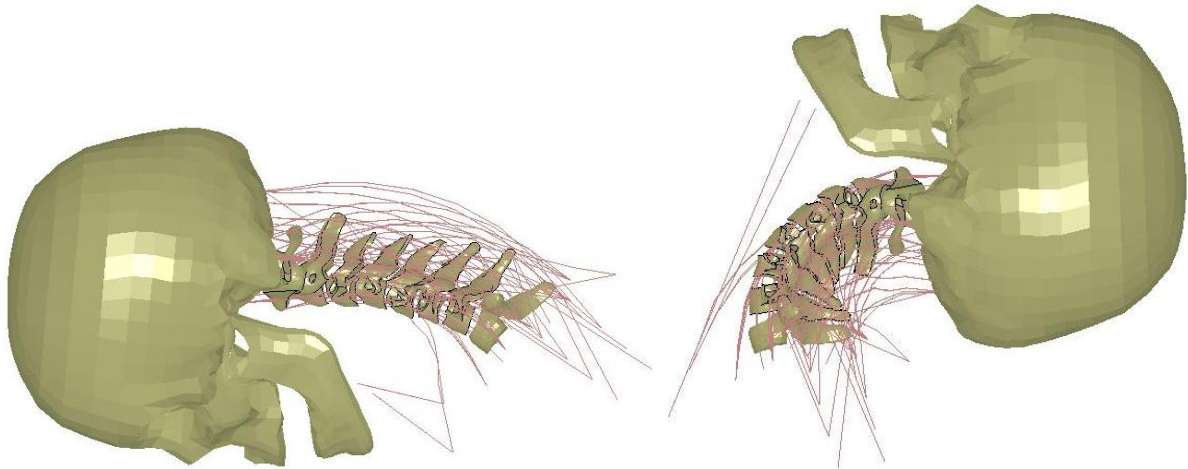
Figure 3-20: Neck muscles in the UW cervical spine model in flexion (left) and extension (right).

The neck muscles were modeled using the Hill muscle model that is implemented in LS-DYNA. The Hill muscle model consists of two parallel spring elements, one represents the active or contractile properties (F^{CE}) of the muscle and the other represents the passive tissue response (F^{PE}) (Figure 3-21). The model also contains an elastic element in series with the contractile element to represent tendon

compliance. This is not always used because the tendon compliance is often incorporated with the properties of the contractile element. The contractile element is dependent on the activation state $(a(t))$, current muscle length (L^M), and the velocity of contraction (v^M). The passive element is dependent only on the current muscle length. The total force in the muscle (F^M) is equal to the sum of the contractile force and the passive force.
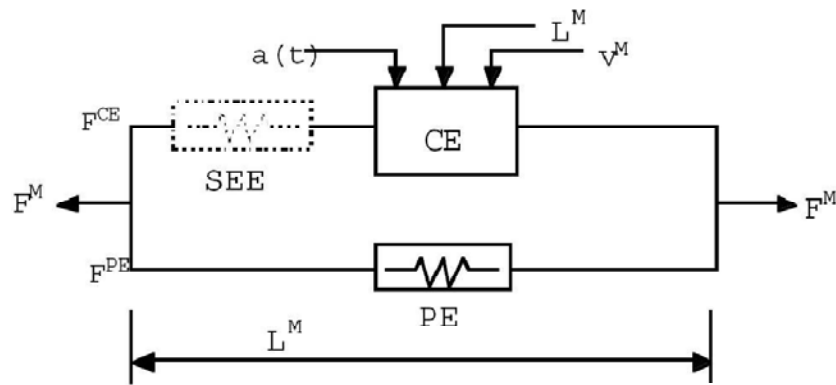
(Adapted from Hallquist, 2003)

Figure 3-21: Schematic of the Hill muscle model.

The contractile force is equal to the peak isometric force times scale factors that are dependent on the activation state, current muscle length, and contractile velocity (Equation 3-2). The peak isometric force of a muscle is equal to the PCSA times the peak isometric stress. In the model, PCSA of each muscle was taken from Knaub & Myers (1998) and the peak isometric stress is 0.5MPa (Winters & Stark, 1988). There is a delay between when the brain desires a muscle to contract and when the electro-chemical process for muscle contraction to occur, which has been modeled by Winters & Stark (1985). The activation state of muscle in the model to 100ms neural input starting at 74ms can be seen in Figure 3-22. The active force of a muscle is highest when the normalized length is equal to 1.05 and decreases in a Gaussian shape when the length increases or decreases (Winters & Woo, 1990; Figure 3-23). When a muscle is stationary, it is able to generate the peak isometric force. When a muscle contracts it is able to generate additional force and while being extended it generates less force (Winters & Woo, 1990; Fung, 1993; Figure 3-24). The velocity used in this function is normalized by the maximum shortening velocity (v^{max}), which is approximated as 5/s times the initial muscle length (Winters & Woo, 1990).

$$F_{CE} = F_{max}a(t)f_{AL}(L^M)f_{AV}(v^M)$$

Equation 3-2

38
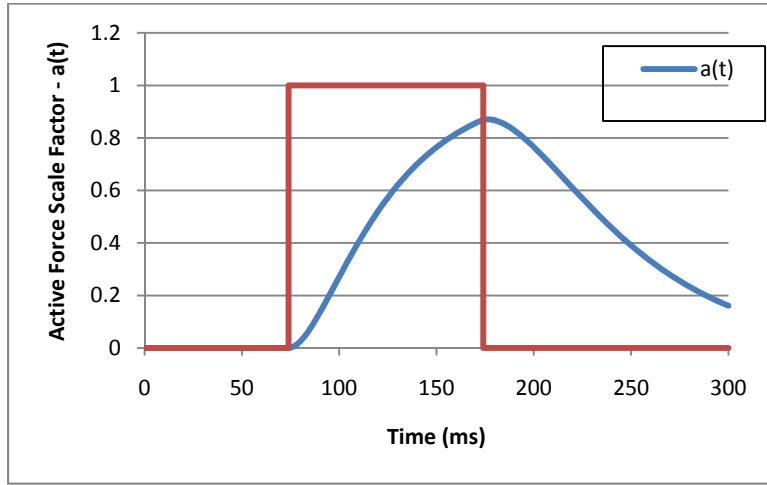
Figure 3-22: The muscle activation function for a 100ms step neural input starting at 74ms.
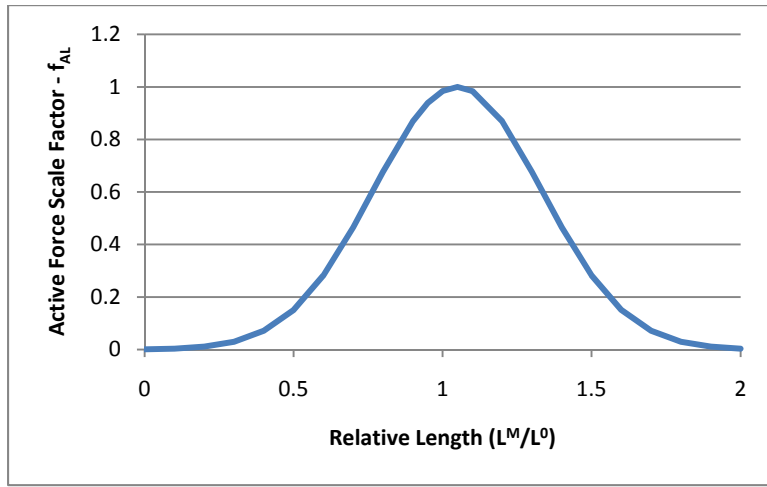
Figure 3-23: The current length dependent active force scale factor.
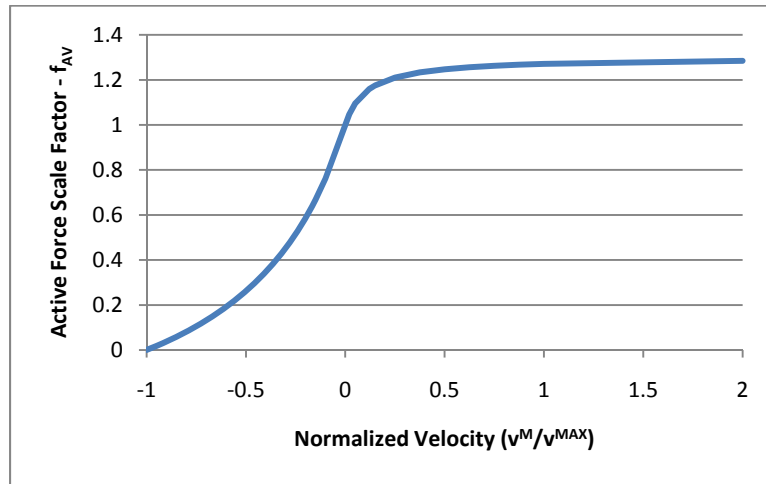
Figure 3-24: The contraction velocity dependent active force scale factor.

The passive element in the muscle model is equal to the peak isometric force multiplied by a scale factor that is dependent on the current muscle length (Figure 3-25). The passive muscle force is zero when the length of the muscle is less than the initial length, because the muscle does not support a compressive force. When the muscle is stretched by 1.6 times the original length, the passive force will be equal to the peak isometric force.
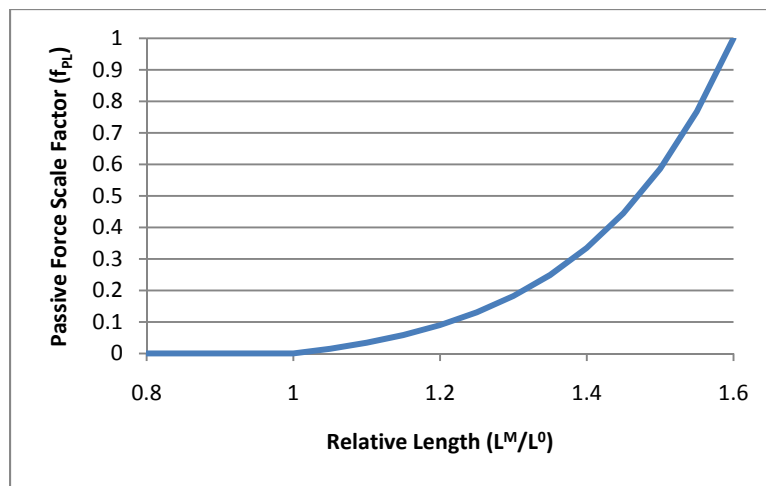
Figure 3-25: Passive force scale factor, which is dependent on current muscle length.

3.6 Model Improvements

The UW neck model has proved to be stable, biofidelic, and accurate. Due to the expanded range of loads applied to the model compared to previous work (full spine in rear impact and tension), some

areas for improvements were identified. Previously, the model was using mass scaling to achieve a time step of 4.5E-7s, which resulted in a 0.15% increase in mass that had no influence on the model response in frontal impact. For this thesis, the mass scaling was removed because it caused contact instabilities in rear impact that resulted in unrealistic axial rotations of the head and vertebrae. The full spine tension simulations revealed that the model was initially lax compared to cadaver tests, which led to literature review of ligament pretensions and ultimately ligament preloads being incorporated into the model. Finally, the ligaments attaching the hyoid bone to the cricoid cartilage were added based on a previous finite element model which showed they influence the head kinematics in rear impact (Lee et al., 2004a).

Chapter 4

Whiplash Review

4.1 Whiplash Symptoms

The first step in modeling whiplash injury is to understand what the symptoms of a whiplash injury are, and which symptoms occur most frequently. Neck pain, shoulder pain, headache, cognitive difficulties, visual obscuration, dizziness, paresthesia (pins and needles feeling), tinnitus (ringing in the ears), and back pain are all reported symptoms of whiplash (Cusick et al., 2001; Bogduk, 2006). In 2006, Bogduk did a comprehensive review of literature reporting which symptoms whiplash patients suffer from most frequently (Table 4-1). He found that neck pain, headache, and shoulder pain are the most common whiplash symptoms in both acute and chronic cases.

Table 4-1: Proportion of patients reporting symptoms, reproduced from Bogduk (2006)

	Proportion of Patients Reporting Symptoms (%)						
	Acute				Chronic		
Symptom	A	B	C	D	E	F	G
Pain							
Neck pain	89	90	92	88	74	100	95
Headache	26		57	54	33	88	20
Shoulder pain	37	80	49	40			61
Other							
Paresthesia		50	15		45	68	
Weakness						68	
Dizziness		62	15	23		53	12
Visual problems				9	2	42	14
Tinnitus		30	4	4	14		
Cognitive impairment		26				71	
Back pain		42	39		42		
Sample size	102	320	117	93	43	68	866

A: Maimaries et al., 1988; B: Dvorak et al., 1989; C: Radanov et al., 1995; D: Hildingson and Toolanen, 1990; E: Sturzenegger et al., 1994; F: Lord et al., 1996; G: Ovadia et al., 2002.

4.2 Pain

In the first chapter of *Physical Therapy of the Cervical and Thoracic Spine* (2002), Bogduk provides a detailed description of pain related to the cervical spine, which will be summarized here. Whiplash symptoms can fall under two categories: somatic pain where the source of pain is nociceptive nerve signalling related to tissue damage in the neck, or radicular pain where pressure is exerted on nerve tissue sending erroneous signals to the central nervous system.

A subset of somatic pain is referred somatic pain, where the pain originates in a structure in the neck, but pain is also felt in other parts of the body (head, shoulders, etc.). Clinically, the most suitable theorized mechanism of referred somatic pain is that multiple nerves from different parts of the body converge into the same neuron in the central nervous system, and the brain will interpret pain from either nerve as pain in both regions of the body. Several researchers have attempted to map somatic referred pain patterns, but due to differences between people only approximate patterns have been discovered; referred pain in the head is caused by damage to the upper spine (C1 to C3), referred pain to the upper limbs originates in the lower cervical spine (C5-T1), and referred pain in the shoulders can occur from any level in the cervical spine.

Radicular pain is often used to describe pain in other parts of the body which were caused by trauma to the neck, but only a small proportion of cases can be fully described by this type of pain. If neck pain is the only symptom, the pain cannot be radicular in nature because there is no known mechanism that nerve root pressure can cause localized symptoms in the neck. Nerve root compression will influence both small and large diameter nerves (nociceptive pain nerves and other sensory/motor control nerves respectively), so radicular pain must be accompanied with symptoms like paresthesia, numbness, and weakness. The nerve roots in the upper cervical spine (C1 and C2) are not susceptible to compression, so radicular symptoms are not a suitable explanation for upper cervical spine injuries. Finally, radicular pain caused by nerve root compression has been described as sharp shooting pain, so if the pain is dull and diffuse the source is not likely radicular. Therefore, to fully capture all whiplash symptoms with a numerical neck model, the nerve roots and spinal cord would need to be modeled. Due to the high prevalence of neck pain and the lower prevalence of other symptoms, the neck model in this thesis will focus on the causes of somatic pain.

Whiplash injuries can be grouped into two categories based on the amount of time symptoms have remained; acute injuries last a short period of time and chronic injuries can last for a long time or

never fully heal. The European Foundation of IASP (International Association for the Study of Pain) Chapters (EFIC) defines chronic pain as pain lasting longer then 3-6 months (Niv & Devor, 2007). Researchers have reported that 24% to 66% of whiplash patients that initially seek medical attention still had symptoms one year after their injuries occurred (Radanov et al., 1995; Deans et al., 1987; Norris & Watt, 1983). Chronic pain is defined as a disease, and acute pain is a symptom according to the EFIC (Niv & Devor, 2007). According to J.D. Loeser (2006), "For reasons not yet understood, some acute injuries lead to changes in the central nervous system that perpetuate the painful process long after any peripheral stimulus has ceased." The changes to the central nervous system have been documented by changes in brain activation to chronic pain as compared to acute pain (Apkarian, 2004). The most commonly accepted mechanism for these changes is pain central sensitization in the brain after an injury in the periphery (Ren & Dubner, 1999). Studies have supported the pain central sensitization theory in whiplash by showing that whiplash victims have lower pain thresholds in their neck and in other parts of their bodies when compared to healthy controls (Sterling et al., 2002; Koelbaek Johansen et al., 1999). Considering that the transition between acute pain and chronic pain is a poorly understood process involving the brain, numerical injury prediction is currently not able to identify which injuries will become chronic and which will not. The computational model in this thesis will be able to show tissue damage, which will then be compared with clinical studies for chronic pain when available.

4.3 Sources of Whiplash Pain

Researchers have proposed and investigated several structures in the neck as possible sources of whiplash injury. These structures include the capsular ligaments and facet joints, other ligaments, the vertebral discs, the vertebral artery, the dorsal root ganglion and dorsal root, and muscles. This section will provide a review of literature of how each of these structures relate to whiplash injuries.

4.3.1 Capsular Ligaments and Facet Joints

The cervical facet joints have been clinically identified as the source of pain in 54 to 60% of chronic whiplash patients (Barnsley et al., 1995; Lord et al., 1996) and 60% of the general population who suffer from chronic neck pain (Manchikanti et al., 2002). In their double-blind studies, Barnsley (50 patients) and Manchikanti (160 patients) both used short term and long term anaesthetic blocks in the facet joints of patients and reported positive pain relief when both blocks reduced pain and the duration of pain relief was increased with the long term block. Similarly, Lord et al. (1996) used an

anesthetic block and a placebo in a double blind study with 68 patients. In 2006, Bogduk stated that "Facet joint pain is the single most common basis for chronic neck pain after whiplash. There are no data on how commonly chronic neck pain stems from muscles, ligaments, or discs." This author has not found any research that relates to the prevalence of chronic neck pain in other structures of the neck which would disagree with Bogduk's statement.

Two theories exist for the cause of facet joint injury; pinching of the synovial fold and excessive strain of the capsular ligament. In rear impact, pinching of the synovial fold is caused by a dynamic change of the vertebrae's axis of rotation during extension, which causes the posterior edge of the superior facet to contact the inferior surface and possibly trap the synovial fold (Yoganandan et al., 2002; Kaneoka et al., 1999). The synovial fold has been shown to contain nociceptive nerves (Inami et al., 2001), but no biomechanical evidence has shown that the synovial fold is loose enough to be pinched by the facet surfaces. Excessive strain in the capsular ligaments can be caused by the opening of the facet joint in extension or flexion, and shear can magnify this effect. Currently, the synovial fold is not modeled in the UW cervical spine model and the evidence to support its injury is not complete, so the focus on the facet joint will be excessive CL strain, which will be discussed subsequently.

Several authors have identified nociceptive nerve afferents capable of transmitting pain signals are present in the capsular ligament (Cavanaugh, 2000; Siegmund et al., 2009). Researchers have also been able to show that pain occurs when the facet joint is distracted in animal models. Lee et al. (2004b) was able to show that rats experienced pain up to 14 days after distraction of a facet joint by measuring paw withdrawals from a non-noxious stimulus. This showed that the rat was experiencing neck pain because the nerve that feeds the paw of rats was shown to be the same the feeds the capsular ligaments. Using a goat model, Lu et al. (2005) was able to measure the electrical impulses generated by nerves when the facet joint was distracted. They showed that local principal capsular strains of $46 \pm 17\%$ lead to high threshold nerve discharge, which they reasoned to be nociceptive pain signalling. In the rat model, isolated testing of rat capsular ligaments showed that a drop in force before the ultimate force (sub-catastrophic failure) occurred at strains of $23.1 \pm 9.3\%$ (Lee et al., 2006). The sub-catastrophic failure distraction agreed well with the distraction that caused behavioural sensitivities for up to 14 days in the rat, showing that sub-catastrophic failure of the capsular ligament is an indication of prolonged pain (Lee et al., 2004b; Quinn & Winkelstein, 2007).

The sub-catastrophic failure of human isolated facet joints from cadavers has been shown to range from $35 \pm 21\%$ (Siegmund et al., 2001) to $65 \pm 74\%$ (Winkelstein et al., 2000).

Using full cadavers and cervical spines, authors have shown that peak capsular strain in low speed rear impacts range from 28.5 to 39.9% (Panjabi et al., 1998b; Deng et al., 2000; Pearson et al., 2004). Deng used 6 cadavers in a series of 26 rear impacts, and measured the motion of each vertebra using a high speed X-ray to track implanted spheres and inferred a facet joint distraction. The strain results reported by Deng came from two tests at 5g and 6g, and have been scaled by a factor of Deng's initial gage length divided by CL lengths reported by Panjabi et al. (1998b). Panjabi et al. (1998b) used a specially designed spinal ligament transducer affixed across the facet joint to track joint distraction during rear impacts (2.5g to 10.5g) of four T1 to occipital cadaveric spines and divided the distraction by measured ligament lengths to get strain. Pearson et al. (2004) used a bench top sled with muscle force replication to impose rear impact loads (3.5g to 8g) on six occipital to T1 spine sections and measured vertebral motion by tracking marker flags using high speed cameras, and then inferred facet joint distraction that was divided by measured ligament lengths to get strain. Panjabi and Pearson also found that the peak physiologic CL strain ranged from 6.2 to 21.4% by applying a quasi-static extension moment of 1.0Nm and 1.5Nm respectively. They found that the peak strains in rear impact were above the physiologic strains, suggesting that injury is possible.

Ivancic et al. (2008) showed damage occurs to the CL in rear impact by showing the average elongation at 5N tensile force of rear impact exposed CLs was 0.9mm greater than control CLs. Their experiment involved testing isolated capsular ligaments from six cadaver spines (70.8 average age) that had been exposed to rear impact of up to 8g and six cadaver spines without any impact exposure (80.6 average age). They performed a two-factor ANOVA analysis to show that the average elongation increase of 0.9mm was statistically significant ($P<0.05$). This study suggests that some microscopic damage had occurred in the rear impact exposed CLs to reduce their mechanical strength despite no visual indication of damage being present.

4.3.2 Other Ligaments

To study the effect of whiplash exposure on the mechanical properties of ligaments, Tominaga et al. (2006a) dissected and tested the mechanical properties of the ALL, PLL, CL, LF, ISL, and middle third disc that had been exposed to 8g rear impact and compared their properties to control ligaments from a previous study. Their study used six control spines (80.6 average age) and six spines exposed

to whiplash using a bench-top sled with a surrogate head (70.8 average age). They showed that the average failure force of whiplash exposed ligaments compared to control ligaments was 149N vs. 186N, which was significantly different (P<0.05). This shows that some of the ligaments in the spine are being damaged altering their mechanical properties during an 8g rear impact. This paper did not compare the control vs. whiplash exposed specimens for each ligament or for each spinal level, which may have helped identify the ligaments being damaged and what spinal level is the most at risk.

The flexibility of cadaver cervical spines was measured by Pearson et al. (2005) before and after incremental frontal impact of 4, 6, 8, and 10g. A total of six cervical spines from three males and three females with average age of 71.3 years (range 54-87years) were used for the experiment. First, the spines were exposed to a non-injurious 2g frontal impact using a bench-top sled with muscle force replication. Then the baseline neutral zone and range of motion were measured by applying a 1.5Nm moment and recording the motion of each vertebra using markers and high-speed video. Next, the spines were exposed to a higher impact level and flexibility was measured again, which was repeated until all the impact levels were completed. They found that the flexibility of the spine was significantly increased over the baseline during an 8g impact (P<0.05) at the C6-C7 level, with up to 51.4% more flexibility. Following a 10g impact, significant flexibility increases were seen at every spinal level from C2-C3 to C7-T1. The increase in flexibility shows that damage is occurring to the soft tissues of the cervical spine, which can potentially include ligament injury.

Panjabi et al. (2004a) measured the dynamic strains of the PLL, CL, LF, and ISL during frontal impacts of 4, 6, 8, and 10g using a whole cervical spine on a bench-top sled with muscle force replication. The specimens used were the same ones used by Pearson et al. (2005). The dynamic strains were compared to physiologic limits, which were computed by applying 1.5Nm moment in both flexion and extension. This moment was shown to produce peak physiologic intervertebral rotations. They found that at a 4g impact the ISL and LF experienced significant (P<0.05) increases over the physiologic strains, and at 10g the CL experienced increases over the physiologic strains. The PLL strain did not exceed the physiologic limits in any test. At 10g frontal impact, the peak strains for the PLL, CL, LF, and ISL were 20.7, 36.1, 94.5, and 83.5% respectively. An increase in dynamic strain over physiologic limits indicates a possibility of ligament injury.

Recently, researchers have been using magnetic resonance imaging in an attempt to find lesions in the upper spinal ligaments which can be attributed to chronic whiplash pain. Several authors were not

successful in finding lesions, or found high-intensity signal fluctuations in a significant portion of non-injured volunteers reducing the clinical relevance of such structural changes (Roy et al., 2004; Pfirrmann et al., 2001; Wilmink & Patijn, 2001; Willauschus et al., 1995). Krakenes & Kaale (2006) have defined an imaging protocol for the craniovertebral junction that uses high spatial resolution with good contrast and 2mm thick sections to successfully indentify lesions to the alar ligament, tectorial membrane, posterior atlanto-occipital membrane (PAOM), and transverse ligament. Their study examined 92 whiplash patients (mean age 40years; range 14–61 years) and 30 control volunteers without neck injury (mean age 46 years; range 28–66 years). They used three radiologists blinded to the injury status of the patients to inspect the MRI reports and found interobserver kappa values of 0.41 to 0.82, depending on the observers and the ligaments being inspected, which represents a moderate to good agreement. The authors created a grading scheme which assigned a value of 0 or 1 if the ligaments were normal or had minor lesions and a grading of 2 or 3 for high-grade lesions. They were able to show that whiplash patients had more high-grade signal changes than the control group (66.3% vs. 6.7% for the alar ligament) suggesting that their MRI protocol is a useful tool in predicting injury in the upper cervical spine (Table 4-2). Krakenes & Kaale also provided questionnaires to the whiplash group asking them if their head was rotated at the moment of impact and if they were involved in a frontal or rear-end impact. They found significantly more high-grade (2 and 3) alar ligament lesions among those with rotated head position than among those with neutral head position (85.1% vs. 46.7%, $P < 0.001$) (Table 4-2). High-grade changes were significantly more common in frontal than in rear-end collision for the transverse ligament (61.1% vs. 10.5%, $P<0.001$) and atlanto-occipital membrane (37.1% vs. 5.3%, $P<0.001$) (Table 4-2).

Table 4-2: Percentage of patients with high-grade (grade 2 or 3) signal changes in MRI study by Krakenes & Kaale (2006).

	Control Group (n=30)	WAD Group (n=92)	WAD Group (n=92)			
			Neutral Head Position (n=45)	Rotated Head Position (n=47)	Frontal Impact (n=54)	Rear Impact (n=38)
Alar Ligaments	6.7%	66.3%	46.7%	85.1%	72.2%	57.9%
Transverse Ligament	20%	40.2%	27.8%	42.5%	61.1%	10.5%
Tectorial Membrane	0%	17.4%	17.8%	17.0%	22.2%	10.5%
PAOM	3.4%	24.0%	22.2%	25.5%	37.0%	5.3%

Jónsson et al. (1991) studied 22 cervical spines from traffic accident victims with fatal craniocerebral injuries (19 male, 3 female, mean age 26 years) and found 77 facet joint or ligament flavum lesions and 22 disc lesions. During aggressive impacts, Clemens & Burow (1972) found ligament and intervertebral disc damage to cadavers that had been exposed to frontal and rear impacts. They used 53 human torsos with average age of 70years (range 50-90years), which were separated at T10, attached to a rigid plate, and dropped with a controlled deceleration. In frontal impacts up to 38g, they found that 80% of the cadavers had disc damage, 75% had vertebral fractures, 50% had CL ruptures, 40% had LF ruptures, and 35% had PLL or ALL ruptures. The lower, middle, and upper cervical spines experienced 46.7, 14.1, and 21.2% of the injuries respectively in frontal impact. In rear impact up to 16g without headrests, 90% of the cadavers had disc injury, 80% had ALL ruptures, 40% had CL ruptures, 30% had vertebral fractures, 10% had LF ruptures, and 10% had PLL ruptures. The majority of injuries in rear impact occurred at the C56 and C67 vertebral levels. Although the impact levels in these studies are severe, they show that the ligaments and disc are susceptible to injury in automotive accidents.

4.3.3 Vertebral Discs

In a clinical MRI study of whiplash patients, Petterson et al. (1997) found that 33% of patients had moderate to severe disc herniations. They used a group of 39 patients (20men, 19 women, mean age 32 years, range 18-52 years) who had been admitted to a hospital within 24 hours after a car accident.

They found that five of the six patients with severe disc herniations had persistent symptoms up to two years after the accident, and they concluded that these symptoms related to impingement of the medulla oblongata (inferior portion of the brain stem, which is continuous with the spinal cord). In the two year study, the authors were not able to show decreased MRI signal intensity of the disk, which would be an indication of disc degeneration. The study shows that disc herniations are a plausible cause of whiplash symptoms, but failed to show that disc degeneration occurs as a result of whiplash injury.

The Biomechanics Research Laboratory at Yale University used a bench-top sled with muscle force replication to expose fresh-frozen cervical spines to frontal and rear impact loads to study the response of the disc (Panjabi et al., 2004b; Ito et al., 2005). Ito et al. exposed six spines (mean age 71.3, range 54-87 years) to frontal impact and inferred the disc response using high speed cameras to track vertebral motion. Panjabi et al. used the same method to measure the response of the discs in rear impact of six spines (mean age 70.8 years, SD 11 years). Before exposing the spines to impacts, both authors applied 1.5Nm flexion and extension moment to define the physiologic deformations of the disc. In frontal impact, the annular tissue strain at C2-C3 significantly ($P<0.05$) exceeded physiologic limits during a 6g impact and spread to all spinal levels (except C4-C5) at 10g, and the disc shear strain exceeded physiologic limits beginning at 4g at C2-C3 and all spinal levels except C4-C5 at 10g. The peak annular strains recorded were 43.1% (C2-C3) and 29.6% (C5-C6) and the peak shear stains were 0.9 and 1 radians at C2-C3 during a 6g and 8g impacts respectively. During rear impact, the annular strains were significantly ($P<0.05$) greater than the physiologic limits starting at 3.5g and spread to all levels except for C2-C3 at 5g, with the greatest strain of 51.4% during an 8g impact. The disc shear strains in rear impact exceeded ($P<0.05$) physiologic limits in the C5-C6 disc at 3.5g and spread to all levels at 8g, with a peak shear strain of 1 radian during the 8g impact. These authors found that the disc may be a location of injury during car crashes because strains exceeded the physiologic limit. They also showed that the annular tissue of the disk is potentially injured at a lower impact level for rear impact compared to frontal impact (3.5g vs. 6g) and that the spinal level with the highest risk for frontal impact is C2-C3, compared to C5-C6 for rear impact.

4.3.4 Vertebral Artery

The vertebral artery supplies blood to the head, brain, and neck. It enters the neck at the C6 and runs superiorly in the transverse foramen up to C1, where it exits along the posterior arch and enters the

skull (Gray, 1918). Several authors have hypothesized that the vertebral artery could be injured in coupled extension and axial rotation (Siegmund et al., 2009). These authors have proposed that the stretching of the vertebral artery will cause decreased blood flow rates due to Poison's effect contraction of the vessel diameter and stretching or pinching of the artery along its course can cause damage. Compromised blood supply to the brain may cause whiplash-related symptoms such as headache, dizziness, and vertigo.

Cadaveric neck models with muscle force replication have been used to investigate the elongation of the vertebral artery in frontal, side, rear, and head-turned rear impact (Carlson et al., 2007; Ivancic et al., 2006). The authors used 6 spines for each impact direction, with average ages of 71.3, 82.5, 70.8, and 80.2years for frontal, side, rear, and hear turned rear impacts respectively. The vertebral artery elongation was measured using a custom transducer that ran along the anatomical path of the artery. Physiological elongations were measured by applying 1.5Nm, 3Nm, and 1.5Nm moments in flexion-extension, axial rotation, and lateral bending respectively. The peak physiologic elongation was significantly exceeded in a side impact (P<0.05) starting at 6.5g and a head-turned rear impact at 5g. During frontal and rear impacts with the head looking forward, peak physiologic elongations were not exceeded. The peak physiologic elongation for looking forward frontal and rear impact was 8.1mm compared to 17.4mm and 30.5mm for side impact (8g) and head-turned rear impact (6.5g) respectively.

The scope of this thesis is frontal and rear impacts with the occupant in position. Vertebral artery elongation has only been shown to exceed physiologic limits in side and head-turned rear impact. There is insufficient evidence that vertebral artery injury will cause compromised blood flow rate for a significant amount of time (>3 months), so its influence on chronic whiplash is unknown. Also, this hypothesis does not explain the principle whiplash symptom, neck pain. For these reasons, the vertebral artery will not be investigated further in this thesis.

4.3.5 Dorsal Root Ganglion and Dorsal Root

The cervical spinal nerve roots stem from several rootlets that protrude from the anterior and posterior surfaces of the spinal cord and combine at each spinal level to form the posterior (dorsal) and anterior (ventral) nerve roots (Taylor et al., 1998; Gray, 1918). At each spinal level, the nerve roots extend antero-laterally through the intervertebral foramen where they proceed inferiorly into the periphery to innervate structures outside the spinal column. The intervertebral foramen is the space bounded by the

articular pillars, pedicles, and vertebral bodies of two adjacent vertebrae. There are two dorsal roots at each spinal level that combine into the dorsal root ganglion (DRG). The nerve roots are not enclosed by a thick epineurial sheath, as the peripheral nerves, which potentially exposes nerve roots to increased risk of injury when loaded (Siegmund et al., 2009).

Researchers have proposed two methods that the dorsal nerve roots and ganglion can be injured in automotive impacts. Pressure changes in the spinal canal during rapid motion put a pressure load on the nerves and narrowing of the intervertebral foramen apply mechanical load on the nerves (Siegmund et al., 2009).

The volume of the spinal canal changes when the neck goes into flexion, extension, or lateral bending, and during physiologic motion blood flow into or out of the venous plexa can maintain a constant pressure in the spinal canal (Siegmund et al., 2009). During dynamic loads caused by car crashes, it has been proposed that the inertial resistance of blood flow causes transient pressure gradients in the spinal canal, which can apply pressure to nerve roots and the DRG, potentially causing whiplash symptoms (Aldman, 1986).

Using anesthetized pigs, a group of Swedish researchers were able to show that dynamic pressure gradients existed in the spinal canal during whiplash motions (flexion, extension, and lateral bending) (Svensson et al., 2000). In these tests, the anaesthetized pigs were lying on their side, and their head was strapped to a plate, which was pulled in the anterior, posterior, or lateral direction. The magnitude of force varied from 150 to 900N, and the duration of force application was approximately 200ms. During the tests, the pressure in the spinal column was measured using a catheter transducer implanted into the vertebral foramen. Using Evans Blue dye, a histopathological investigation of the DRG from the pigs showed nerve cell membrane dysfunction in the pigs exposed to a dynamic 600N force, but not in pigs with a quasi-static 600N force or sham-exposed controls. The peak pressure presented was 130mmHg, which occurred at the C4 during an extension motion.

The same group of researchers was able to show similar pressure measurements in cadavers exposed to rear impact (Eichberger et al., 2000). They used a sled with a Volkswagen seat to expose four cadavers (mean age 65 years; range 30-87 years) to 28 rear impacts (mean 11g; range 4.6-15.2g). The pressure inside the spinal canal was measured using two small transducers inserted into the canal. A peak pressure of 200mmHg was measured at approximately the C4. These results compared well with

the measurements taken in pigs. The researchers were not able to show if nerve tissue damage had occurred, because they did not perform a histological investigation of the DRG.

In a separate study, Taylor et al., (1998) was able to show the dorsal root ganglion can be injured during rapid extension motion. They showed neural tissue disruption in 15 of 109 cervical spines from victims of fatal blunt force trauma to the face. The cervical spines from the victims were frozen, sectioned into 2.5mm transverse slices, and then examined under a microscope. The 15 spines with neural tissue disruption were confirmed using a histological examination. The most common location of injury was C4 (8 of 44 injured DRGs), followed by C7 (8) and C3/C6 (7 each). Although this study showed the DRG can be injured during rapid extension motion, these loads are not representative of non-fatal rear impacts.

To investigate the narrowing of the intervertebral foramen during rear impact and head turned rear impact, cadaveric neck models with muscle force replication have been used (Tominaga et al., 2006b; Panjabi et al., 2006). The authors used 6 spines each with an average age of 70.8 and 80.2 years for rear impact and head-turned rear impact respectively. The motion of each vertebra was tracked using opaque markers and the motion of six points around the vertebral foramen was inferred. They found that the peak foramen narrowing was 1.8mm during an 8g head-turned rear impact. It was shown that this narrowing was significantly (P<0.05) above a baseline measurement taken at 2g, but no effort was made to deduce if this amount of narrowing could cause neural tissue damage. They did conclude that the lower cervical spine, especially C5-C6 and C6-C7 are at the highest risk of DRG damage due to intervertebral foramen narrowing.

The DRG structures are not included in the current UW cervical spine model. Therefore, despite biomechanical evidence that supports these structures as a possible source of whiplash symptoms, this mechanism of injury will not be investigated further in this thesis. It should also be noted that injury to the DRG would produce radicular pain symptoms and as discussed in section 4.2 these symptoms are not the focus of this thesis. This could be an area of future development.

4.3.6 Muscle

Muscle tissue can be injured when undergoing eccentric-contraction, which is muscle lengthening during contractive activation (Garrett, 1996). Brault et al. (2000) showed that the sternocleidomastoid was stretching while active using EMG measurements of 42 volunteers exposed to rear-impact loads. Vasavada et al. (2007) used a biomechanical model of a human spine, which had EMG data and

kinematic data from volunteers tests imposed onto the T1 and skull in rear-impact, to measure muscle strain. During muscle activation, they found average (SD) sternocleidomastoid strains of 7% (5), 21% (14) for the splenius capitis, 18% (16) for semispinalis capitis, and 5% (4) for the trapezius. The cervical muscle strains measured in this study exceed the previously-reported injury threshold of 5 to 20% (Macpherson et al., 1996; McCully & Faulkner, 1985). However, there is a lack of evidence to support direct muscle injury can cause long-term (>3 months) whiplash symptoms.

In a clinical study of 25 whiplash patients, Scott & Sanderson (2002) measured the serum creatine kinase levels in their muscle tissue, which is a measurement of muscle tissue injury. They found that 2 of 25 patients had increased levels of serum creatine kinase indicating muscle injury, but neither of these patients had symptoms beyond three months. In the eight patients that did experience symptoms beyond three months, none of them had increased levels of serum creatine kinase. They concluded that prolonged symptoms following whiplash injury cannot be explained by biochemically measurable muscle damage.

Muscle may still play a major role in whiplash injury in two ways; distribution and magnitude of forces in the neck, and altered muscle activation after injury may contribute to chronic pain (Siegmund et al., 2009). Researchers have shown that muscle activation in neck pain patients during exercise is different from non-injured controls (Nederhand et al., 2002; Falla et al., 2004). These researchers asked volunteers with and without chronic neck pain (>3 months of symptoms) caused by automotive rear impacts to perform upper body tasks and measured their neck muscle response using surface EMG. They found statistically different magnitudes of EMG signals and deactivations times amongst the two groups. However it remains unclear, whether muscle dysfunction is a cause or effect of pain or merely an associated correlation.

Biomechanical evidence of direct muscle injury as a cause of long term whiplash symptoms is not sufficient to warrant further investigation in this thesis. The role of muscle activation on strains in other structures that are possible sources of whiplash symptoms will be investigated. At this time, it is not possible to predict the altered neuromuscular control caused by automotive crash using a numerical neck model, so this mechanism of sustaining whiplash symptoms cannot be investigated.

4.4 Numerical Modeling of Whiplash Injuries

Several research groups have investigated whiplash using computational models of the cervical spine for automotive research. A summary of finite element models that were reviewed prior to the

construction of the UW cervical spine model is given elsewhere (Panzer, 2006, Chapter 5). In this section, literature covering the use of numerical models to predict whiplash injury has been reviewed. A summary of models reviewed is provided in Table 4-3. The table gives a brief overview of each model, the validated loadings, injuries studied, and references. Below, a summary of the findings from each model is discussed.

Using the TNO neck model, Stemper et al. (2005) studied the effect of spinal curvature on capsular ligament strains. Lordosis curvature of the spine can be described as concave on the posterior surface, and it is the normal curvature of a healthy individual. There are spinal conditions that can cause the spine to straighten or form a kyphosis curvature, which is concave on the anterior surface. The authors exposed their model to an impact with mean acceleration of 2.3g, and 2.6m/s velocity change. They found peak CL elongations of 1.9, 2.2, and 2.6mm in the normal, straight, and kyphosis initial postures respectively. These peak strains where in the lateral region of the C6-C7 capsular ligament for each initial posture. Therefore, they concluded that individuals with non-normal spinal curvature where at a higher risk for sustaining CL injury during a rear-impact, specifically in the lower cervical spine. In a separate study, Stemper et al. (2006) used the same model to predict elongations of the ALL during rear impact with up to 3.6m/s velocity change. The peak elongations measured were 2.6 and 3.8mm at the C5-C6 and C6-C7 spinal levels. These elongations correspond to 52 and 28% of failure distractions of those ligaments respectively. They found that these elongations occur 85ms into the impact, which is likely before head restraint contact. Therefore, they concluded that mitigation of whiplash injury may be achieved by minimizing head retraction early in the impact.

Tropiano et al. (2004) applied a 15g rear impact to the HUMOS full body model to study ligament strains and vertebral stresses in the cervical spine. They found that Von Mises stress in the bone did not exceed 15MPa, which is significantly below the injury levels reported in literature. The ALL experienced 30% engineering strain at C5-C6, and during the initial phase of upper cervical spine flexion the ISL at C2-C3 experienced 62% strain. These injuries approach or exceed published failure strains of those ligaments, which is likely due to the aggressive impact acceleration.

The effect of an active head restraint on CL strain and the neck injury criteria (NIC) was investigated using the THUMBS human body model (Kitagawa et al., 2008). They found that peak capsular strain was reduced from 26 to 8.5% with the use of an active head restraint during a 16g rear impact. The

NIC value was only reduced from 20 to 17. They concluded that the active head restraint was effective in reducing the risk of whiplash injury.

The ETH neck model with fluid structural interaction in the spinal canal was used to study the pressure in the spinal fluid during a 4g rear impact (Schmitt et al., 2003). They measured a peak pressure of 87mmHg at the C4 spinal level. The pressure measured was much lower than the average of 200mmHg measured in cadavers during approximately 11g rear impacts, but the difference is likely attributed to the different impact severities (Eichberger et al., 2000). The shape and timing of the pressure spike compared favourably with the cadaver study. Neither the cadaver study nor the numerical model where able to comment on the likely hood of DRG damage, but their results are similar to a study performed on pigs where nerve damage was identified (Svensson et al., 2000).

The models reviewed here all have their limitations. The TNO model does not use elements to represent the IVD and facet joints, but rather uses elastic constraints between the vertebrae to model these joints. This method is able to accurately predict global kinematics but cannot assess injury to the disc. Also, the TNO model is a multi-body model rather than a finite element model, which means the model cannot predict stress or strain in the vertebrae. Vertebral strain is essential for predicting bone fracture during severe impacts, which is a future direction for the UW cervical spine model. The HUMOS model was not validated for rear-impact, yet they present vertebra stress and ligament strains from a 15g rear impact. Both the HUMOS or THUMBS model have less than 80,000 elements for full body models and the UW cervical spine model has 108,000 elements for a neck model. The only model reviewed with active musculature was the ETH model, but they have only used that model to study one mechanism of whiplash. Compared to the UW cervical spine model, none of the models reviewed here have been validated to the same extent for kinematics or local tissue response, and they are not modeled with the same degree of detail.

Table 4-3: Summary of numerical cervical spine models used to study whiplash injury.

Model Name	Type	Description	Validated for	Injuries studied	References
TNO Neck Model	Multi-Body	Skull to T1 Vertebrae: Rigid, scanned from cadaver Ligaments: Piecewise linear springs Discs: 3D point restraint Facets: 1D point restraint Muscle: 68 passive pairs	Quasi-static facet response ALL response Rear impact	ALL strain Effect of posture of CL strain	Stemper et al., 2004 Stemper et al., 2005 Stemper et al., 2006
HUMOS	Finite Element	Full body 50th percentile male in seated position Approx. 50,000 elements Vertebrae: solid elastoplastic Ligaments: 1D non-linear springs Discs: solid elements, incompressible fluid for nucleus, linear elastic for annulus. Facets: two layers of solid elements with springs for CL. Muscles: Passive, non-linear springs for elastic properties, plus solid linear viscoelastic volumes.	Quasi-static segment response Frontal, oblique, and lateral impact.	Vertebral stresses Ligament strains	Behr et al., 2003 Tropiano et al., 2004
THUMS	Finite Element	Full body 50th percentile male in seated position Approx. 80,000 elements Vertebrae: linear elastic solids Ligaments: piece-wise linear discrete Facets: no cartilage, shell elements for CL Discs: Solid linear elastic Muscles: passive, 1D discrete	Quasi-static facet response Rear impact	CL strains and NIC Influence of active head restraints	Kitagawa et al., 2008 Kitagawa et al., 2006
ETH Neck Model	Finite Element with CFD of spinal canal	Skull to T1 Vertebrae: Rigid Ligaments, facets and discs modeled Muscles: 1D discrete, active Hill type Fluid representation of spinal canal	Rear-impact	Dynamic pressure spikes put the DRG at risk	Schmitt et al., 2003

Chapter 5

Model Validation

The UW cervical spine model has been previously validated at the segment level (Panzer, 2006; Panzer & Cronin, 2009). A spine segment consists of two adjacent vertebrae with the intervertebral disc and ligaments that connect them. In the segment level validations the lower vertebra was fixed, a quasi-static force or moment was applied to the upper vertebra, and the displacement or rotation of the upper vertebra was measured. The motion segments were validated in flexion, extension, lateral bending, axial rotation, tension, compression, and shear in the anterior, posterior, and lateral directions. The model agreed well with most of the experimental measures, but it was too lax in anterior and posterior shear. For full results see Panzer (2006).

In this chapter, the results of further model validation were presented. The model in tension without any musculature was compared to an experimental study that used cadaver spines. Next, the local response of the ligaments and the discs were compared to cadaver studies that used a bench-top sled that exposed cadaver spines to frontal and rear impact. Finally, the global kinematic response of the model was compared to full body sled tests involving cadavers and volunteers in frontal and rear impact at various severity levels.

5.1 Full Spine in Tension

The tensile response of the full ligamentous cervical spine model was validated against experimental results reported by Dibb et al. (2009). This is an important step in the validation of the whole cervical spine model because neck tension is often coupled with extension and flexion motion in both rear and frontal impact respectively. The researchers used a custom designed test fixture that allowed the skull to translate in the anterior-posterior direction and rotate in the sagittal plane about the centre of gravity (Figure 5-1). Their fixture measured the translation and rotation of the head as a hydraulic actuator applied a quasi-static tensile force up to 300N on the T1 in the inferior direction (Figure 5-1).
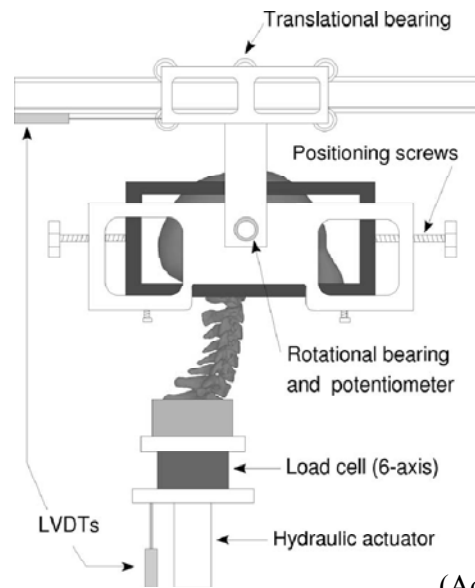
Figure 5-1: Experimental test fixture for quasi-static tensile loading of the cervical spine.

To model the experimental tests the musculature was removed and the T1 was oriented at 25° to the horizontal as per the tests. The head was constrained at the centre of gravity in all directions except for anterior-posterior translation and sagittal plane rotation. The location of the skull centre of gravity in the model was representative of how they located it in the experiments. The T1 was constrained in all directions except inferior-superior translation. A prescribed displacement was applied to the T1, and the tensile force was recorded along with the translation and rotation of the skull.

In tension, the inferior displacement of the T1 in the model agreed closely with the average response measured by Dibb et al. (2009) up to 100N (Figure 5-2). After 100N, the response of the model was slightly more lax but still remained within one standard deviation of the average cadaver response. The posterior displacement of the head in the model was slightly greater then measured experimentally, but did not deviate beyond one standard deviation of the average experimental results (Figure 5-3). For head rotation, the opposite was true as the head did not extend as much, but remained within one standard deviation of the average experimental results (Figure 5-4). Overall, the tensile response of the whole neck without musculature agreed excellently with the experimental tests by Dibb et al. (2009), because the responses always remained within one standard deviation of the experimental average.
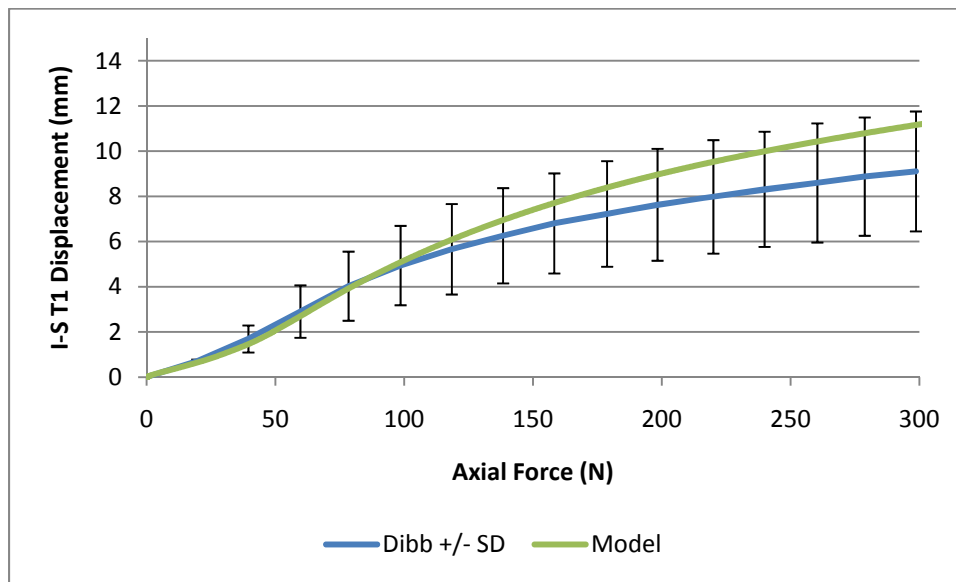
Figure 5-2: The T1 inferior-superior displacement of the model.

The inferior direction is positive.
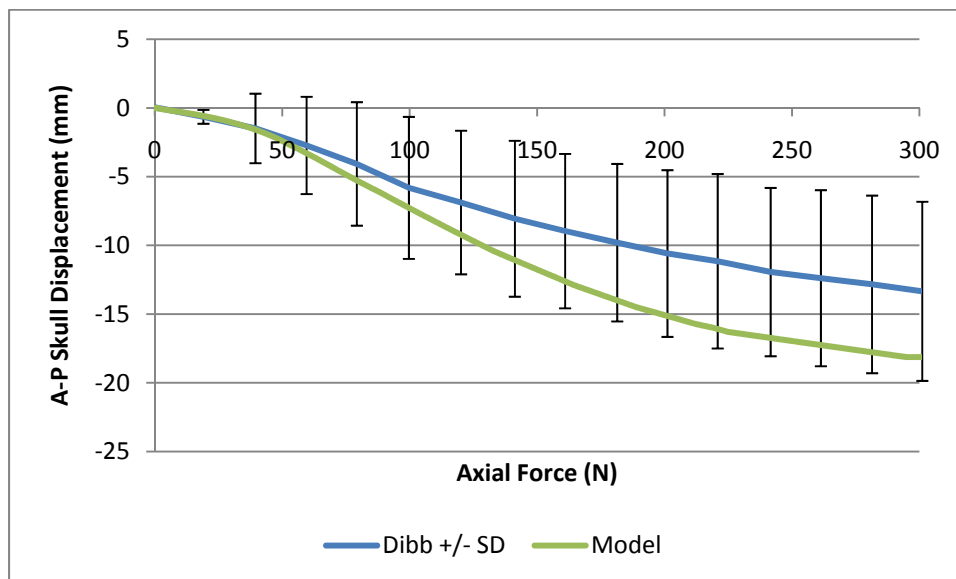
Figure 5-3: The skull anterior-posterior displacement of the model.

The anterior direction is positive.
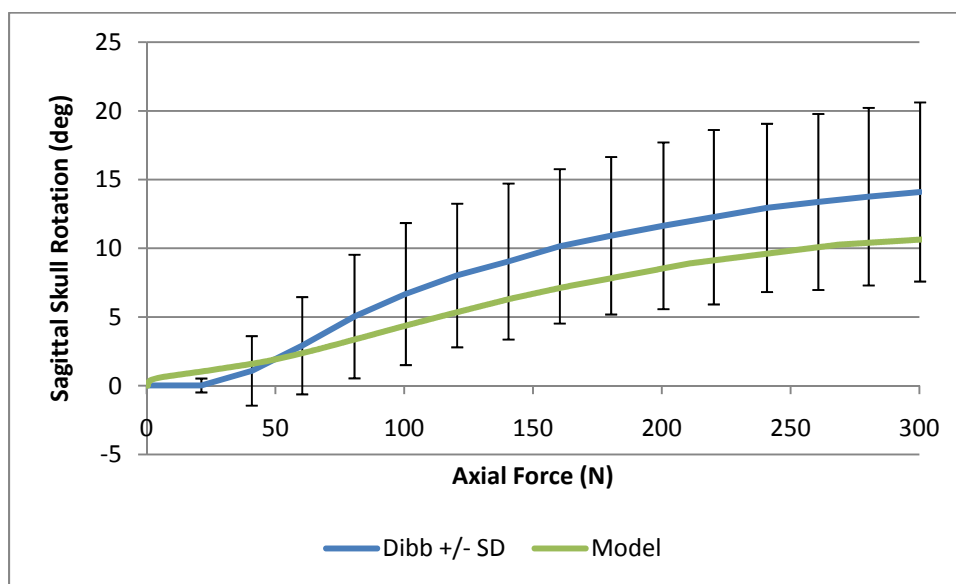
Figure 5-4: The sagittal plane head rotation of the model.
Extension is positive rotation.

5.2 Ligament and Disc Local Validation

The Biomechanics Research Laboratory at the Yale University of Medicine developed an in-vitro model of the cervical spine, which is able to measure tissue strains during simulated impacts (Figure 5-5; Ivancic et al., 2005). The results from these cadaver studies were used to validate ligament and disc strains predicted by the UW cervical spine model during an 8g frontal impact and 8g rear impact. Accurately predicting local soft tissue strains is essential to modeling whiplash injury.

The cadaver model of the cervical spine uses whole spines from T1 to C1 (Figure 5-5). The T1 was angled to preserve the natural posture of the spine and then potted in resin for attachment to the bench-top sled. Then a surrogate head with a mass of 3.3kg and 0.016 kg m^2 sagittal plane moment of inertia was affixed to the C1. The mass of the head was below reported values for a 50th percentile male, but the researchers wanted to avoid damaging the spines. Next, cables were added to model the passive response of anterior, posterior, and lateral spinal muscles. The cables ran through wire loops attached to each vertebra, and a pulley was installed at C4 for the anterior cables. At the base of the spine the cables were attached to springs, each with stiffness of 4N/mm. To model contact between the chin and the chest, a cable was installed between C0-C2, which limited flexion to in-vivo amounts. Finally, rods were installed in each vertebra, so that the rigid body motion of each vertebra

could be tracked using high-speed camera during each impact simulation. The soft tissue strains were calculated by inferring distractions based on the rigid body motion of the vertebrae. The head extension and intervertebral rotations of the cadaver model were compared to in-vivo volunteer studies during rear-impact (Ivancic et al., 2005). They found the head extension remained in the volunteer corridor for a 3.6g impact and the intervertebral rotations were either just above or within the 95% confidence interval of a volunteer during a 4.6g rear-impact.
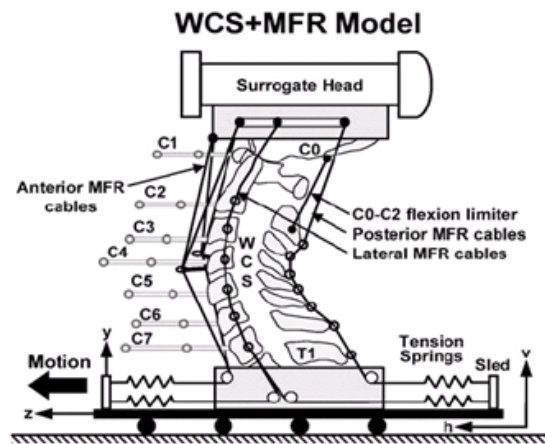
(Adapted from Ivancic et al., 2005)

Figure 5-5: The cadaver whole spine bench-top sled with muscle force replication.

The response of the UW cervical spine model was compared to the cadaver tests by applying the experimental T1 acceleration trace on the T1 of the model (Figure 5-6). The head was free to move in all directions, and the T1 was only allowed to move in the anterior-posterior direction. The mass and sagittal plane moment of inertia of the model were changed to reflect the values used in the experiments. Muscle activation was turned off to simulate the passive cable system used in the experiments. The ligament strains were calculated by dividing ligament distraction by the initial length. The disc shear strains were calculated by measuring the location of points on the inferior and superior surface of the disc as a function of time and then calculating shear strain using Equation 5-3, as per the experiments. The directions were relative to a coordinate system fixed to the lower vertebra, with the z direction aligned with the superior surface of the vertebral body and y was oriented superiorly. Delta z was the change in distance between two points in the z direction and y_0 was the distance between the two points in the neutral posture.
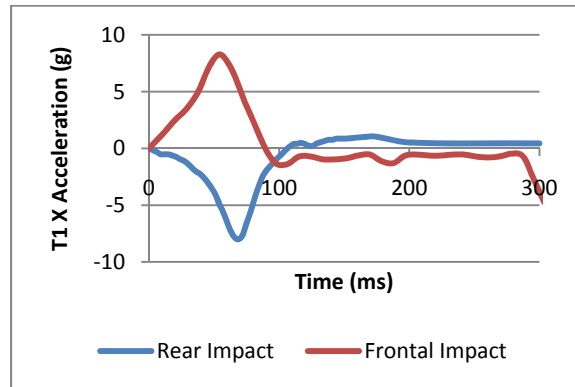
Figure 5-6: T1 acceleration profile for ligaments and disc validation in frontal and rear impact.

$$\gamma = arctan\left(\frac{\Delta z}{y_0}\right)$$

Equation 5-3

5.2.1 Frontal Impact

In frontal impact, the ligament strains predicted by the model during an 8g impact were compared to experimental results presented by Panjabi et al. (2004a). The model predicted within one standard deviation of the experimental average for 26 out of 30 locations measured (Figure 5-7). The model predicted below the error bars for the posterior aspect of the ISL at C3-C4 and the anterior ISL at C2-C3 and C5-C6. The only location where the strain predicted by the model exceeded the error bars was the anterior aspect of the C6-C7 CL. For several of the ligaments, the model was able to capture the trends between vertebral levels. Generally, the strains predicted by the model were below the experimental average reported by Panjabi et al. (2004a).
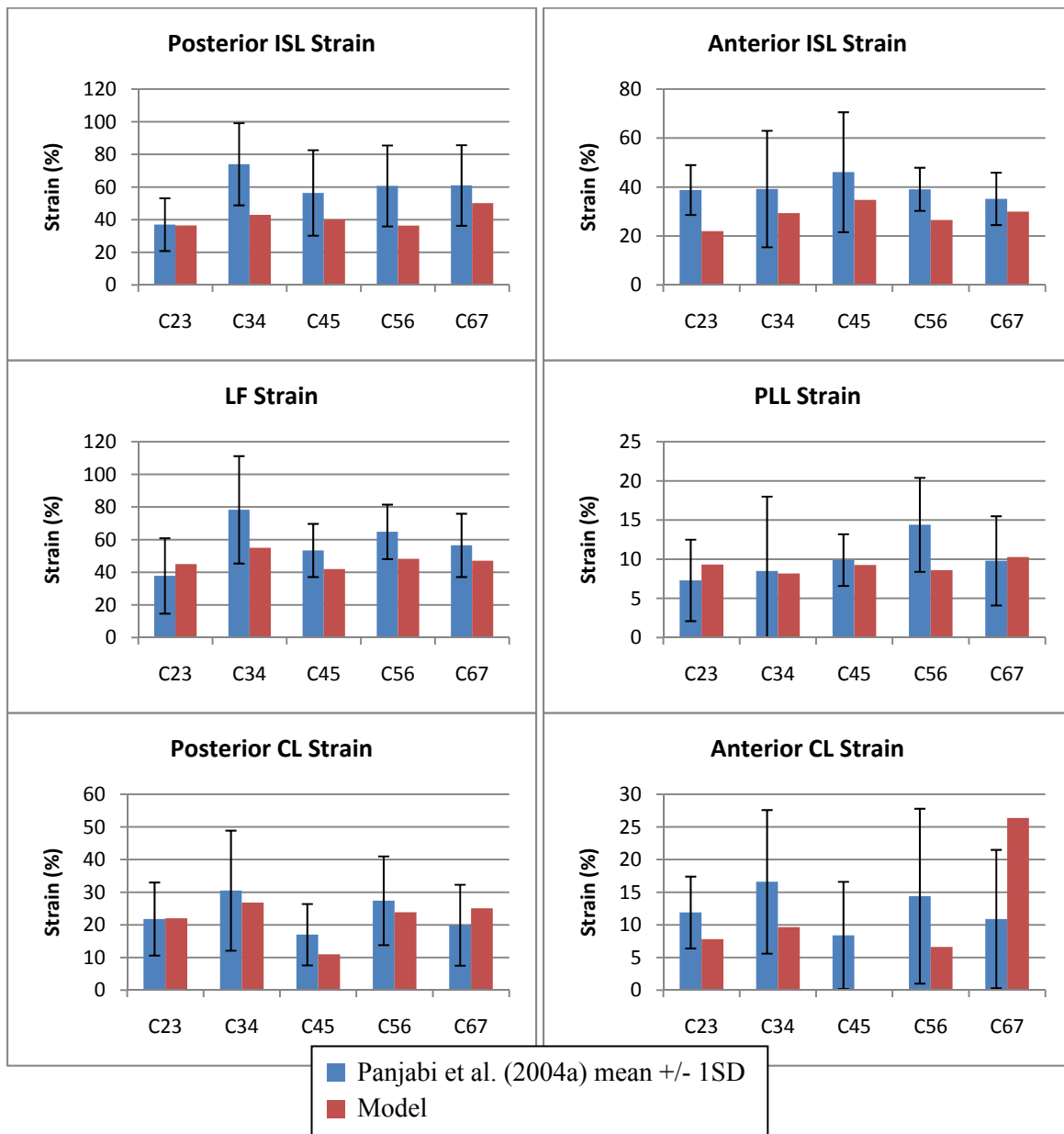
Figure 5-7: The peak ligament strains in the model during an 8g frontal impact.

The disc shear strains calculated from the model in an 8g frontal impact were compared to tests performed by Ito et al. (2005). The disc shear strains predicted by the model fell within one standard deviation of the experimental average for C3-C4 to C6-C7 in the anterior, middle, and posterior aspects of the disc (Figure 5-8). The disc shear strains in the model were well below the experimental error bars at C2-C3 for all locations in the disc.
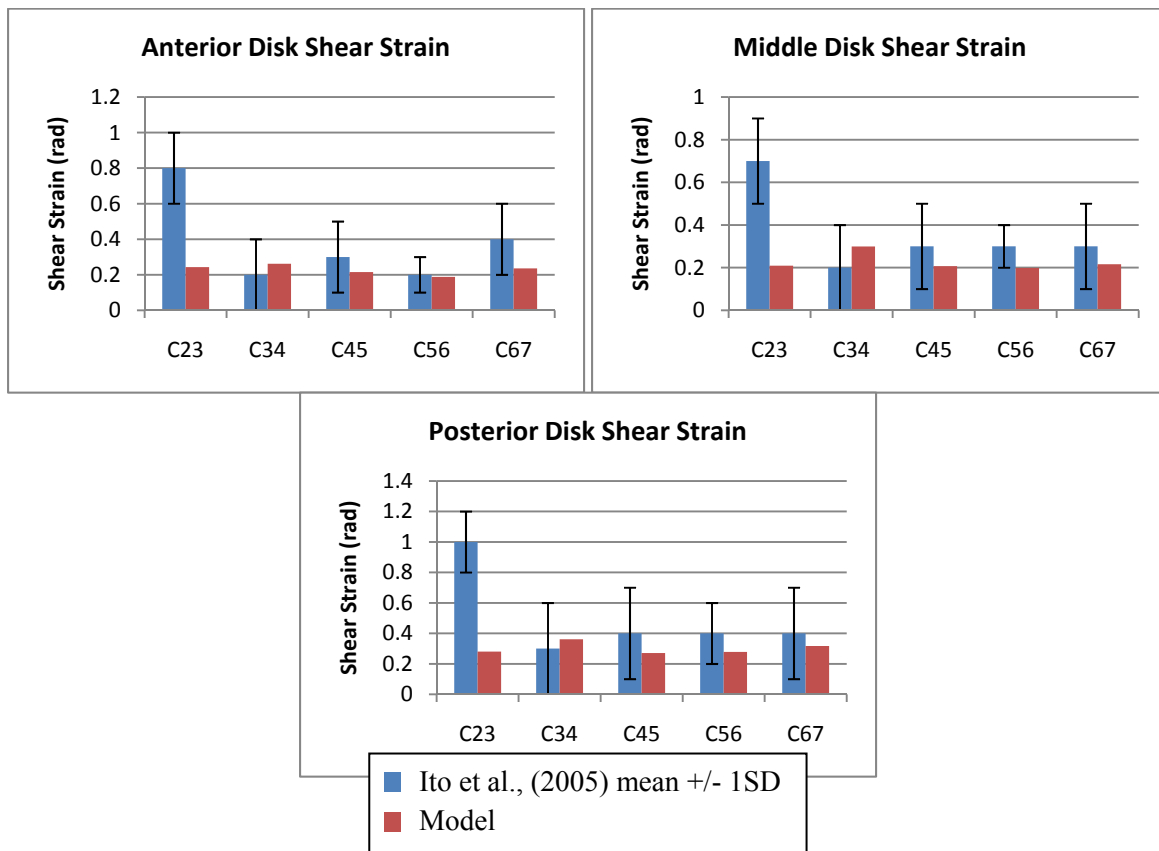
Figure 5-8: The peak disc shear strains in the model during an 8g frontal impact.
Anterior, middle, and posterior refer to the location were the strain measurement was taken.

5.2.2 Rear Impact

The response of the ALL in the model during an 8g rear impact was compared to a study by Ivancic et al. (2004), and CL strain response was compared to results by Pearson et al. (2004). The ALL strain in the model was within the one standard deviation error bars at all the vertebral levels except C4-C5 (Figure 5-9). CL strains calculated in the model were all within the error bars at every vertebral level. It should be noted that at the spinal levels C2-C3, C3-C4, and C6-C7 the CL strain in the model was just above or at the lower limit of the error bars.

Panjabi et al. (2004b) measured the disc shear strain during an 8g rear impact, which was used to validate the shear strain response of the discs in the UW cervical spine model. The disc shear strain was measured at the anterior, middle, and posterior aspects of each disc between C2-C3 to C6-C7. It was found that the shear strain measured in the model was within 1 SD of the experimental averages

for every spinal level except C5-C6 for each location of measurement (Figure 5-10). The shear strains measured in the model at C5-C6 were less than 50% of the average experimental values.
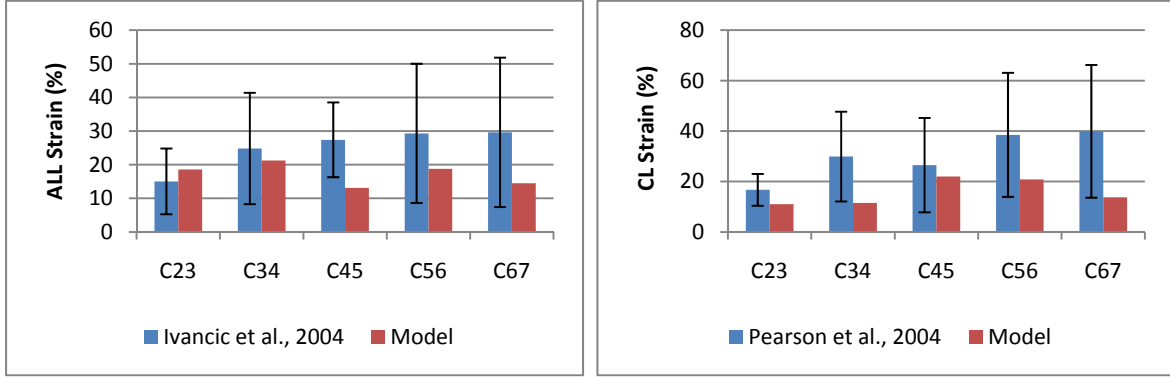
Figure 5-9: The peak ligament strains in the model during an 8g rear impact.

The experimental results are shown as mean +/- 1SD.
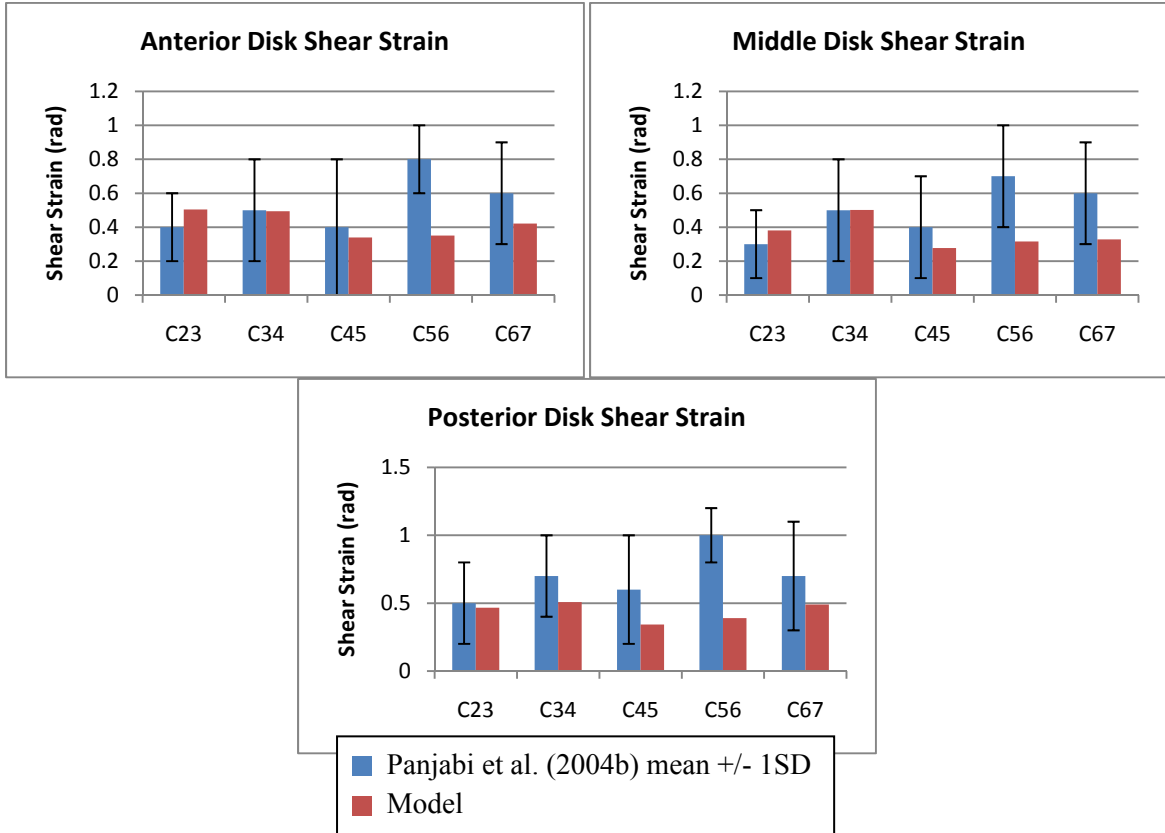
Figure 5-10: The peak disc shear strains in the model during an 8g rear impact.

Anterior, middle, and posterior refer to the location were the strain measurement was taken.

5.3 Global Kinematic Validation

Validating the global kinematic response of the model is an important aspect of producing a biofidelic human model. Accurate global response will provide further assurance that the local soft tissue strains predicted by the model are representative of in-vivo humans. In this chapter, the results of validating the model in frontal impact at 8 and 15g, and rear impact at 4 and 7g will be presented. The frontal 15g validation results have been presented previously (Panzer, 2006), but they will be presented again with the model modifications outlined in Chapter 2 included.

Muscle activation is critical for a cervical spine model to evaluate the response of a human subject (Brolin et al., 2005; Panzer, 2006). Studies have found that flexor and extensor muscles activate at approximately the same time during an impact, and that EMG signals start at 60 to 79ms after impact initiation (Siegmund et al., 2003; Ono et al., 1997; Roberts et al., 2002; Szabo and Welcher, 1996). For live human simulations, both the flexors and extensors in the model were excited 74ms after impact and remained active for 100ms (Siegmund et al., 2003). Muscle activation was included for both frontal impact cases and the 4g rear-impact, but not for the 7g rear-impact which was based on a PMHS study.

5.3.1 Frontal Impact

The Naval Biodynamics Laboratory (NBDL) performed a series of 39 frontal impacts on eight volunteers that were selected from a group of physically fit marines (Ewing et al., 1968, 1969; Thunnissen et al., 1995). The average weight and height of the volunteers were 73.2 kg and 173.6 cm, with standard deviations of 10.0 kg and 8.2 cm respectively. The volunteers sat in a rigid seat and were restrained with a wide belt strap and a standard aircraft shoulder restraint. These restraints ensured that the T1 did not move in the vertical direction, but Thunissen et al. (1995) showed that the T1 still rotated. The rigid seat was fixed to a 12" HYGE acceleration sled, which was accelerated backward from rest with a specified profile to simulate a frontal impact. Each volunteer was fitted with a gyroscope and accelerometers in the mouth, over the spinous process of the T1, and over the superior posterior aspect of the head (Figure 5-11). These instruments captured the acceleration and rotation of the T1 and head CG in the mid-sagittal plane and were confirmed using high-speed video to track markers on the accelerometers.

Figure 5-11: Volunteer instrumentation set-up for the NBDL frontal impacts.

The NBDL tests were simulated by applying the experimental T1 anterior-posterior acceleration and T1 rotational acceleration traces to the T1 of the UW cervical spine model (Figure 5-12). The T1 was constrained in all other directions and the head was free. Muscle activation was included to model live volunteers as discussed at the beginning of this chapter. The resulting linear and angular accelerations were measured at the centre of gravity of the head and compared to response corridors by Thunnissen et al. (1995).
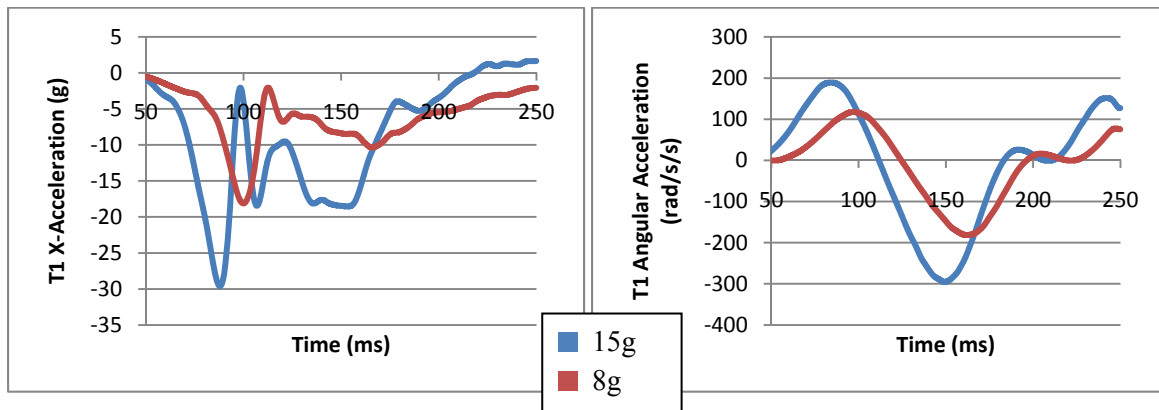
Figure 5-12: The T1 inputs for the NBDL validation cases (Thunnissen et al., 1995).

The time-lapse response of the model to an 8g frontal impact is shown in Figure 5-13. At 50ms, the head was beginning to move into flexion, with 1.1° of rotation at that time. From 50ms to 100ms, the

68

head reached a flexion angle of 6.5° which is relatively modest and the T1 displaced 30mm away from the head, meaning the neck was mostly loaded in anterior shear. Up to 150ms, the head continued to rotate in flexion and the neck was loaded in a combination of flexion and tension. The peak head rotation of 46.6° occurred at 180ms. After this time, the head and neck rebounded towards an upright position, but the neck did not rebound fully before the end of the simulation.
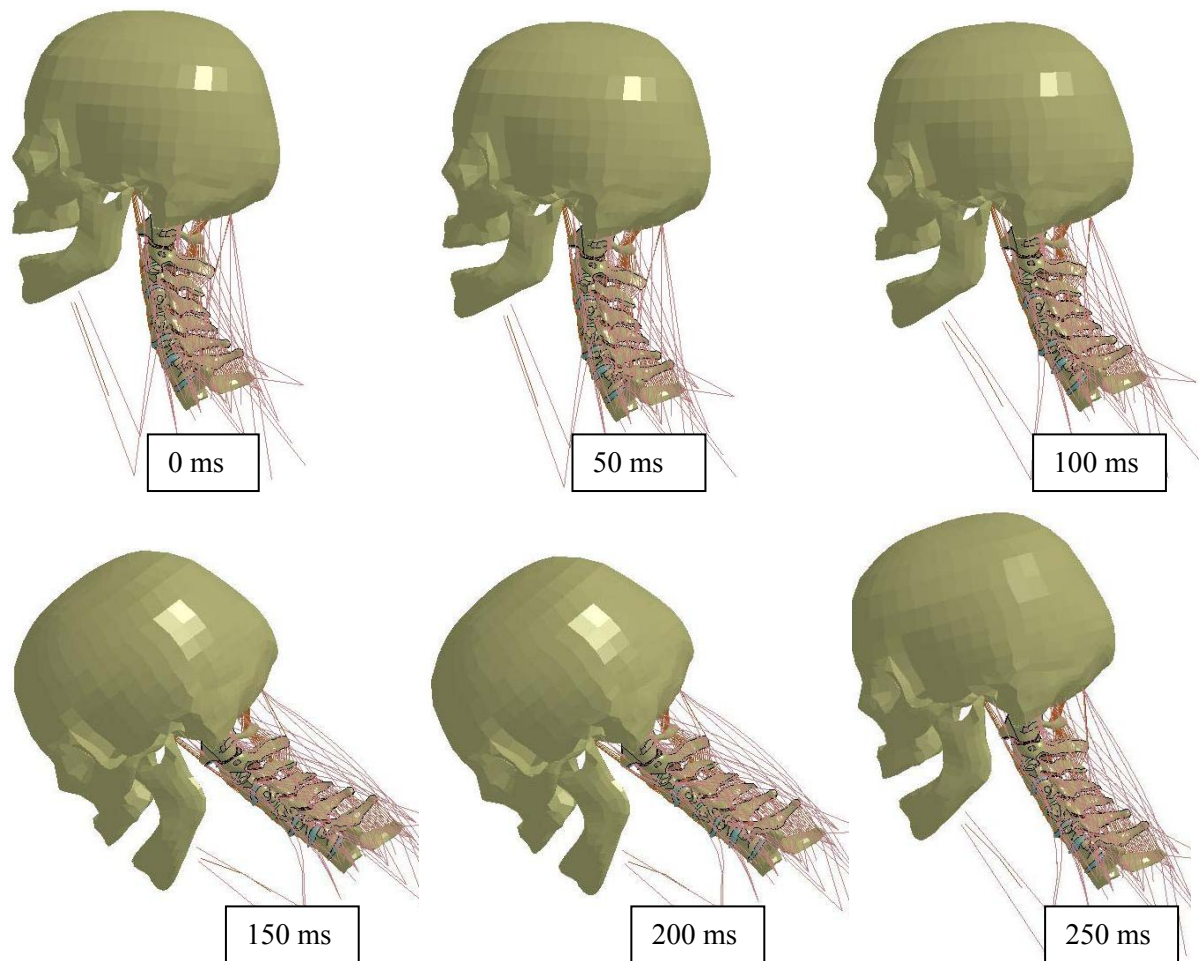
Figure 5-13: Time-lapsed response of the model to an 8g frontal impact.

The volunteer response corridors presented below represent an average plus minus one standard deviation of the tests performed at an 8g peak sled impact severity (Thunnissen et al., 1995). Overall, the posterior acceleration of the head CG was a representative shape and remained mostly in the volunteer corridor (Figure 5-14). The initial trough experienced by the model was of appropriate magnitude, but occurred approximately 6ms too early when compared to the volunteer corridor.

Similarly, the peak predicted by the model at 113ms was approximately 20ms too early. Finally, after 170ms the response of the model was predominantly linear, where as the volunteer corridor takes a more curved shape, resulting in the model coming out of the corridor.
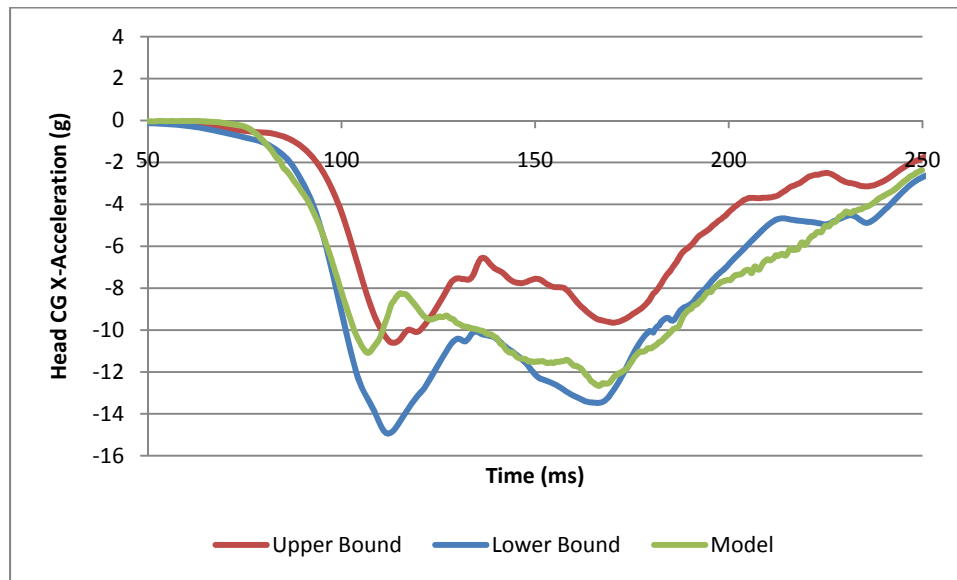
Figure 5-14: The head CG X-acceleration response of the model to an 8g frontal impact. Negative acceleration in the posterior direction.

The inferior-superior response of the head CG in the model was also a good to excellent fit with the volunteer corridor, because the shape was representative and the response did not deviate significantly from the corridor (Figure 5-15). The main deviation in response was at the trough that occurred at 120ms, which was approximately 20ms too early compared to the volunteer corridor. Other discrepancies in the response of the model included the oscillations at 85ms and the height and timing of the final peak.
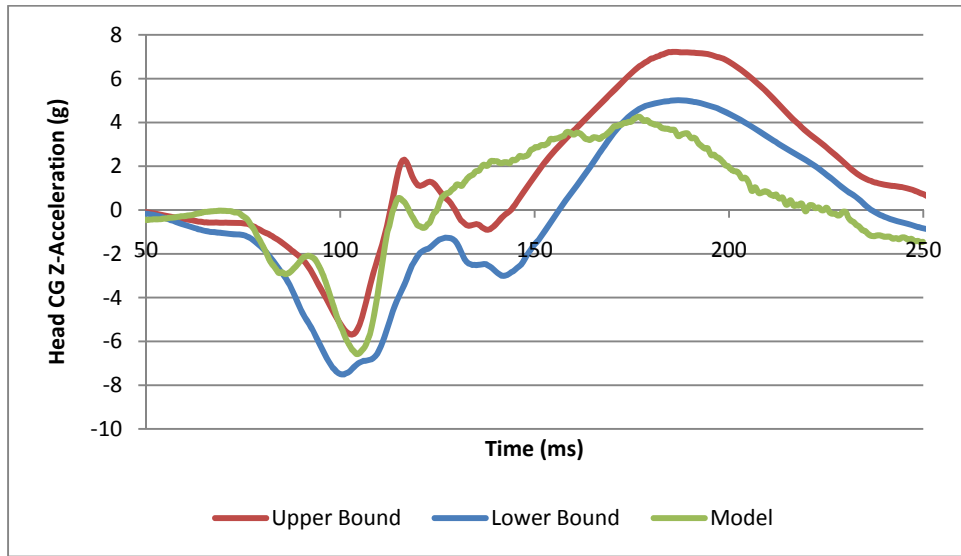
Figure 5-15: The head CG Z-acceleration response of the model to an 8g frontal impact. Positive acceleration in the superior direction.

The rotational acceleration of the head CG in the model was offset by approximately 10 to 15ms from the volunteer corridor (Figure 5-16). Other than that discrepancy, the model was an excellent fit with the volunteer corridor as the magnitude of the peaks and troughs and their relative timing was similar to the volunteer corridor.
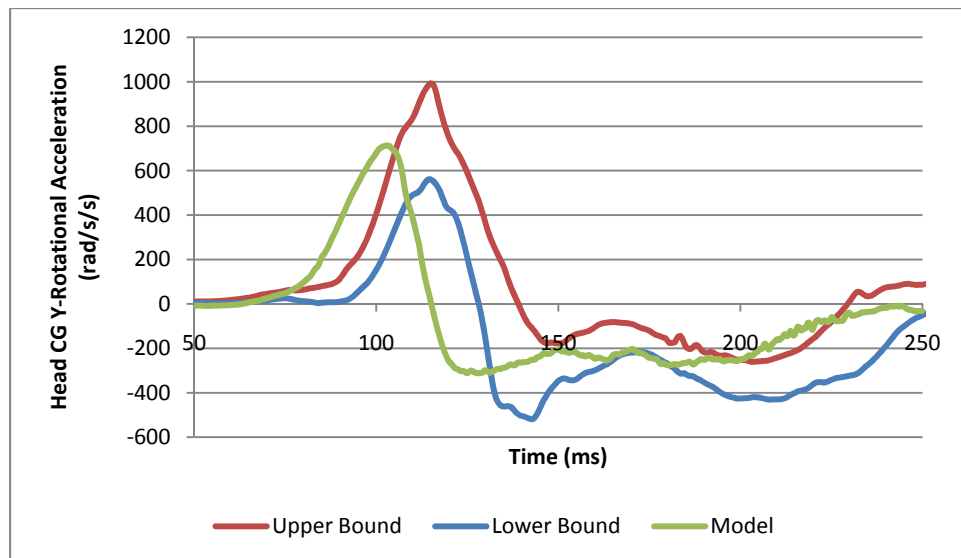
Figure 5-16: The head CG rotational acceleration response of the model to an 8g frontal impact. Flexion is positive acceleration.

For the 15g frontal impact, the head only rotated into a small flexion angle (1.2°) and the T1 moved less than 1mm away from the head 50ms into the simulation (Figure 5-17). The neck in the model also exhibited the same transition from anterior shear to combined tension and flexion, but in the 15g impact the transition occurred more rapidly. By 162ms, the head reached its maximum flexion angle of 93.6° and started to rebound. At the 15g impact severity the rebounded past the neutral posture into an extension angle of 7.8°.

| 0 ms | 50 ms | 100 ms |

| 150 ms | 200 ms | 250 ms |
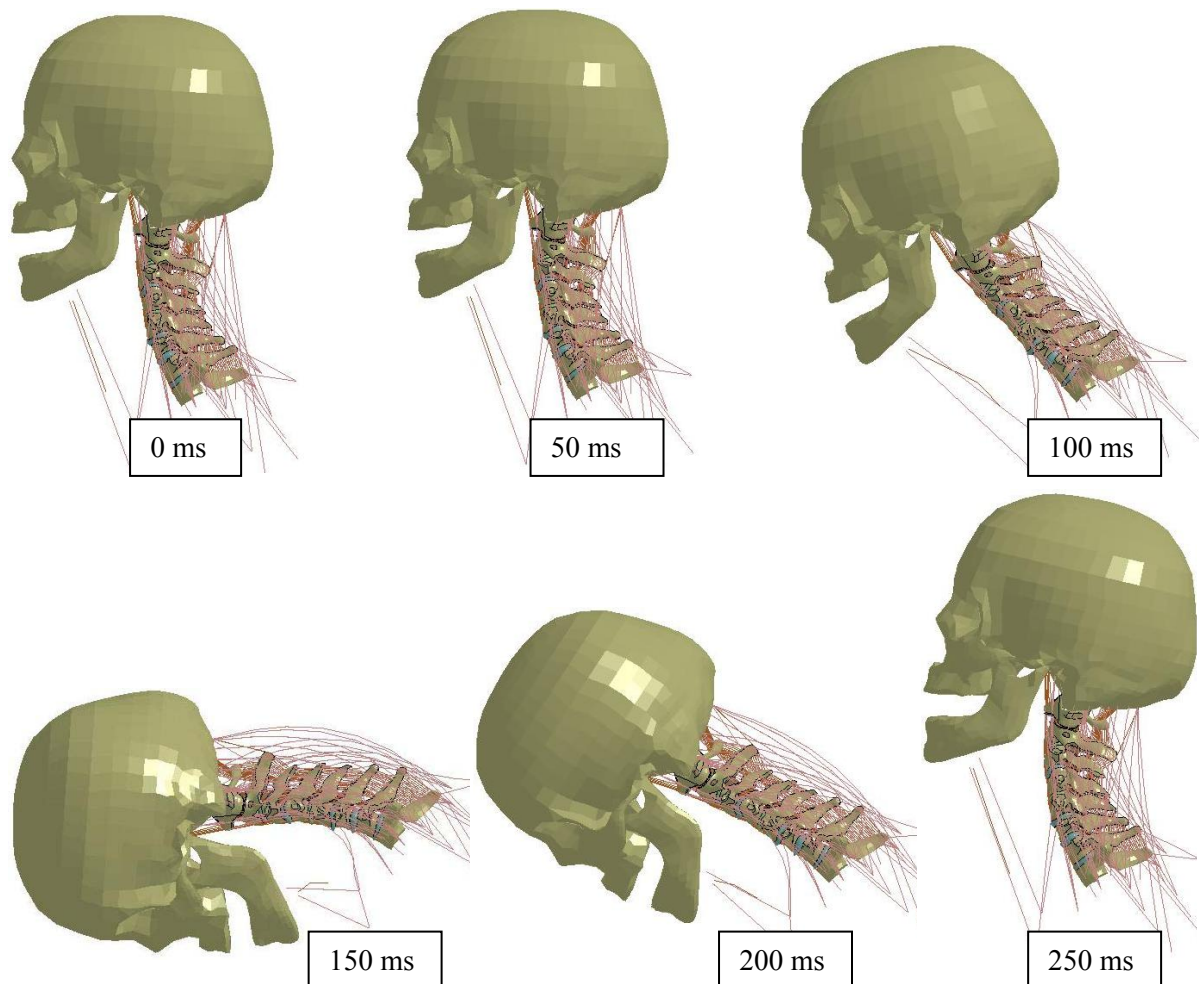
Figure 5-17: Time-lapsed response of the model to a 15g frontal impact.

In a 15g frontal impact, the posterior acceleration of the head CG in the model deviated from the mean plus minus one standard deviation volunteer corridor (Thunnissen et al., 1995), but was still a reasonably good fit (Figure 5-18). The initial trough experienced by the model occurred 3ms too early and was 3g less than the upper bound of the volunteer corridor. After that, the model experienced an

additional oscillation that was not seen in the volunteer response. From 120ms on, the response of the model had an accurate shape, but the acceleration dipped below the lower bound of the volunteer corridor between 165ms to 225ms.
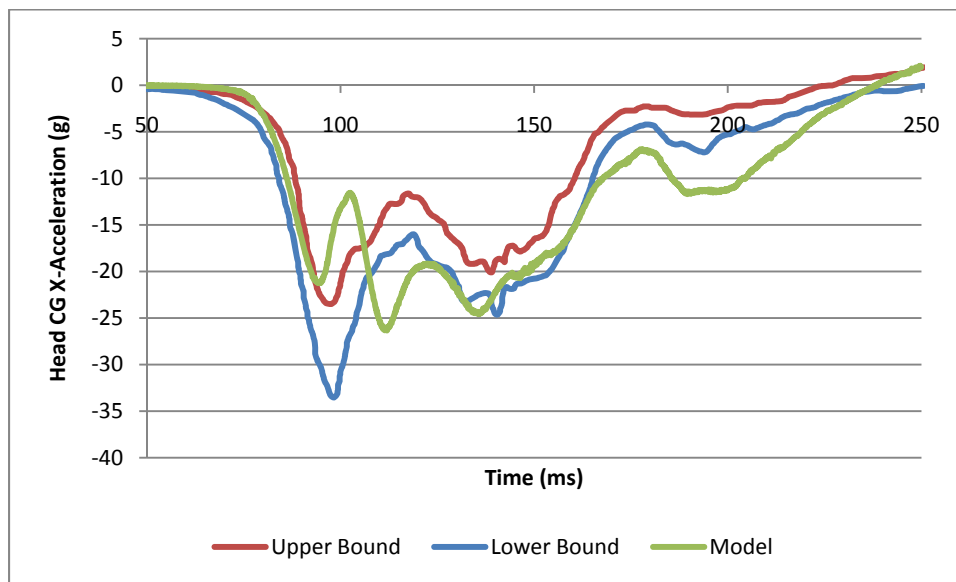
Figure 5-18: The head CG X-acceleration response of the model to a 15g frontal impact. Negative acceleration in the posterior direction.

The inferior-superior acceleration of the head in the model remained mostly within the volunteer corridor and the shape compared well with the corridor (Figure 5-19). The first two troughs in the response of the model were 3g and 1g respectively outside the lower bound of the volunteer corridor, and the second trough occurred 10ms late. In the last 50ms of the simulation, the response of the model dropped below the lower bound of the volunteer corridor.
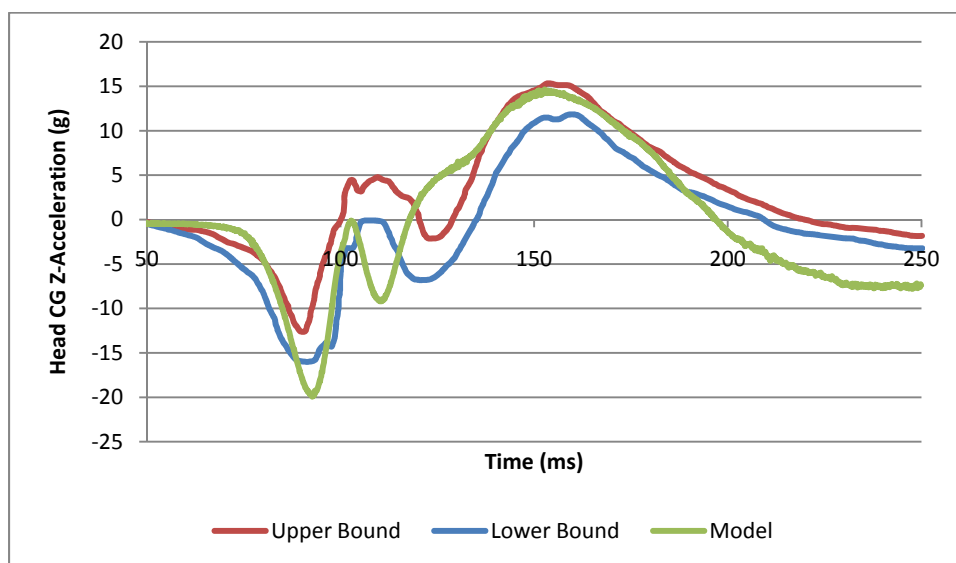
Figure 5-19: The head CG Z-acceleration response of the model to a 15g frontal impact. Positive acceleration in the superior direction.

There are two places where the rotational acceleration of the head CG in the model deviated from the volunteer corridor; the initial peak occurred approximately 5ms too early, and the model lacked a trough at 120ms (Figure 5-20). Despite these differences the model was still a good fit to the volunteer data.
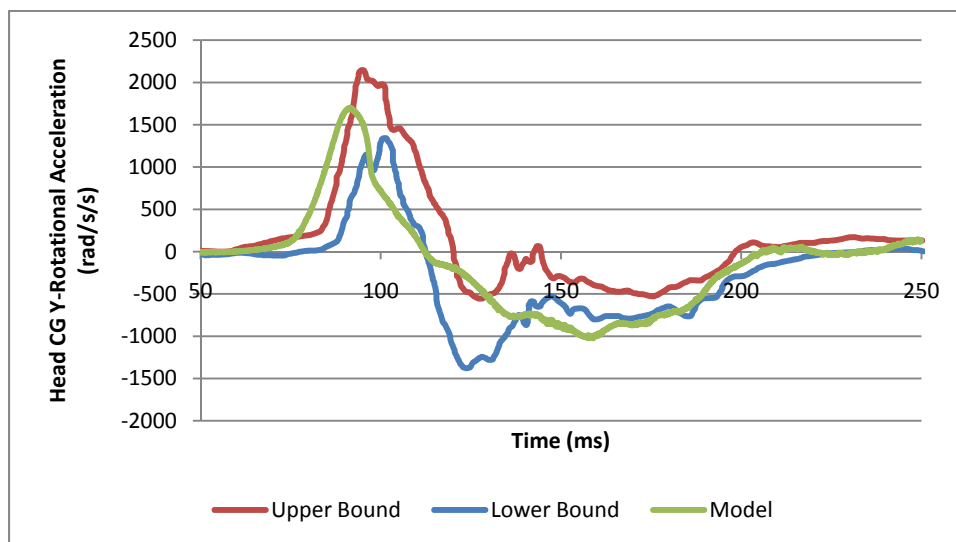
Figure 5-20: The head CG rotational acceleration response of the model to a 15g frontal impact. Flexion is positive acceleration.

5.3.2 Rear Impact

Davidsson et al. (1998) performed 28 rear impacts on thirteen human volunteers at speeds between 5 and 7kph with an average peak acceleration of 3.6g. The test involved the collision of a bullet sled with a stationary target sled, which seated a volunteer on a laboratory seat with a headrest. The laboratory seat consisted of four foam covered back support panels and a head rest attached with springs to two rigid frame rails that were mounted to a 1995 Volvo 850 seat base (Figure 5-21). For the headrest, the stiffness of the springs was 7.0kN/m, the foam was 40mm thick, and the panel weighed 0.659kg. The seat was designed so that it could be easily implemented in computer simulations. The volunteers were fitted with head strap mounted accelerometers and a rotational rate sensor to capture the kinematics of the head. The acceleration and rotation of the T1 was captured using an accelerometer and rotational sensor mounted over the skin.
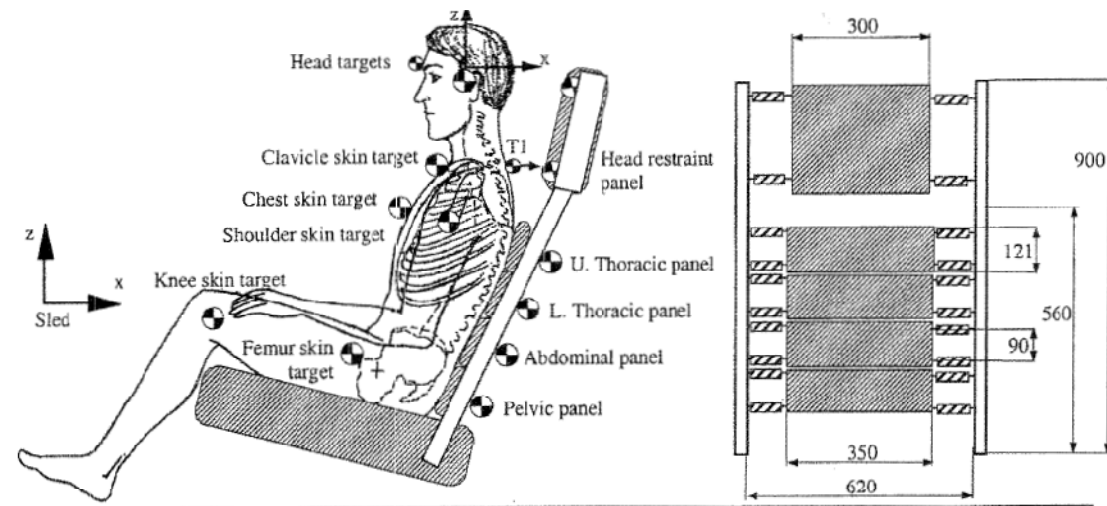
(Adapted from Davidsson et al., 1998)

Figure 5-21: The laboratory seat used by Davidsson et al. (1998).

To model these rear impacts, the average T1 accelerations in the inferior-superior and anterior-posterior directions, along with the sagittal plane rotation were input onto the cervical spine model T1 as prescribed motion constraints (Figure 5-22). The T1 of the model was constrained in all other directions, and the head was not constrained. To model the headrest, the average sled anterior acceleration was input as prescribed motion to the frame attachment points of the springs (Figure 5-22; Figure 5-23). The headrest material properties were non-linear viscoelastic based on automotive seat cushion material tested at UW and the stiff backing was assumed to be pine with orthotropic elastic material properties (Green et al., 1999; Campbell & Cronin, 2007). The mass of the headrest

75

and stiffness of the springs were input using values provided by Davidsson et al. (1998). The headrest was initially positioned 86mm away from the skull, which was the average value used in the experiments. Muscle activation was included for validation against Davidsson et al. (1998) to mimic the behaviour of volunteers.
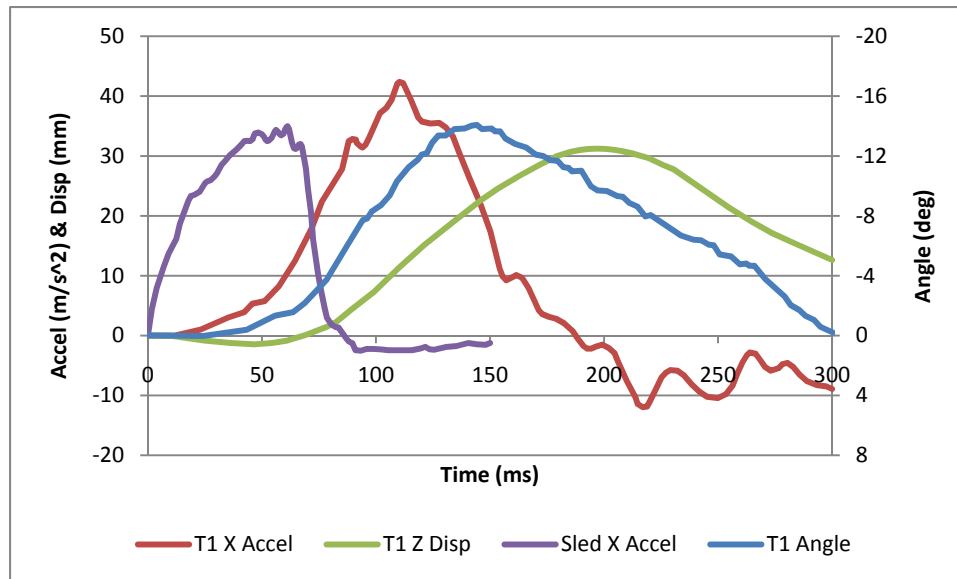
Figure 5-22: The T1 and head rest inputs for the 4g rear-impact simulation.

(Davidsson et al., 1998). The X acceleration is positive in the anterior direction, Z is positive in the superior direction, and the angle is positive in extension.
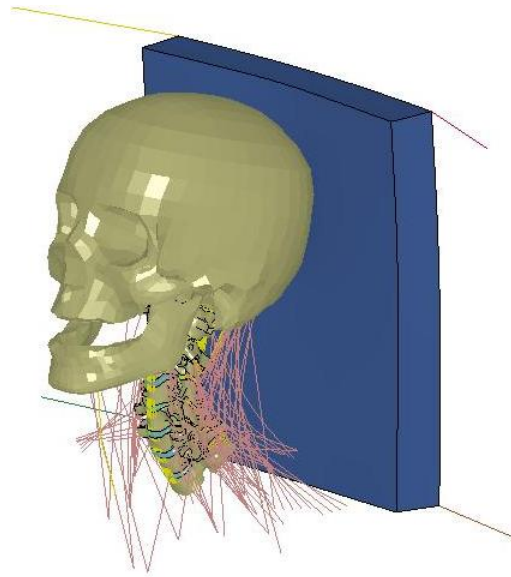
Figure 5-23: UW cervical spine model shown with headrest for 4g rear impact.

The time-lapse response of the model to a 4g rear impact showed that for the first 50ms of the impact, the head and neck remained relatively stationary as the headrest moves towards the head (Figure 5-24). Looking at the time history of head rotation reveals that the head actually rotated in flexion for the first 92ms of the simulation reaching a peak flexion angle of 1.3° at a time of 67ms. This finding agrees with experimental tests of cadavers, which report the head and upper cervical spine are initially in flexion and the lower spine in extension in what has been called the S-curve phase of rear impacts (B.Deng et al., 2000; Grauer et al., 1997). Just after the head started to rotate into extension, it was found that the head contacted the headrest at 96ms, which compares favourably with the average (SD) headrest contact time of 98 (12) ms in the experiments (Davidsson et al., 1998). This shows that the headrest in the model was behaving similarly to the one used for the experiments. From 100ms to 200ms, the head moved into the head rest and the neck went further into extension, with the peak head extension of 34.2° occurring at exactly 200ms. The T1 input includes a superior displacement of the T1, which occurs because of straightening of the spine and ramping of the torso (Ono & Kaneoka, 1999; Davidsson et al., 1998; Deng et al., 2000). The peak T1 superior displacement of 31.9mm occurred at 196ms, which means that at peak extension the neck was also experienced a high compressive load. After 200ms, the model begins to rebound and move away from the headrest.
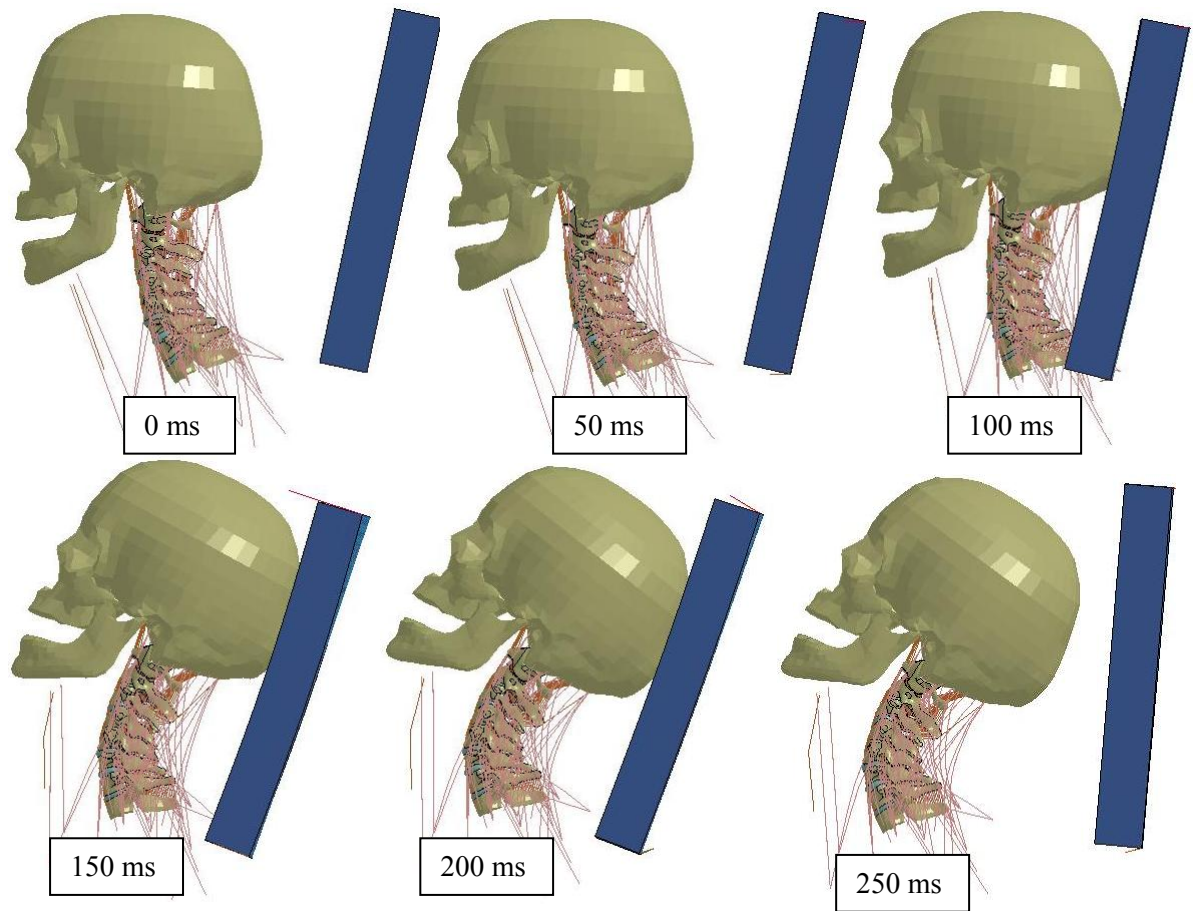
Figure 5-24: Time-lapsed response of the model to a 4g rear impact.

The global kinematic response of the model was compared to corridors presented by Hynd et al. (2007), which represent the average volunteer response plus minus a standard deviation from the experiments by Davidsson et al. (1998). The anterior displacement of the head CG in the model fell within the volunteer corridor for the entire impact duration when computed with respect to the sled (Figure 5-25). When the anterior displacement of the head was computed with respect to the T1, the final displacement of the head was 38mm more posterior of the T1 than the lower bound of the volunteer corridor. This means that the head CG of the model displaced too far in the posterior direction.
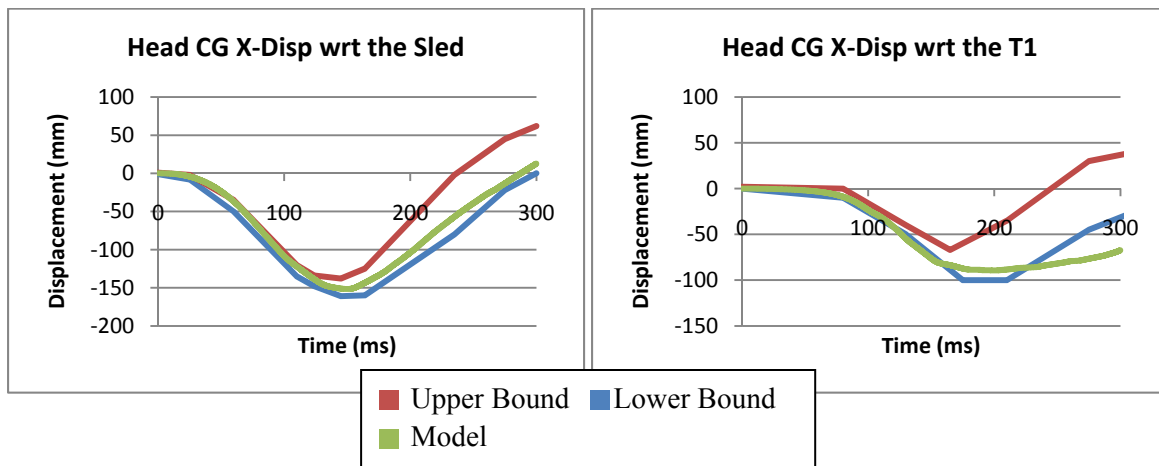
Figure 5-25: The head CG X-displacement response of the model to a 4g rear impact.
A negative relative displacement means that the head has displaced posteriorly relative to the structure being compared to.

The plots of occipital condyle displacement (O.C.) in the superior direction showed that between 140ms and 240ms the head in the model did not displace enough in the superior direction (Figure 5-26). The relative displacement between the O.C. and the T1 was mostly negative, which showed that the neck was either in compression, extension, or in this case a combination of the two.
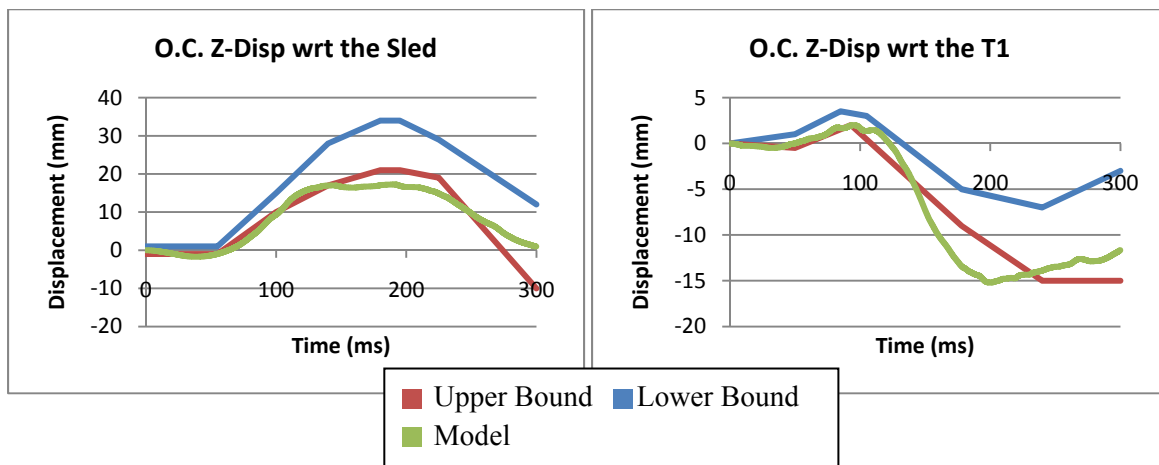
Figure 5-26: The head O.C. Z-displacement response of the model to a 4g rear impact.
A positive relative displacement means that the head has displaced superiorly of the structure being compared to.

Initially, the head of the model went into flexion with respect to the T1 and changed into extension at 120ms (Figure 5-27). The response of the model matched the volunteer corridor up to 140ms, but then continued into extension as the volunteers straightened their heads. With head extension, the head CG of the model displaced inferiorly and posteriorly. Therefore if the head did not rotate an additional 17° into extension compared to the lower bound of the volunteer corridor, the response of the model in the anterior and superior directions would likely be improved.
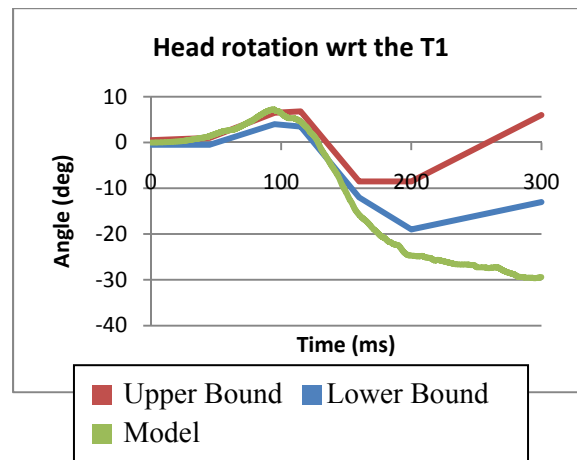
Figure 5-27: The head CG rotational response of the model to a 4g rear impact. Extension is negative.

A series of 26 rear impacts on 6 whole body cadavers at delta velocities ranging from 5 to 15.5kph, and accelerations from 5 to 9.9g were performed by B. Deng (1999). These experiments involved a cadaver seated in a custom rigid seat, with or without a headrest, and being accelerated from rest using HYGE mini-sled. The average (SD) age, weight, and height of the cadavers were 72.3 (20.5) years, 59.4 (11.4) kg, and 165 (4.6) cm respectively. Accelerometers and rotational rate sensors were drilled into the skull and T1 to capture the linear accelerations and rotations of these parts.

A specific run with 7g sled peak acceleration was chosen to simulate, based on the impact severity and available data. The response of the model was compared to tests in which the sled peak acceleration was within plus minus 1g of the chosen run. The experimental T1 superior and anterior accelerations and sagittal plane rotation were input into the model as prescribed motion (Figure 5-28). The coordinate system used rotated with the T1 and was initially 20° in flexion, as per conversation with B. Deng. The T1 was constrained from moving in any other direction and everything else was

free in all directions. Muscle activation was not included in the validation to mimic the behaviour of cadavers.
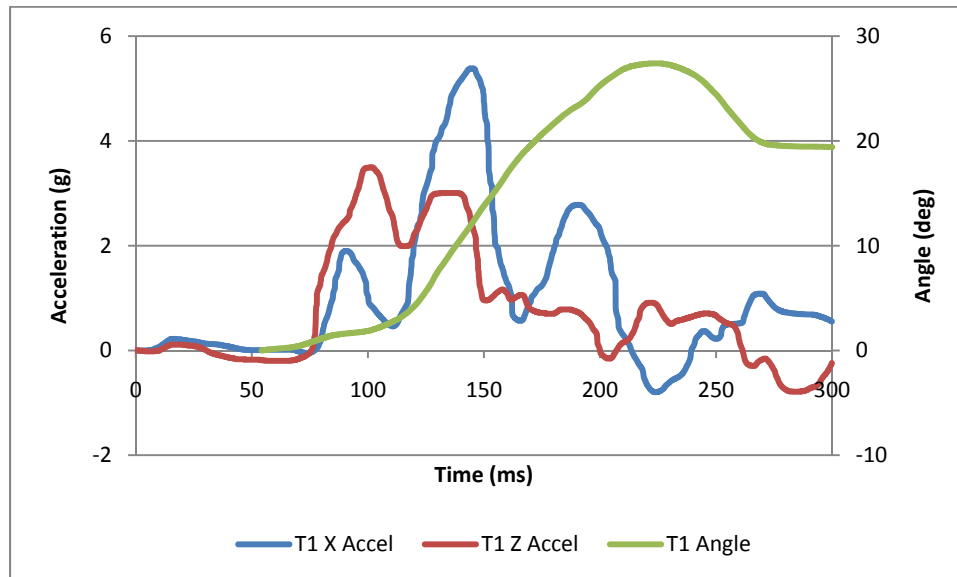
Figure 5-28: T1 prescribed motions for a 7g rear-impact (B.Deng 1999).

X acceleration is positive in the anterior direction, Z is positive in the superior direction, and the angle is positive in extension.

In a 7g rear impact, the model went through the same transition of S-curvature to full extension when compared to the 4g impact (Figure 5-29). The head of the model was in flexion for the first 66ms, with a peak flexion rotation of 1° at 49ms. The peak extension angle of the head was 89.7°, which occurred at 210ms.
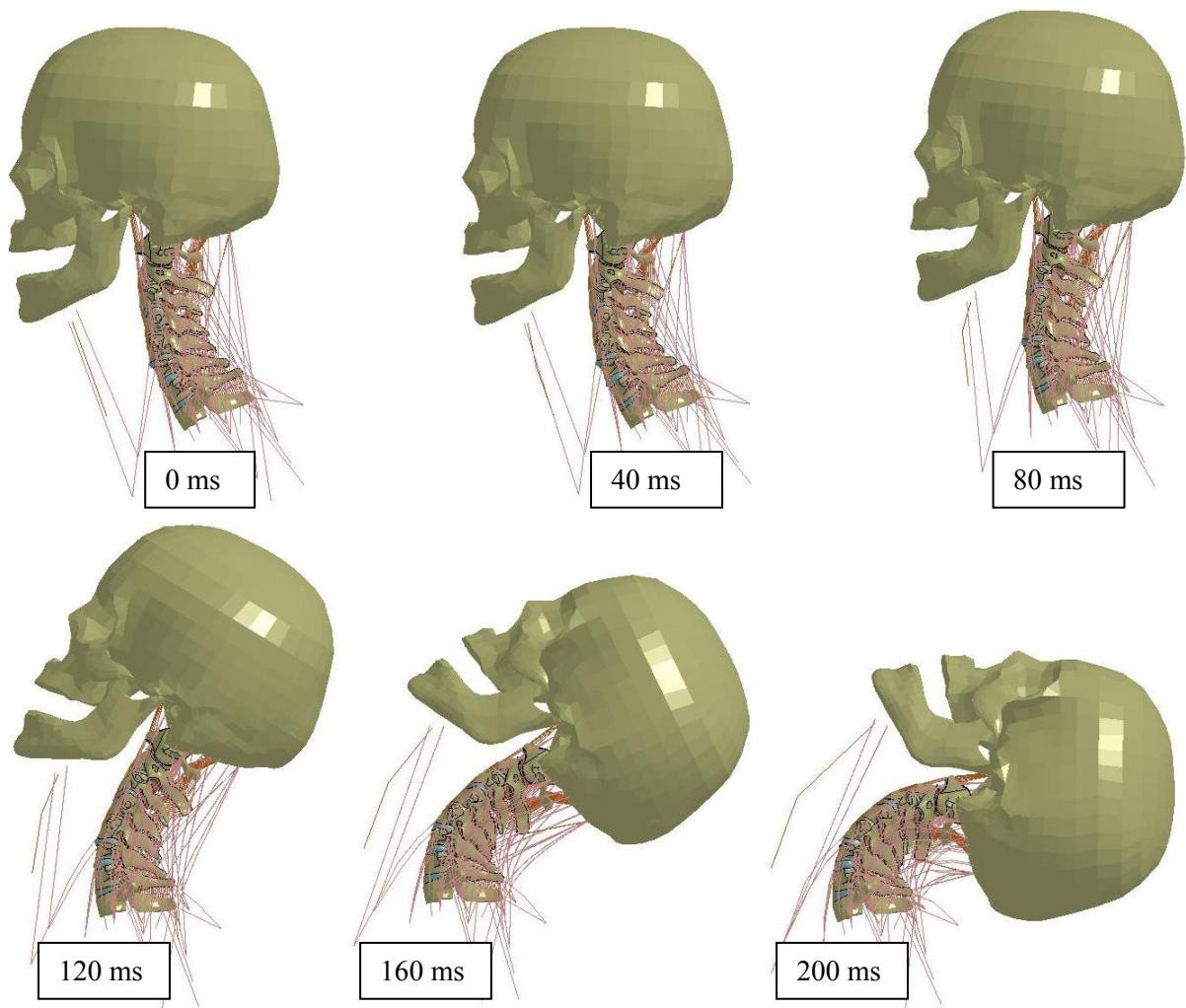
Figure 5-29: Time-lapsed response of the model to a 7g rear impact.

The rotation of the head in the model initiated in the same manner and at the same time as the experiments, and the slope of head angle vs. time was also representative of the experiments (Figure 5-30). The only deviation in the response of the model was the peak extension angle of the head was 6° beyond the highest experimentally measured value. A similar trend was found with the rear impact simulations at 4g.
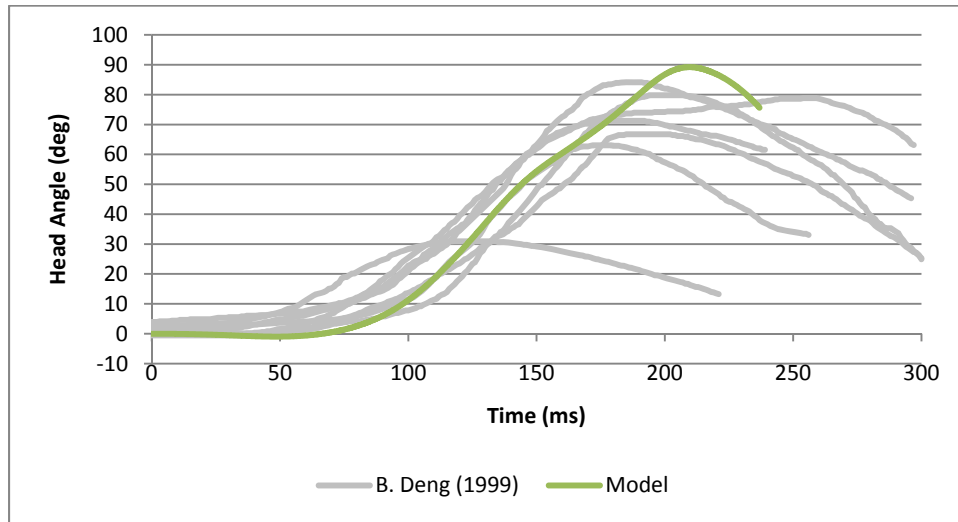
Figure 5-30: Head rotation of the model during a 7g rear-impact.
Positive angle is extension.

The anterior acceleration of the cadaver's head displayed wide variation, but generally there was a peak near 100ms and one or two peaks of 6 to 10g between 150ms and 225ms (Figure 5-32). The response of the model was similar, with three peaks of 1.7g, 6.5g, and 4.3g at 110ms, 181ms, and 216ms respectively. The response of the model remained well within the wide scatter of the experimental results.
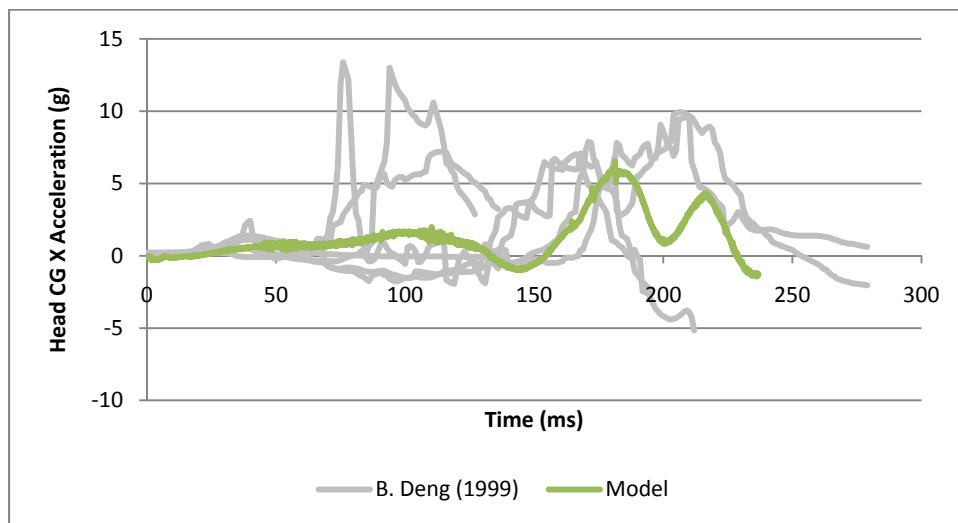
Figure 5-31: Head CG X-acceleration of the model during a 7g rear-impact.
Positive acceleration is in the anterior direction.

In the inferior-superior direction, the first peak acceleration of the head CG in the model was too high compared to all but one of the experimental PMHS tests (Figure 5-32). Then from 50ms to 150ms the acceleration of the head remained above the experimental scatter. Overall, the model's response in the interior-superior head CG acceleration was a moderate fit to the experimental measures.
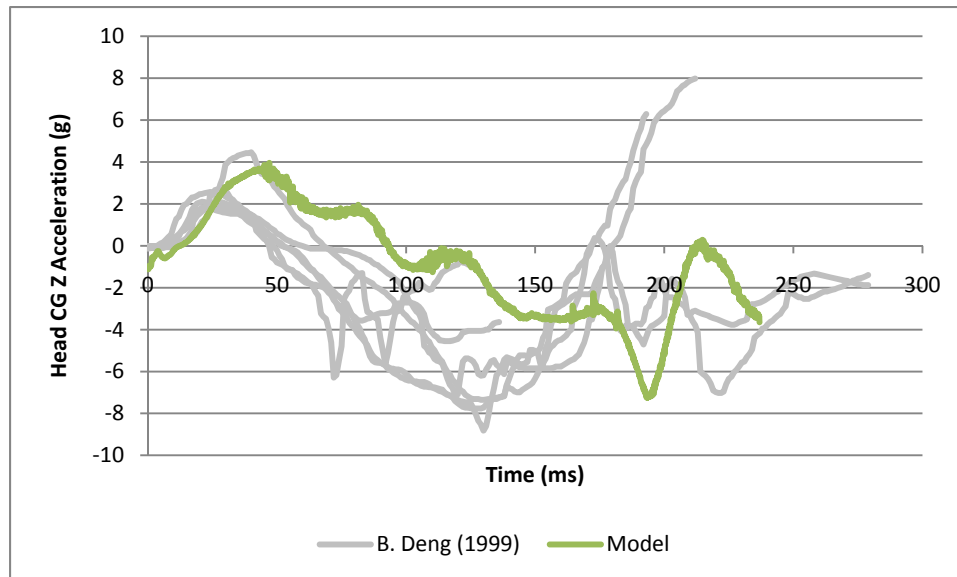
Figure 5-32: Head CG Z-acceleration of the model during a 7g rear-impact.
Positive acceleration is in the superior direction.

In addition to validating the global response of the head in the model, it is also valuable to validate the relative vertebral rotations at each spinal level. If the intervertebral motions in the model are accurate, the soft tissue strains predicted by the model will also be accurate. Early in the impact (<150ms) the C1-C2, C2-C3, and C3-C4 segments of the cadavers went into relative flexion as their chin tucks in, and later in the impact they went into extension (Figure 5-33). This was seen in the model but the peak flexion angle predicted by the model was on the low end of the experimental results. At 100ms, the cadaver C4-C5 and C5-C6 segments go directly into extension, which was predicted by the model. The slope of the relative rotation vs. time predicted by the model was accurate at the C4-C5 and C5-C6 levels, but in both cases there was a delay relative to the PMHS.
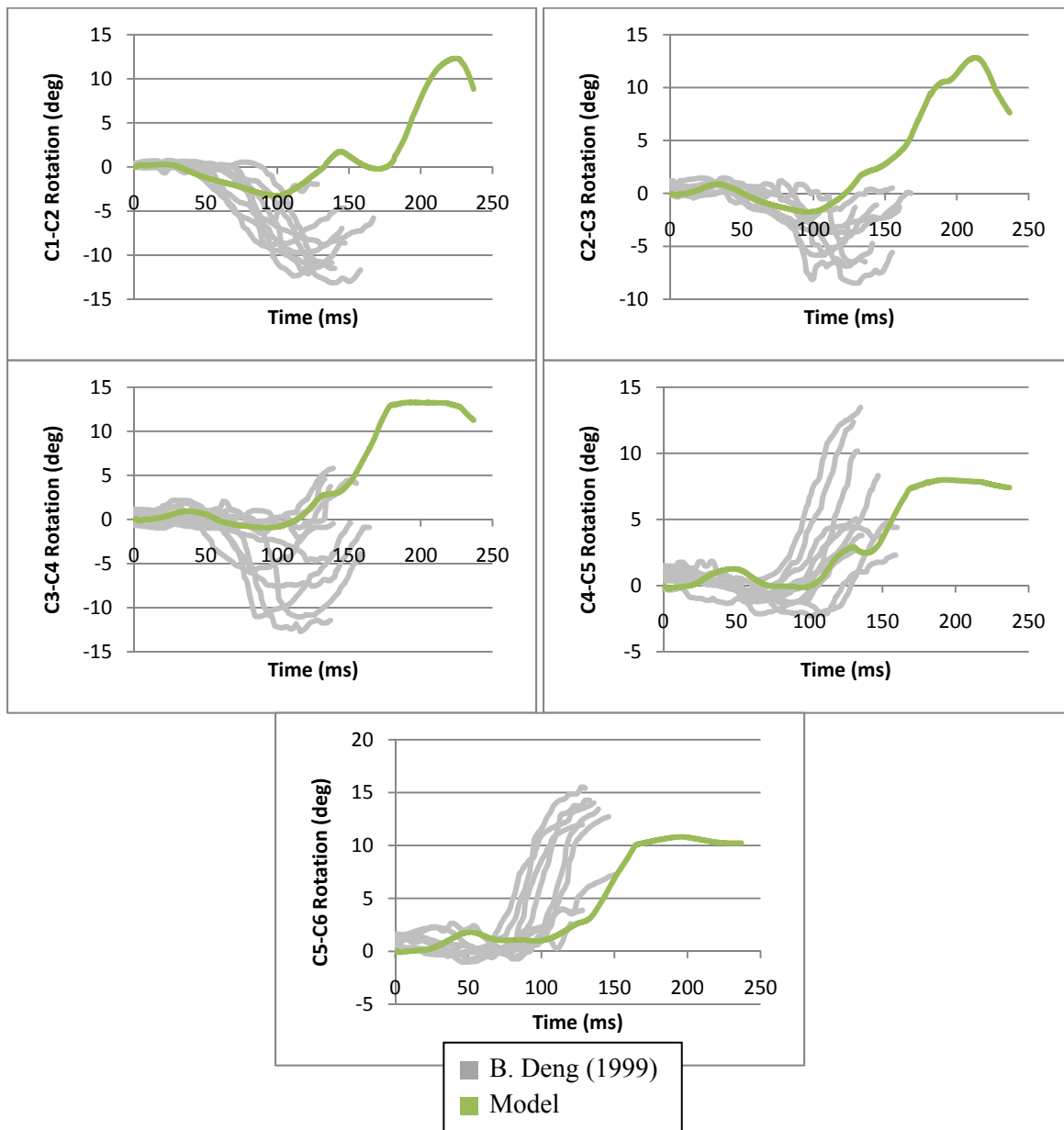
Figure 5-33: The intervertebral rotations of the model during a 7g rear impact. Positive angles are extension.

5.4 Discussion

The full cervical spine with musculature removed exposed to a tensile load of 300N compared well with the experiments performed by Dibb et al. (2009). The inferior displacement of the T1, and the rotation and translation of the skull remained within one standard deviation of the experimental

average for the entire range of force from 0 to 300N. The model slightly deviated from the experimental averages after 100N where the T1 displacement and the posterior displacement of the head were larger. This subtle difference could be due to the friction of the head mount in the anterior-posterior direction or the mass of the head mount in the experiments. Both of these explanations would provide resistance for the head to move in the anterior-posterior direction, which would also stiffen the inferior displacement of the T1. This phenomenon can be described by considering a case where the head is completely fixed and an inferior displacement is applied to the T1, such that displacement can only occur by stretching of the ligaments and discs, but if the head is free to translate and rotate the displacement of the T1 can occur by straightening of the spine or stretching of soft tissue. The case where the head is fixed will be inherently stiffer, so providing additional resistance to the anterior-posterior translation of the head will move the experiment closer to the head fixed case and stiffen the inferior displacement of the T1. The rotation of the head in the model was 3.5° less at 300N compared to the experiments. The head translates and rotates in the experiments because it was trying to form a straight load path through the T1 to the occipital joint to the head centre of mass. Some combination of head translation and rotation are required to achieve this load path, so the rotation of the head in the model could be low because the translation of the head was high as discussed previously. Another explanation is that the occipital joint in the model may be too stiff, preventing the head from extending, but the over extension of the head in rear impact discredits this theory. This is the first time a full cervical spine model has been tested in this important mode of loading.

The ligament response of the model in frontal impact compared well with the experiments, with 26 out of 30 ligaments in the model falling within one standard deviation of the experimental average. Generally, the strains measured in the model were below the experiments, which may be due to the advanced age of the specimens (mean 71.3 years; range 54-87) or a lack of stiffness created by the cable system meant to model passive tissue response in the experiments. In a 3.6g rear impact, the cadaver cervical spine with muscle force replication model exhibited peak head extension of 37.1°, which was within the range measured in a series of volunteer tests at similar impact loads (Ivancic et al., 2005). Also the intervertebral rotations from one volunteer test measured with cineradiography were within the 95% confidence interval measured by the cadaver model for C4-C5 and C5-C6, and within 1.3° of the 95% confidence interval for C23 and C34 (Ivancic et al., 2005). This level of validation would not be acceptable for a numerical model and no such validation has been published

for the cadaver model in frontal impact. This leaves the possibility that their muscle replication force was not creating enough resistance. The only location the model over predicted peak strain was the anterior aspect of the C6-C7 CL, which measured a value of 26.4% and the posterior aspect of the C6-C7 CL had a peak strain of 25.1%. The fact that the posterior and anterior CL strains were so similar suggests that this vertebral level was loaded more in anterior shear then in flexion. This trait can be traced back to the segment level validations were the model was shown to be too lax in anterior shear (Panzer, 2006).

The model accurately predicted peak disk shear strains in frontal impact as measured experimentally by Ito et al. (2005) for spinal levels C3-C4 to C6-C7. The model under predicted the peak shear strain at C2-C3 by an average of 0.59 radians compared to the mean experimental results. This can be explained by the C0-C1-C2 flexion limiter that was used to limit the flexion of these vertebrae to 30° to simulate chin-sternum contact (Ivancic et al., 2005). By limiting the flexion of these vertebrae, they become stiff beyond 30° flexion and transferred more load via shear strain to the C2-C3 disc. The flexion limiter was not modeled numerically, so it stands to reason that the C2-C3 shear strains would be lower in the numerical model.

In rear impact, the ALL and CL strains predicted by the model were mostly within one standard deviation of the experiments, but generally the strains predicted by the model were below the experimental average. This can be explained by a lack of resistance from the experimental cables meant to model passive muscle resistance, as discussed previously. The disc shear strains in the model during rear impact were accurate at every level except C5-C6, which was on average of 0.48 radians below the mean experimental results. There is no apparent reason the shear strain at the C5-C6 level in the model would be particularly low, considering these strains are similar to the vertebral levels above and below. Also, there is no clear explanation why the cadaver model would consistently predict high shear strains at the C5-C6 level for each of the three positions measured. One possible explanation is that the initial posture of the cadaver model and the numerical model are different causing the spinous process contact to occur at different times. The spinous process limits the vertebrae in extension and when in contact transfers load into adjacent vertebrae.

The global kinematic response of the model in frontal impact was generally very representative of the volunteer tests performed at the Naval Biodynamics Laboratory. One major discrepancy was the tendency of the model to oscillate more than the volunteers, which can be seen in the 15g X-

acceleration and 8g Z-Acceleration. This can be attributed to a lack of damping in the model. The viscoelastic function for the ground substance was fit to relaxation tests performed at low strain rates and the annulus fibrosus was lacking rate dependent properties due to a lack of available experimental data. Therefore, the discs may not be contributing enough damping for impact situations. Another source of damping that the model does not include is soft tissues such as but not limited to the skin, subcutaneous fat, oesophagus, and spinal cord. The other disagreement between the model and the volunteers was the early onset of head rotational acceleration, which was seen in both the 8g and 15g impacts. This difference may be explained by the lack of muscle pretension that would be required by the volunteers to maintain an erect posture prior to the impact. The muscle pretension would provide resistance to the head rotating and may delay the onset of rotational acceleration. A final source of error in the model may be the muscle activation scheme, which was both the flexor and extensor muscles contract at 74ms and remain active for 100ms (Siegmund et al., 2003). The scheme was based on research using EMG data on volunteers during rear impact, which showed that sternocleidomastoid and trapezius activate at approximately the same time (Roberts et al., 2002, Szabo and Welcher, 1996). This activation scheme indicates a 'strap-down' muscle control strategy as proposed by Nashner (1985). No data is currently available to support a more intricate muscle activation scheme.

The rear impact kinematic response of the model was generally a good fit to the volunteer data at 4g and the cadaver tests performed at 7g. The experimental data for the 7g rear impact exhibited large variations because in addition to the usual experimental variations the researcher did not attempt to expose the cadavers to consistent impact severities, and the results were shown for impacts that were greater than 6g and less than 8g. In both the 4g and 7g rear impact severities the head over extended. If the excessive extension of the head was resolved in the 4g case, the head would not have moved so far posteriorly or inferiorly, which would bring the model into the other response corridors. Two aspects of the model that can contribute to increased extension of the head are the facet joints and the uncovertebral joints. When the articular surfaces of the facet joint come into contact, they provide resistance for further extension. Unfortunately, there is no data available for the facet gap in a human spine in-vivo or in-vitro and it was possible to match other postural data with variation of the facet gaps. The uncovertebral joints are formed between protuberances extending from the superior-lateral to superior-posterior surface of a vertebral body to the posterior surface (Figure 5-34). Kotani et al. (1998) performed progressive transactions of the uncovertebral joint on vertebral segments and found

that the stiffness in extension dropped by 36% when the posterior portion of the joint was removed. This research also noted similar decreases in stiffness in torsion and lateral bending, but only an 11% decrease in flexion stiffness. Despite the biomechanical evidence of the role of these joints, no numerical cervical spine model has attempted to model them. The reason for this is likely the size of the protuberance is small compared to the vertebral body and would be difficult to capture with the imaging modalities used to create geometry for numerical models. Another difference between the experiments and the model was the excessive vibrations seen in the Z-acceleration and to a lesser extent the X-acceleration of the head during the 7g impact. This difference can be explained by the lack of damping in the model as discussed previously.
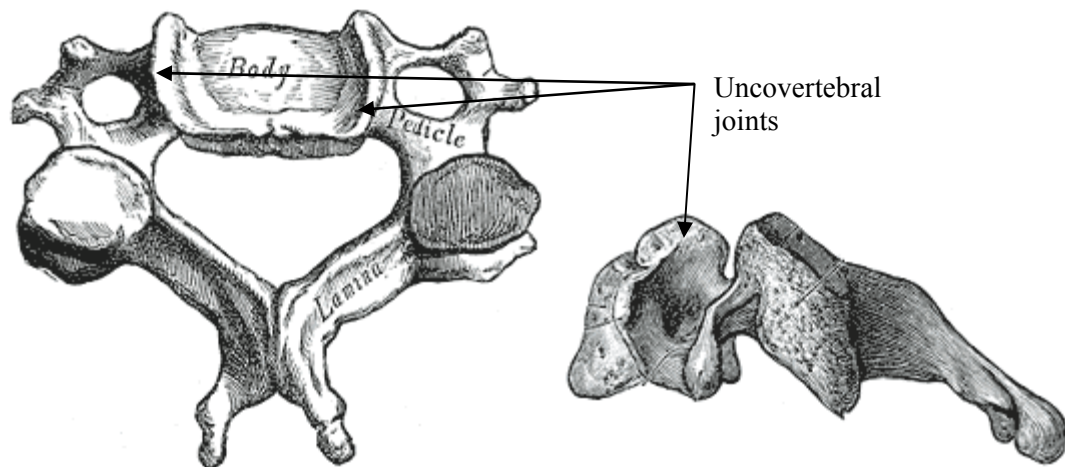
(Adapted from Gray, 1918)

Figure 5-34: The uncovertebral joints in the cervical spine.

The muscles in the model were modeled as a series of 1D discrete elements, which ignores the volume of the muscle tissue. Hedenstierna and Halldin (2008) implemented a continuum muscle model in the KTH cervical spine model and found that modeling the continuum muscle volume increased the stiffness of the neck. The change in stiffness of the neck was quantified by the required muscle activation to keep the model in the response corridors, and the largest percent difference between the discrete muscles and continuum muscles was 31% in the hyoid muscles in rear impact. In frontal impact, the largest percent difference between the two muscle models was 10%. The stiffening of their model occurred by friction between the muscles as they slide over one another and compressive stiffness of the tissue. Therefore, if the UW neck model incorporated muscle volume the over extension of the head would be reduced in rear impact and the early onset of head rotation in frontal impact would be delayed.

89

Chapter 6
Soft Tissue Strains

Once the tissue response predicted by the model was successfully validated against bench-top cadaver models, an investigation into the strains predicted by the model in both frontal and rear impact was undertaken at a range of impact severities. In frontal impact, the soft tissue strains were calculated for the 8g and 15g NBDL volunteer tests used in Chapter 5. The soft tissue strains were also calculated for a 22g impact, whose T1 inputs came from a series of cadaver tests performed at the University of Virginia (Bolton et al., 2006; Figure 6-1). These cadaver tests were not suitable for validation, because an airbag was used and this was not being modeled. In rear impact, the 4g and 7g impact cases were analyzed for soft tissue strain, but muscle activation was included for both the 4g and 7g case to mimic the strains experienced in-vivo. The T1 inputs for a 10g rear impact were taken from a cadaver impact performed by B.Deng (1999) (Figure 6-2), and used to calculate soft tissue strains for this impact severity. This load case was not suitable for model validation because only two cadavers were impacted at this severity and this was not enough to get a meaningful comparison. Finally, the soft tissue response of the model to higher severity rear impacts was investigated by scaling the X-direction acceleration from the 10g impact to achieve impact severities of 12g, 14g, and 16g.

The soft tissues injuries that were investigated included strain in the ligaments and annulus fibres of the intervertebral discs. Ligament strain was calculated by measuring the distraction of 1D elements representing the various ligaments in the cervical spine and then dividing by anatomical ligament lengths reported in literature (Ivancic et al., 2004; Panjabi et al., 2004a; Panjabi et al., 1991). The strain in the annulus fibres were output directly from a history variable in LS-DYNA. This history variable outputs strain in the fibre direction of the material model used for the fibre lamina shell elements. The ligament strains, except for the CL, were compared to a failure corridor that represented the average plus and minus a standard deviation of strain at the ultimate stress from in-vitro tensile tests of dissected cervical spine ligaments (Yoganandan et al., 2001). The CL strains were compared to reported values for sub-traumatic failure of isolated facet joint exposed to tensile load (Winkelstein et al., 2000, Siegmund et al., 2001). Sub-traumatic failures have been linked to prolonged pain response in animal models as discussed in Chapter 4, section 4.3.1. The annulus fibre strains were compared to a failure strain derived from the reported AF circumferential failure strain of 21% (Iatridis et al., 2005), which was then re-oriented assuming a fibre orientation of +/- 30°.

It was also of interest to calculate the strain rate of the ligaments and discs in the model to aid future experimental tissue research and guide the development of future rate dependant properties in numerical models. The ligament strain rates in frontal and rear impact were calculated by numerically differentiating the strain vs. time plots and then filtering the data using a Butterworth (BW) filter with a cut off frequency of 100Hz. The disc strain rates were output from the 1st principle strain rate feature in LS Prepost software (LSTC, Livermore, CA) for the annulus shell elements, and then filtered with a 100Hz BW filter.

The last section of this chapter investigates the role of active musculature and T1 inputs on the strain measured in the model. It was hypothesized that strains predicted by bench-top whole cadaver cervical spines experiments would be high because they do not include the full sagittal plane motion of the T1 and active musculature. For a rear impact, full T1 inputs include extension and inferior-superior acceleration. Numerical models in the past have shown that muscle activation influences global kinematics (Brolin et al., 2005; Panzer, 2006). The model was used to investigate this hypothesis.
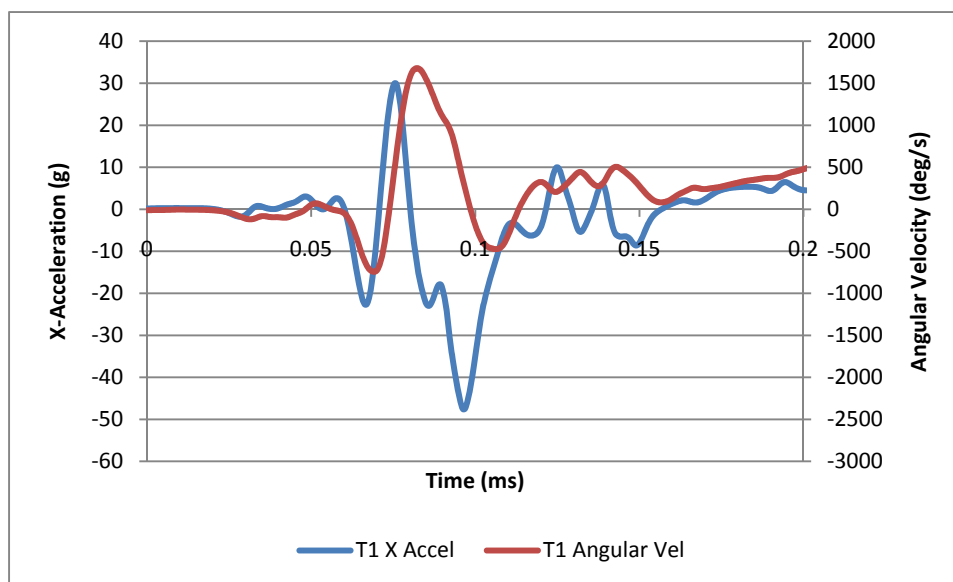
Figure 6-1: T1 Inputs for a 22g frontal impact (Bolton et al., 2006).
Negative X in the posterior direction and positive angular velocity in flexion.
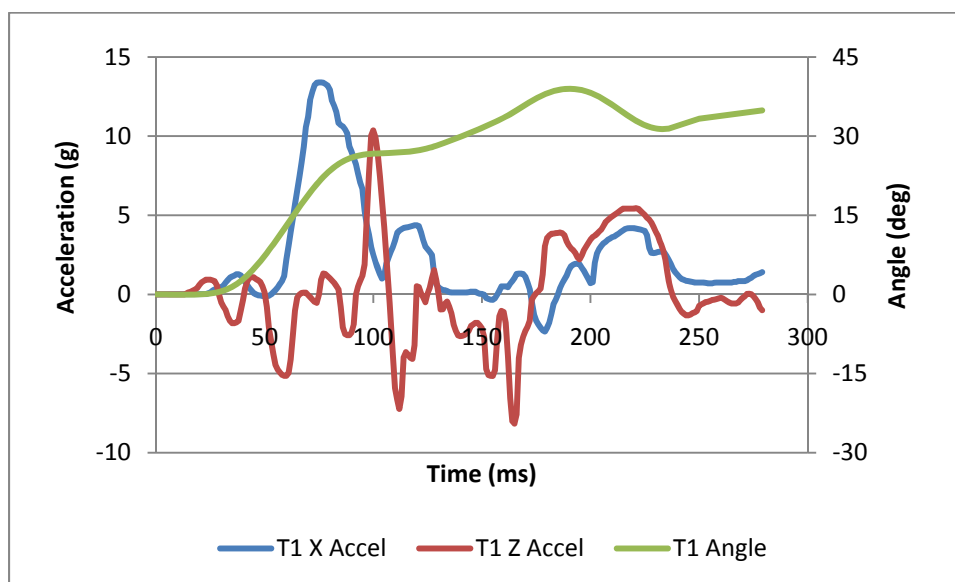
Figure 6-2: T1 Inputs for a 10g rear impact (B. Deng 1999).

X acceleration is positive in the anterior direction, Z is positive in the superior direction, and the angle is positive in extension.

6.1 Soft Tissue Strains in Frontal and Rear Impacts

6.1.1 Frontal Impact

With increasing impact severity, the strains predicted by the model increased for every ligament examined (Figure 6-3). The strains were generally the greatest for ligaments located more posteriorly (i.e. the ISL and LF). The peak ligament strain was 0.99 at the C3-C4 LF during a 22g impact. Ligaments that entered their failure corridor for a 22g impact include the PLL, CL, LF, and ISL at several spinal levels. Also the Apical Ligament from the upper cervical spine ligament exceeded the lower bound of the failure corridor by a strain of 0.078. For a 15g impact, the ligaments exceeding the lower bound of their failure criteria included the C6-C7 CL, C3-C4 & C7-T1 LF, and C4-C5, C6-C7 & C7-T1 ISL.
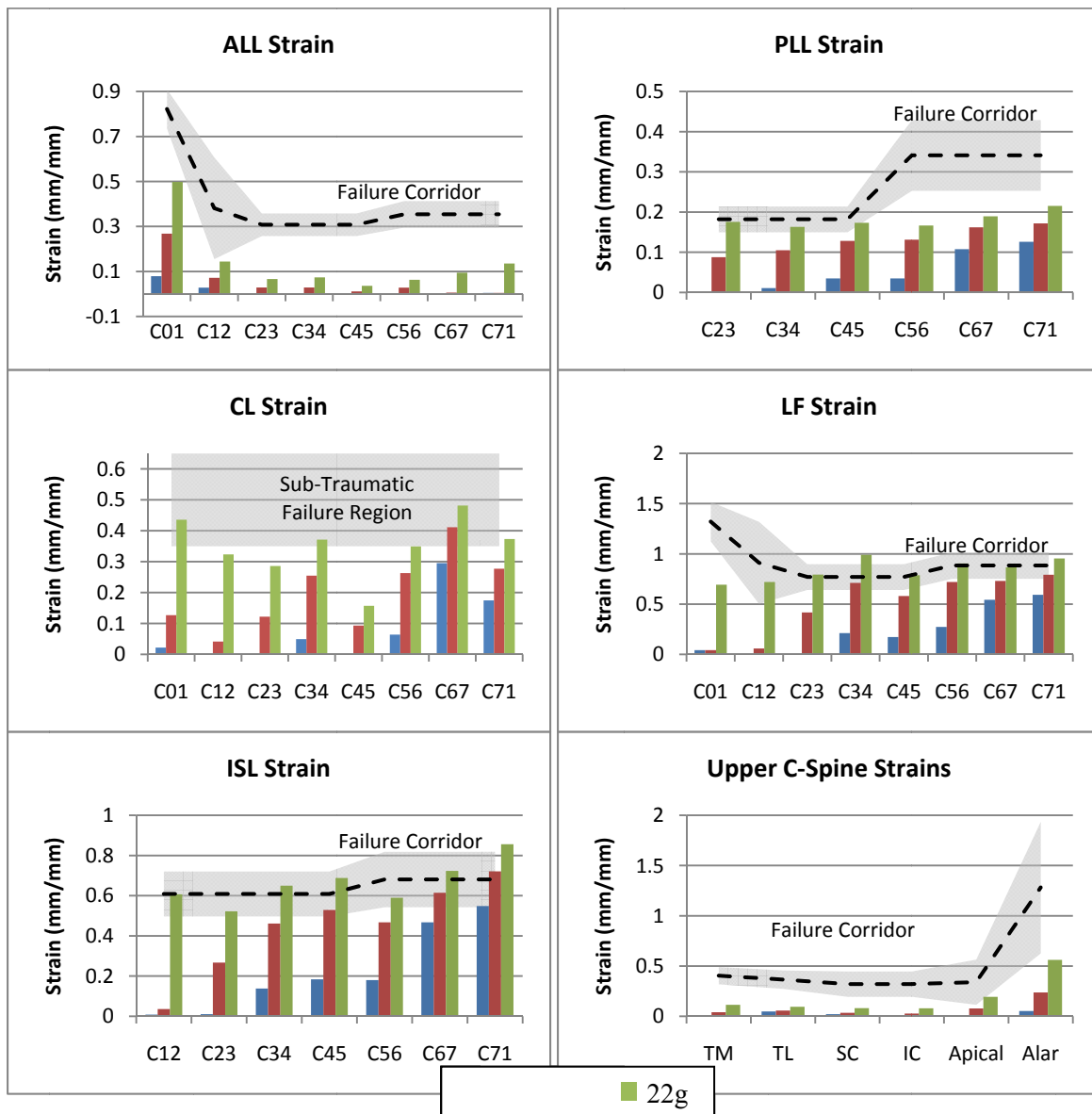
Figure 6-3: Predicted ligament strains in frontal impact.

The C7-T1 disc predicted the highest average annulus strains when compared to other vertebral discs (Figure 6-4). The annulus strains along the fibre direction reached a maximum of 0.719 for the outer layer of the C7-T1 annulus fibrosus during a 22g impact. The minimum disc fibre strain was 0.136 at the second most outer layer at the C3-C4 during a 7g impact. The disc fibre strains did not vary significantly depending which layer was measured. The average disc fibre strains increased with increasing impact for all vertebral levels.
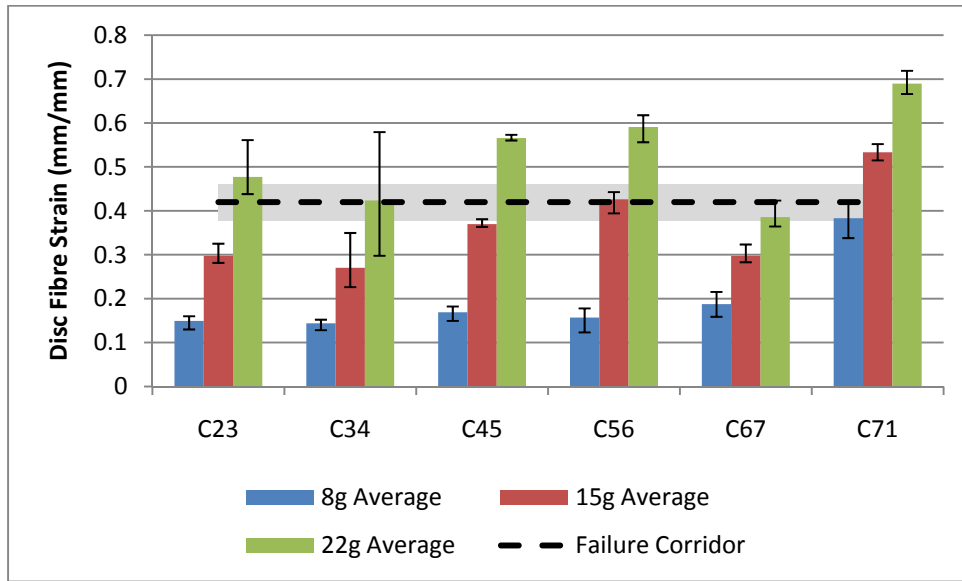
Figure 6-4: Predicted annulus fibrosus strain along fibre direction in frontal impact.
The average value measured at different annulus layers is reported along with the range.

The average ligament and disc annulus fibre strain rates predicted by the model along with the range measured at different vertebral levels are shown in Figure 6-5. Once again the more posterior ligaments experienced higher strain rates and the average ligament strain rate increased with increasing impact severity. The highest ligament strain rate was 67.3/s for the C7-T1 ISL. The average disc strain rates also increased slightly with increasing strain rate, but the highest disc strain rate of 231.7/s occurred at the C5-C6 disc during an 8g impact.
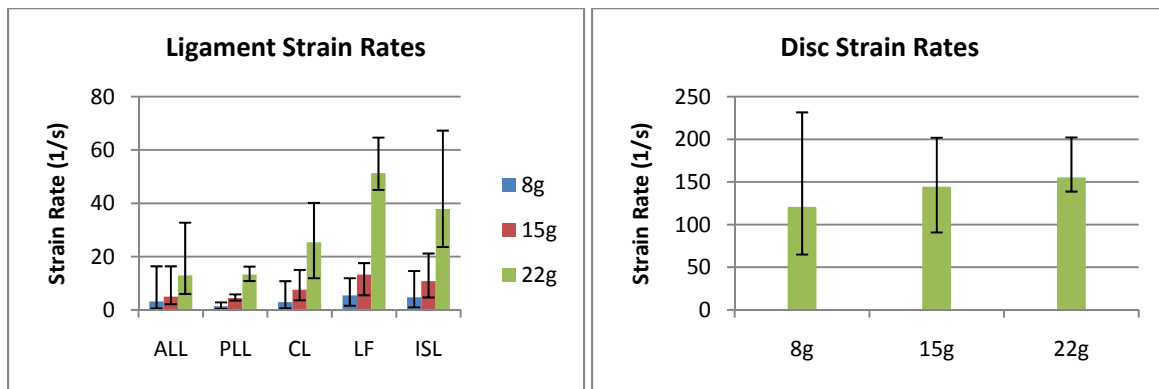
Figure 6-5: Predicted ligament and disc strain rates in frontal impact.
Average and range shown.

6.1.2 Rear Impact

In rear impact, none of the ligament strains exceeded the failure criteria for the three impact severities investigated (Figure 6-6). For the lower spine, the strains were highest in the CL and ALL. The posterior ligaments including the PLL, LF, and ISL exhibited the highest strains in the upper cervical spine from the occipital condyles (C0) down to C3. The highest strain measured in rear impact was 0.529 in the LF at C0-C1 during the initial S-curve phase of the 10g rear impact. When the 10g rear impact was scaled to achieve more severe rear impacts, the strain of the ALL entered the failure corridor at a 12g impact (Figure 6-7). During a 14g impact, both the ALL and CL strains were in their respective failure corridor.
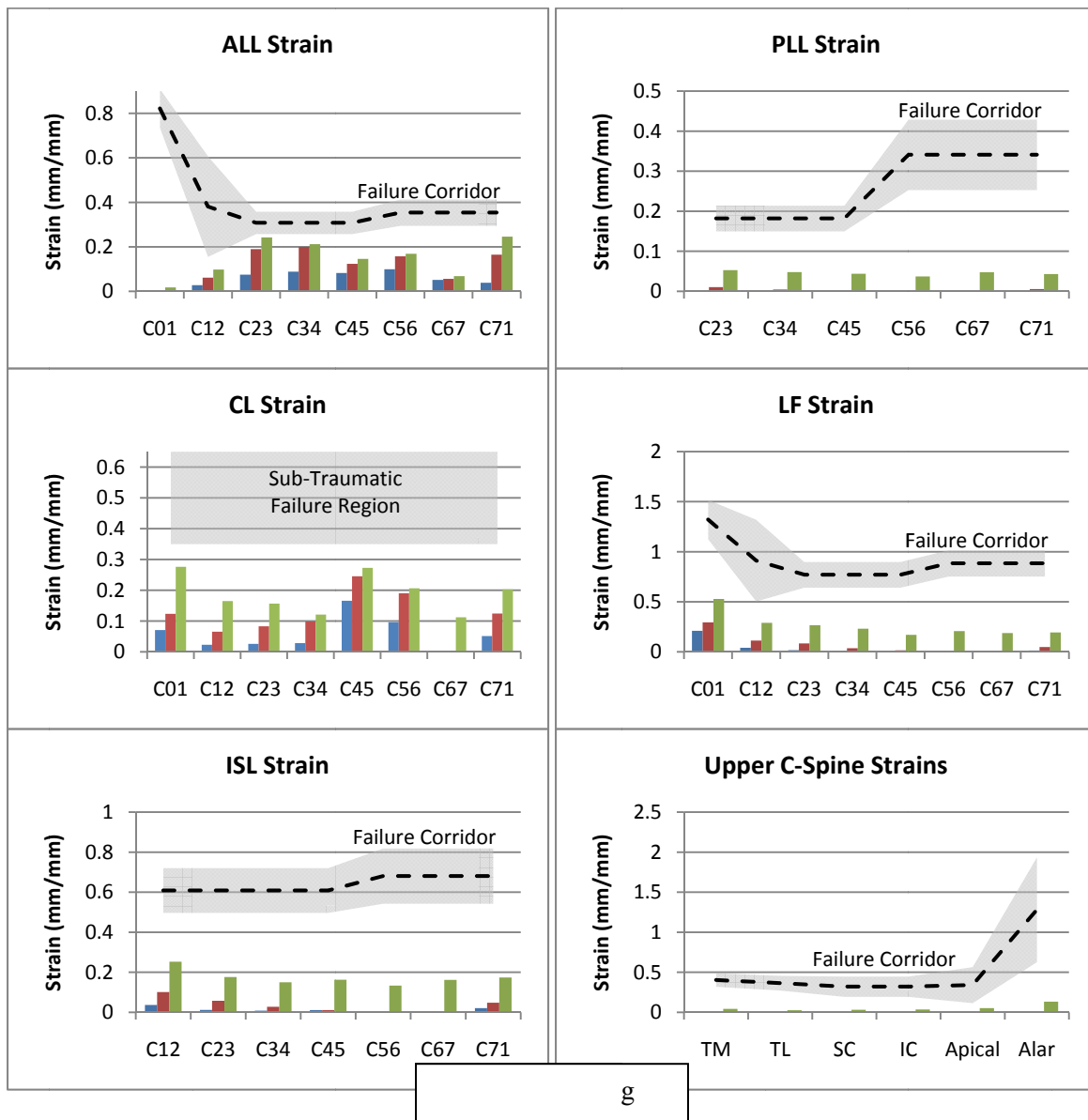
Figure 6-6: Predicted ligament strains in rear impact.
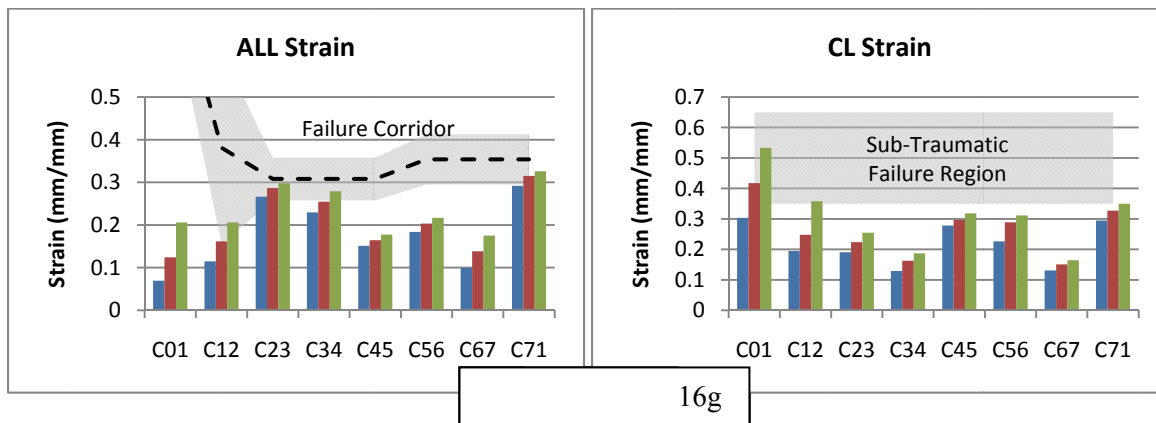
Figure 6-7: Predicted ALL and CL strain during more severe rear impacts.

The disk fibre strains generally increased with increasing impact severity (Figure 6-8). As with frontal impact, the strain measured in the different annulus layers did not vary greatly, except for at the C2-3 level in both a 7g and 10g rear impact. For a 7g and 10g impact, the C2-C3 level had the highest average fibre strain, and the average strain exceeded the failure strain during a 10g impact.
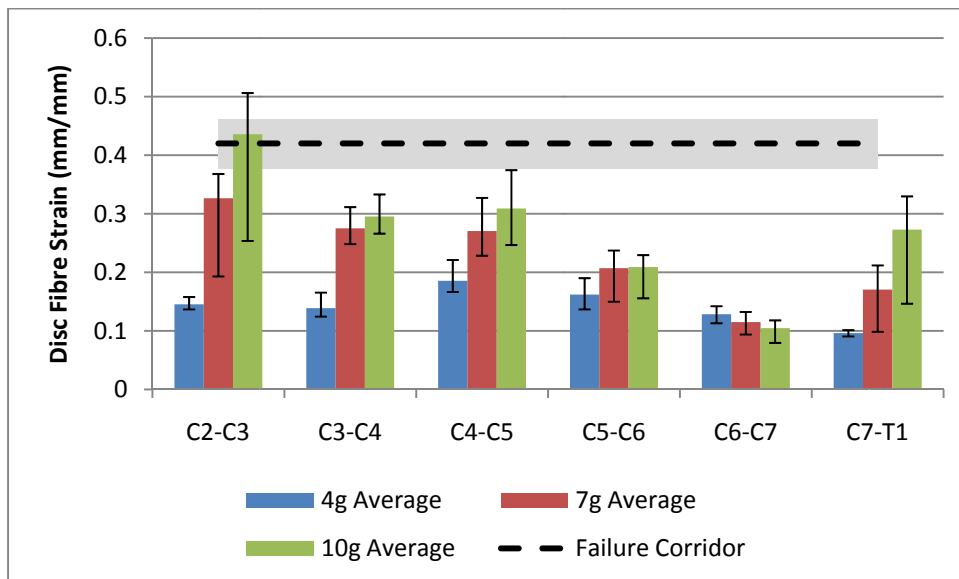
Figure 6-8: Predicted annulus fibrosus strain along fibre direction in rear impact.
The average value measured at different annulus layers is reported along with the range.

The highest strain rate measured in the ligaments was 28.8/s in the LF of C0-C1 during a 10g impact, and the highest annulus fibre strain rate was 149.4/s in the C5-C6 disc during a 10g impact (Figure 6-

9). The location of highest disc strain rate was the same in frontal and rear impact. The average ligament strains increased with increasing impact severity.
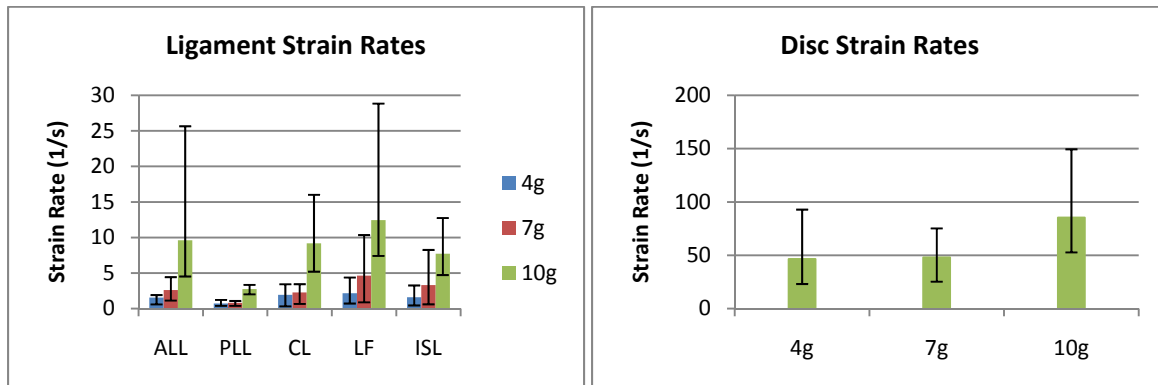
Figure 6-9: Predicted ligament and disc strain rates in rear impact.

Average and range shown.

6.2 The Influence of Muscle Activation and T1 Inputs on a 7g Rear Impact

The model was evaluated with and without muscle activation during a 7g rear impact to investigate the role of muscle activation on ligament strains. The model was also evaluated with full T1 inputs and with only anterior acceleration in a 7g rear impact. The T1 inputs for the 7g rear impact were the same used for model validation in Chapter 5. The anterior direction acceleration for the X only T1 inputs was the resultant acceleration of X and Z directions used previously. The T1 input study was performed with passive muscles so a comparison with bench-top cadaver cervical spine tests could be made. The global head kinematics and ALL & CL strains were compared for the two studies. The ALL and CL strain were chosen to represent the influence of muscle activation and T1 inputs because these ligaments were stretched the most severely in rear impact.

The global kinematics of the head were largely influenced by the addition of active musculature (Figure 6-10). The peak head extension was reduced by 17.2° or 19% and the X acceleration of the head CG occurred over a longer time frame with smaller peaks with the inclusion of muscle activation. When the T1 inputs were reduced to the anterior direction only, the peak head extension was reduced by 11.2° or 12.5% and the peak X acceleration of the head CG increased by 1.13g or 17.3% (Figure 6-11). It should also be noted that the timing of the peak head extension and the X-acceleration peak both occurred approximately 40ms earlier.
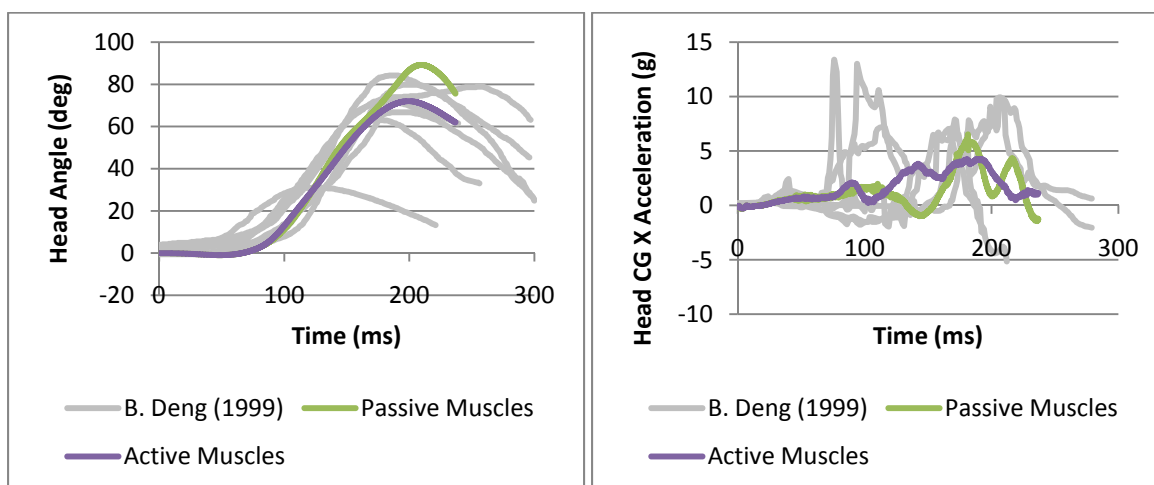
Figure 6-10: Comparing global kinematic response of the head for active and passive muscles.
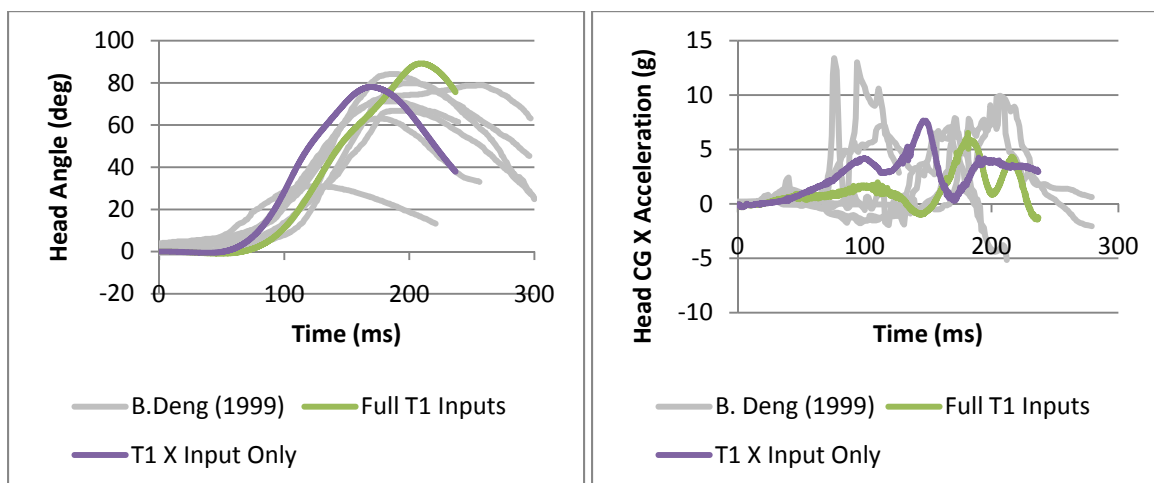
Figure 6-11: Comparing kinematic response of the head for full T1 inputs and X only T1 inputs.

When muscle activation was included, the strain in both the ALL and CL was either reduced or remained the same at every vertebral level, except for the CL at C4-C5 (Figure 6-12). The largest percent difference between active and passive muscles was 100% at the ALL of C0-C1, followed by 68% at the ALL of C6-C7. The largest decreases in strain from passive muscle to active muscles were 0.155 and 0.121 at the CL of C0-C1 and ALL of C6-C7 respectively. The influence of full T1 inputs, including rotation and superior displacement, was less significant on the ALL and CL strains when compared to active muscles (Figure 6-13). With the addition of full T1 inputs, the strains were reduced at all spinal levels except for the ALL of C0-C1 and C6-C7. The largest reductions in strain

99

from X-only T1 inputs to full T1 inputs were 0.050 and 0.023 at the CL of C6-C7 and C0-C1 respectively. These strain reductions were less than one third of the reductions seen when including active muscles.
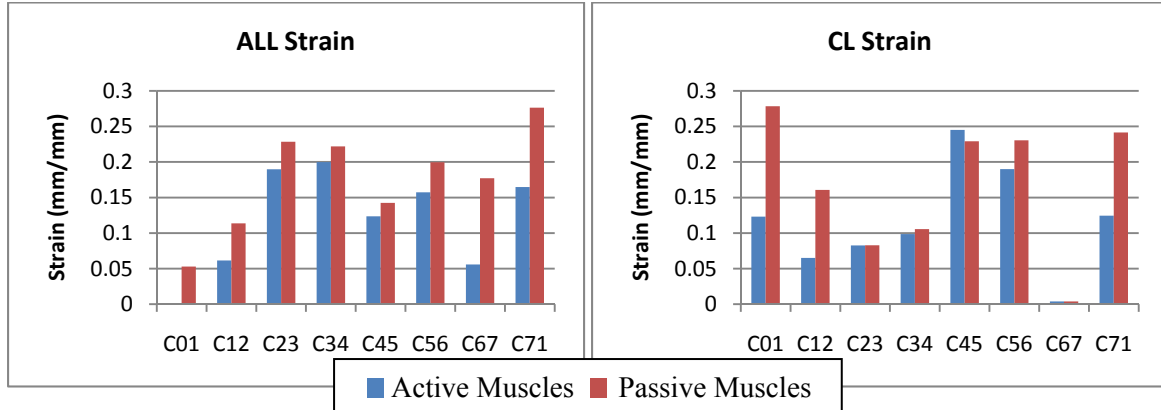
Figure 6-12: Comparing ALL and CL strain for active and passive muscles.
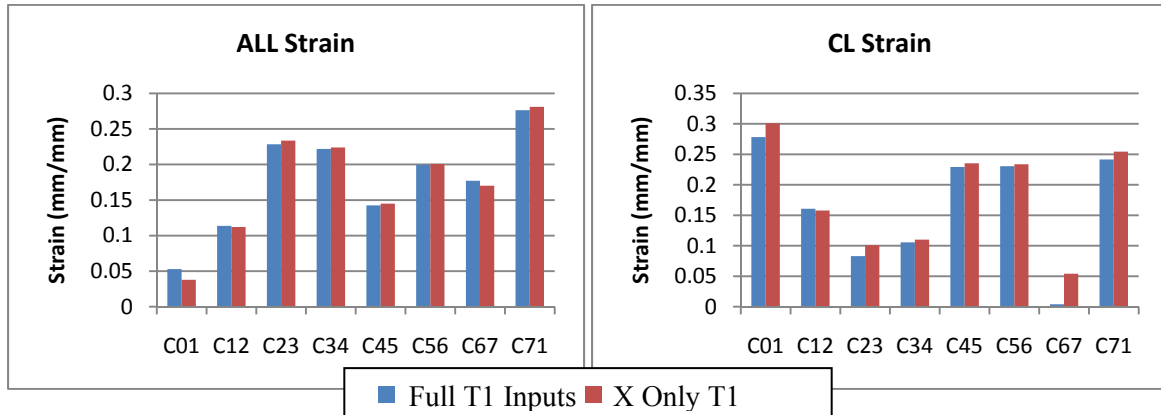
Figure 6-13: Comparing ALL and CL strain for full T1 inputs and X only T1 inputs.

6.3 Discussion

Injury to the facet joints is the most strongly supported whiplash mechanism, based on the wealth of biomechanical and clinical evidence as discussed in section 4.3.1. Clinical double-blind studies have shown that 54 to 60% of whiplash patients have pain originating at the facet joints, with the distribution of positive joints shown in Figure 6-14 (Barnsley et al., 1995; Lord et al., 1996). Both authors found that the C2-C3 facet joint was most likely injured followed by the C5-C6 amongst a population of patients seeking treatment for whiplash pain. To identify facet joint injury in the model, CL strains have been compared to sub-catastrophic failure values of isolated cadaver facet capsules of

35% to 65% (Siegmund et al., 2001, Winkelstein et al., 2000). Sub-catastrophic failure of CLs has been correlated to prolonged pain response in an animal model (Lee et al., 2004b; Quinn & Winkelstein, 2007).
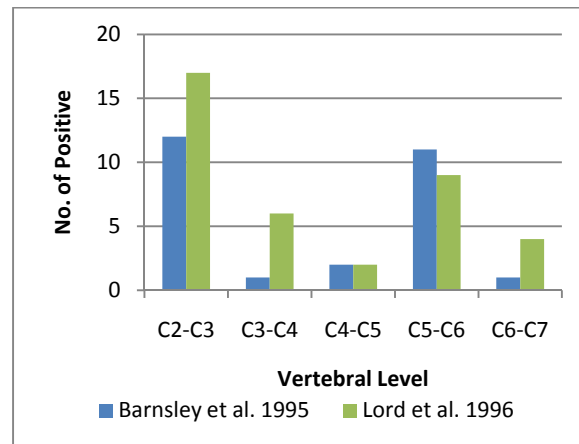
Figure 6-14: Distribution of clinically identified facet joint pain.

The model predicted that the C6-C7 facet joint will be injured during a 15g frontal impact. It is not expected that occupants would be injured at this impact level, as the inputs for this impact severity came from volunteer tests in which no one was injured (Ewing et al., 1968; Ewing et al., 1969). The volunteers for these tests came from a pool of physically fit marines (Ewing et al., 1968), so it stands to reason that they would either have an increased pain tolerance, or higher mechanical tolerance to injury. Therefore, the model predicts that the average population may be at risk for CL injury during a 15g frontal impact. During a 22g frontal impact, the C0-C1, C3-C4, C5-C6, C6-C7, and C7-T1 spinal levels would likely experience CL injury. The locations of CL injury predicted by the model do not fully agree with clinical findings (Figure 6-14), which may be due to the initial position of the vertebrae at each spinal level.

In rear impact, the model predicts CL injury at the C0-C1 level during a 14g rear impact. This impact severity agrees with findings from real life accidents. In a study of 28 instrumented real life accidents with 38 occupants, twenty occupants had short-term consequences at less than 10g, and two had long term consequences at 13g and 15g (Krafft, et al. 2000). In another study of 66 real life accidents, 13 of the 15 people that sustained neck injuries for longer than a month experienced a rear impact of greater than 9g (Krafft, et al. 2002). The model did not predict any injuries during a 7g rear impact, which is supported because this impact severity corresponds to an impact velocity of 7.5mph (B.

Deng 1999), and volunteer tests have been performed up to 6.8mph without mild symptoms, defined as lasting longer than four days (McConnell et al., 1995). The location of predicted CL injury (C0-C1) in the model does not agree with clinical findings (Figure 6-14), but once again the difference could be due to the initial posture of the model.

It is of interest to note that the threshold for CL injury in frontal impact was 15g and in rear impact was 14g. This does not agree with the common perception that soft tissue neck injuries or whiplash injuries only occur in rear impact. The difference may be that the model did not include airbags which help reduce the extent of soft tissue distraction in the neck during frontal impact. It may also be that the model is highlighting the fact that whiplash injuries are likely to occur in frontal impacts, which is supported by epidemiologic data that shows 22.6-27.2% of whiplash cases are caused in frontal impact, compared to 38.1-51.9% in rear impact (Galasko et al., 1993; Berglund et al., 2003).

The posterior ligaments including the PLL, LF, and ISL were at a high risk of injury during a 22g frontal impact, as the peak strains in these ligaments entered their failure corridors. This suggests there was a high risk of tissue damage. In rear impact, the ALL was at risk of tissue damage beginning at an impact severity of 12g. It is difficult to quantify if this damage would result in a painful injury because there is no biological or clinical evidence that any of these sites are commonly a source of whiplash pain. It has been proposed that asymptomatic tissue damage can occur if the damage occurs in a tissue of the neck not associated with neck pain (Bogduk & Yoganandan, 2001). Therefore more information from researchers and medical professions is required to determine if the ligaments of cervical spine other than the CL are associated with neck pain.

It has been proposed that ligament injuries may occur in the initial S-shape phase of a rear impact (Bogduk & Yoganandan, 2001; Grauer et al., 1997). The initial S-shape phase of a rear-impact is when the upper spine goes into flexion while the lower spine is in extension, and later in the impact the whole spine goes in extension which has been labelled the C-shape phase. The model shows that the ISL and LF in the upper cervical spine experience peak strains of 25% and 53% caused by flexion early in the impact, but neither of these ligaments were at risk of tissue damage. However, the model predicted damage to both the CL and ALL later in the impact during the C-shape phase of the impact. The difference may be due to the lack of a head rest for the rear-impacts higher than the 4g severity.

The model predicted that during a 22g frontal impact the alar and apical Ligaments experienced peak strains of 0.56 and 0.19, with the lower limit of their failure corridor at 0.63 and 0.11 respectively. In

a 10g rear impact, the alar and apical ligament strains were 0.13 and 0.05. Krakenes & Kaale (2006) were able to use MRI to find lesions in the upper cervical spine ligaments and found that the alar ligament was the most frequently damaged in both frontal and rear impacts, with 72% and 58% of whiplash patients having lesions in this ligament in frontal and rear impacts respectively. The model agrees with these finding as the alar ligament experiences the most strain in both frontal and rear impacts, but the model suggests the apical ligament was actually at a higher risk of damage. The apical ligament was not investigated by Krakenes & Kaale. The model also agrees that the alar is more likely to be injured in a frontal impact than rear, as during a 7g frontal impact the strain was 0.05 and during a 7g rear impact the strain was only 0.005. The MRI study also showed that 61% of frontal impact whiplash patients had high grade lesions on the transverse ligament, but the model disagrees with this finding because the highest TL strain was less than 10% during a 22g frontal impact. The lower bound of the failure corridor for the TL was 27% strain. This is the first biomechanical evidence reported of the strains in the upper cervical spine ligaments during impact by either a cadaver model or a numerical model in rear impact.

The disc fibre strains were the highest in the C7-T1 disc, followed by the C5-C6 disc in frontal impact and in rear impact the highest fibre strains were in the C2-C3 and C4-C5 disc. The locations of high disc fibre strains predicted by the model partially agree with a MRI study performed by Pettersson et al. (1997), who showed that the C4-C5-C6 region of the spine contained 8 of 12 disc bulges found. The disc strains at C2-C3 and C7-T1 may be high due to the transfer of load from the upper spine or proximity to the applied boundary conditions respectively. The model predicts disc damage beginning at 15g for a frontal impact and 10g for a rear impact. Ito et al. (2005) and Panjabi et al. (2004b) used a cadaver bench-top sled model to measure annulus fibre strains in frontal and rear impact respectively, and found that physiological strains were exceeded beginning at 6g for frontal impact and 3.5g for rear impact. The injury thresholds predicted by the cadaver model occurred at impact severities that are commonly applied to volunteers, possibly because their lack of active muscle resistance or their injury threshold definition. The injury metric used by both the numerical model in this thesis and the cadaver model was excessive strain in the annulus fibrosus along the fibre direction, but this may not be a full representation of disc injury. Researchers have suggested that interlaminar shear stress may be a potential intervertebral disc injury metric (Goel et al., 1995; Iatridis et al., 2005).

The impact severities predicted by the model for tissue injury or damage may be conservative compared to live humans in frontal impact because of the muscle activation scheme. In frontal

impact, the occupants may be visually warned of the approaching impact and could tense their muscles before the impact, which would prevent intervertebral motion and reduce tissue strains. The muscle activation scheme in the model activates 74ms after impact initiation, which models a startled occupant.

This is the first study to show the influence of muscle activation on ligament strains in rear impact. Muscle activation was shown to reduce peak strains of the ALL and CL in a 7g rear impact, with the most dramatic reduction seen at the C0-C1 and C7-T1 regions of the spine. Muscle activation reduces ligament strains because the muscles stiffen the response of the neck and reduce joint distractions as shown by the reduced extension and acceleration of the head. In a 15g frontal impact, Brolin et al. (2005) used a FE human neck model to shown that muscle activation reduced the peak head flexion angle by up to 68°. This model shows that muscle activation reduced peak extension of the head by 17° during a 7g rear impact. The difference between the two simulations is the impact severity used and in rear impact the spinous process of each vertebra come into contact and provide a hard stop for further intervertebral rotations, but in frontal impact the spinous processes move apart from one another.

Using only an anterior acceleration of the T1, rather than extension and anterior/superior accelerations, did not greatly influence the ligament strains predicted by the model. This is despite of the significant changes to the head kinematics that showed with X-only T1 inputs the head extended 11° less and the peak acceleration of the head increased by over 1g. It is thought that the reduction of head rotation and the increase of head acceleration produced a zero net effect on the intervertebral motions. This study shows that the T1 inputs used for bench-top cadaver sled tests should not influence the soft tissue strains predicted, but when considering the soft tissue strain results from these tests one should consider that their strains will be high due to the lack of muscle activation.

Chapter 7

Conclusions and Recommendations

7.1 Conclusions

Whiplash injuries, or soft tissue injuries to the cervical spine, are a leading cause of injury in motor vehicle accidents. Currently, automotive companies use finite element representations of anthropomorphic test devices (ATD) in their crash simulations to predict occupant response and improve crash worthiness. However, these ATDs and their finite element (FE) representations lack the biofidelity to predict local tissue damage, which is essential for the prediction of whiplash injury. To address this deficiency, many of the major automotive companies have formed the Global Human Body Models Consortium (GHBMC) with the intent to produce detailed FE models of the human body that will be used to improve the safety of vehicles. The neck model used in this work was used to investigate whiplash injury. Despite whiplash being commonly associated with rear impacts, this study focussed on both frontal and rear impacts as epidemiological data suggests that up to 27% of whiplash cases are caused in a frontal impact.

The neck model used in this work was developed at the University of Waterloo. The model represents a 50th percentile male and it includes both passive and active musculature, detailed nucleus and annulus model of the discs, rate dependent non-linear ligaments, facet capsules with a squeeze film model of the synovial fluid, and rigid vertebrae derived from CT scans. All of the material properties were determined from independent experimental testing, and implemented using appropriate constitutive models. It should be noted that the properties were not adjusted to improve the model response. The model was previously validated at the segment level under nine loading conditions including but not limited to: flexion, extension, posterior and anterior shear, tension, and compression. It was then assembled into a full cervical spine and validated against experimental data from volunteer sled tests from 15g frontal impacts.

In this work, the full neck model was further validated in three ways; tensile loading up to 300N applied to the model without musculature, local tissue response compared to bench-top whole cadaver cervical spine experiments, and global kinematic response of the head compared to full body PMHS or volunteer sled tests in both frontal and rear impact. The tension experiments were simulated by applying a displacement to the T1 vertebra in the inferior direction while constraining the head in the

superior-inferior direction and allowing it to translate in the anterior-posterior direction and rotate in the sagittal plane. The force-displacement response of the T1 in the inferior-direction, the anterior-posterior translation of the head, and rotation of the head in the model were all within one standard deviation of the average experimental response up to the 300N applied. The tensile response of the model was slightly lax compared to the experiment which was thought to be due to the lack of modeling of the inertial and frictional resistance of the experimental head mount. It is significant that the tensile response of the model was accurate because this mode of loading is often combined with flexion and extension in frontal and rear impacts respectively.

The local tissue validations were performed by applying the T1 acceleration traces from an 8g frontal and 8g rear experimental impact from bench-top cadaver cervical spine testing to the T1 of the model. The experiments used a cable system to mimic the passive muscle resistance, so the active musculature response was turned off. The ligament strains and disc strains predicted by the model were within one standard deviation of the experiments 59 out of 70 times, which shows the model is able to accurately predict local tissue response. All of the ligament strains remained within two standard deviations of the experimental averages. The major difference between the model and the experiments was the disc shear strains predicted by the model were up to three standard deviations below the experiments at the C2-C3 spinal level in frontal impact and the C5-C6 spinal level in rear impact. The cause of the C2-C3 difference was the use of a C0-C1-C2 flexion limiter in the experiments which transferred more shear strain onto the C2-C3 disc. The cause of low shear strain in the C5-C6 disc in rear impact is not obvious, but the model predicts fairly constant shear strains from C4 to C7 and the experiments predict an isolated peak at the C5-C6 level.

Frontal impact volunteer tests performed at 8g and 15g, rear impact volunteer test at 4g, and a PMHS rear impact test at 10g were used to validate the global kinematic response of the model. The experimental acceleration and rotational traces were applied to the T1 of the model and the resulting kinematics of the head were compared to the experiments. Active musculature was used when comparing to the volunteers and passive muscles were used for the PMHS study. The kinematic response of the model was generally shown to be a good fit to the volunteer and PMHS data. The model tended to oscillate more than the human subjects, which is due to the lack of high-rate material characterization in the intervertebral discs and a lack of damping from the soft tissue not modeled such as the skin, fat, the digestive tract etc. In rear impact, the head over extended compared to both the PMHS test and the volunteer tests, which may be caused by the facet gaps or the lack of

uncovertebral joints. The exciting aspect of the successful validation of the cervical spine model is the model has been built from the ground up using the best available material data and none of the material properties or geometry was calibrated to improve the response of the model to a particular measure.

In order to investigate using the model for whiplash prediction, an extensive review of the biomechanical and clinical evidence of organic whiplash causes was reviewed. The capsular ligaments emerged as the most likely source of whiplash pain, as up to 60% of whiplash patients were found to have CL pain using a clinical double-blind study. Other possible sources of whiplash injury include the spinal ligaments other than the CL and the intervertebral discs. Impingement of the nerve roots by either mechanical deformation or dynamic pressure spikes in the spinal fluid was thought to have enough biomechanical evidence for further investigation, but the necessary structures for this mechanism are not currently modeled so it was not investigated. Mechanisms that do not have enough evidence to support further investigation include direct muscle injury and damage to the vertebral arteries.

The model was exposed to increasing impact severities in both frontal and rear impacts with active musculature to investigate CL strain, other ligament strains, and intervertebral disc fibre strains. The model predicted CL injury at a 15g frontal impact and a 14g rear impact. The 15g frontal impact was a volunteer test in which no one was injured, but the volunteers were from a pool of physically fit marines who likely have increased tolerance to injury. The 14g rear impact threshold agrees with data from real-world crashes where of 28 occupants, 20 had short term consequences below 10g and two had long term consequences at 13g and 15g. It is of interest to note that the model predicts similar injury thresholds for frontal and rear impact. This disagrees with the common perception that whiplash is only caused in rear impacts, but the model does not include air-bags that should reduce CL strains. In frontal impact, the model predicts high strains in the alar ligament, which supports MRI evidence that these upper cervical spine ligaments commonly have lesions amongst whiplash patients. This is the first biomechanical evidence of the strain in these ligaments during impact. The model predicts the other ligaments will reach their failure corridor during a 15g frontal impact and during a 12g rear impact. The disc fibre strains reach their failure corridor beginning at a 15g frontal impact and a 10g rear impact. It is concluded that there is not enough clinical evidence to support that the tissue damage predicted by the model in the disc and other ligaments could lead to a prolonged whiplash injury.

Finally, the model showed that the T1 inputs used for bench-top cadaver tests do not significantly alter the ligament strains predicted in rear impact, but these tests over predict ligament strains due to the lack of active muscle activation.

7.2 Recommendations

The model would benefit from material testing data on the intervertebral discs at the strain rates seen in automobile impacts. The primary goal of this improved material data is to increase the damping of the model to reduce the oscillations seen in both frontal and rear impact. The model itself showed that the annulus fibres in the disc experiences peak strain rates ranging from 85/s to 154/s, so these rates could be used for the material testing. Using the model to determine material testing strain rates could be a problem if the new material data significantly changed the strain rates predicted by the model setting up a series of iterations before the best material properties are reached. This is unlikely to be an issue because material properties tend to change on the order of a decade of strain rate.

Another model improvement related to the lack of damping would be the incorporation of soft tissues in the neck that are not currently modeled. These soft tissues include the skin, subcutaneous fat, oesophagus, and spinal cord. Although these tissues are mechanically weak, they would exhibit a viscoelastic response that would increase the damping of the model. Including the spinal cord and the nerve roots would also be the first step towards being able to predict radicular sources of pain during whiplash events. The mechanisms of nerve root damage include mechanical pressure from the deformation of the vertebrae and dynamic pressure spikes in the spinal canal fluid.

The model was not exposed to gravitational forces during impact because a muscle activation scheme to maintain the initial posture is not available. It is thought that initial muscle forces would stabilize the head and delay the onset of head rotation, which would bring the rotational acceleration response of the model in line with the volunteer corridors for a 7g and 15g frontal impacts. The reason a muscle activation scheme for head stabilization has not been developed is there are an endless combination of muscle forces that could stabilize the head and the task of choosing one seems arbitrary and may not be physically relevant. The commercially available Anybody Modeling Software (Aalborg, Denmark) may be able to assist in this task, because it uses inverse dynamics and energy based optimization to determine muscle forces acting across a joint in the human body during physiologic motions.

Knowledge of the in-vivo facet gaps of a seated 50th percentile male occupant would be useful to fine tune the initial position of each vertebra in the cervical spine model. In rear impact, when the facet surface come into contact they help prevent further intervertebral rotations. If the initial facet gaps were reduced it would help prevent the over extension of the head seen in the global kinematic validation of the model in rear impact. Ideally the facet gaps would be measured from MRI data of volunteers, because it may be difficult to quantify the changes in posture between the in-vivo and in-vitro states. Exposing volunteers to the MRI exposure required to accurately measure the facet gaps may not be permissible, but efforts should be made to define a suitable imaging protocol.

Also related to the over extension of the model in rear impact, is the lack of uncovertebral joints. These joints have been shown to increase the stiffness of spinal segments in extension, lateral bending, and rotation (Kotani et al., 1998). The uncovertebral joints had the smallest influence on the spinal segments in flexion, which suggests their influence in frontal impact is not significant. The uncovertebral joint is primarily a bony protrusion from the posterior aspect of the vertebral bodies' superior surface, which may be able to be imaged with high resolution CT scans of cadavers. The joints are likely not being incorporated into current FE neck models because the size of the protrusion relative to the size of the vertebral body means that they get smoothed over by the algorithms used to stitch the CT data into CAD surfaces. Therefore special care for the posterior-superior region of the vertebral bodies would need to be taken to capture the uncovertebral bony protrusions. Once a geometrical representation of the uncovertebral joints is incorporated into the model, it may be possible to validate their function at the segment level using the data from Kotani et al. (1998).

Modeling of the muscle volume may help stiffen the response of the neck model and help reduce the over extension of the head in rear impact and reduce the early onset of head rotation in frontal impact. The muscle volume is expected to stiffen the neck model because it will provide compressive resistance and friction between muscles as they slide over one another (Hedenstierna & Halldin, 2008).

Researchers should investigate the relationship between tissue damage and painful injury for the intervertebral discs and ligaments other than the CL. This would provide valuable information for the use of numerical models to predict whiplash injury. Clinical double-blind studies performed on the discs and ligament of the cervical spine similar to the ones done on the CL would be useful in determining where the other 40 to 46% of chronic whiplash pain originates (Barnsley et al., 1995;

Lord et al., 1996). The facet joints lend themselves to this type of study because the anaesthetic blocks can be injected into the capsule and it is contained, which provides confidence of the location receiving pain relief. The other structures of the neck likely do not lend themselves to the same method, so researchers may have to conceive an alternative approach.

The focus of this work has been frontal and rear impacts with the head looking forwards, but biomechanical studies have shown that soft tissue strains including the CL are higher when the head is turned during the impact (Ivancic et al., 2006; Winkelstein et al., 2000). A muscle activation scheme to maintain the rotated head position at the beginning of the impact will likely be necessary. The model must be able to simulate an out of position occupant to completely capture whiplash injury.

References

Agur, A. M., & Dalley, A. F. (2004). *Grant's Atlas of Anatomy*. Philadelphia: Lippincott Williams & Wilkins.

Aldman, B. (1986). An analytical approach to the impact biomechanics of head and neck injury. In *Proc. 30th Annual AAAM* (pp. 446-454).

Apkarian, A. V. (2004). Cortical pathophysiology of chronic pain. *Novartis Foundation Symposium*, *261*, 239-61.

Barnsley, L., Lord, S. M., Wallis, B. J., & Bogduk, N. (1995). The prevalence of chronic cervical zygapophysial joint pain after whiplash. *Spine*, *20*(1), 20-26.

Bartel, D. L., Davy, D. T., & Keaveny, T. M. (2006). *Orthopaedic Biomechanics: Mechanics and Design in Musculoskeletal Systems*. Prentice Hall.

Behr, M., Arnoux, P. J., Serre, T., Bidal, S., Kang, H. S., Thollon, L., et al. (2003). A human model for road safety: from geometrical acquisition to model validation with radioss. *Computer methods in biomechanics and biomedical engineering*, *6*(4), 263-73.

Berglund, A., Alfredsson, L., Jensen, I., Bodin, L., & Nygren, A. (2003). Occupant- and crash-related factors associated with the risk of whiplash injury. *Annals of epidemiology*, *13*(1), 66-72.

Bogduk, N., & Mercer, S. (2000). Biomechanics of the cervical spine. I: Normal kinematics. *Clinical biomechanics*, *15*(9), 633-48.

Bogduk, N., & Yoganandan, N. (2001). Biomechanics of the cervical spine Part 3: minor injuries. *Clinical biomechanics*, *16*(4), 267-75.

Bogduk, N. (2002). Innervation and Pain Patterns of the Cervical Spine. In R. Grant, *Physical Therapy of the Cervical and Thoracic Spine* (3 ed., pp. 1-12). Churchill Livingstone.

Bogduk, N. (2006). Whiplash Injury. In F. Cervero & T. S. Jensen, *Handbook of Clinical Neurology v81 - Pain* (3 ed., pp. 791-801). Amsterdam: Elsevier.

Bolton, J. R., Kent, R. W., & Crandall, J. R. (2006). *Passenger Air Bag Impact and Injury Response using a Hybrid III Test Dummy and Human Surrogates: Phase 2b*. National Highway Traffic Safety Administration. NHTSA Biomechanics Test Database #8373.

Brault, J. R., Siegmund, G. P., & Wheeler, J. B. (2000). Cervical muscle response during whiplash: evidence of a lengthening muscle contraction. *Clinical biomechanics*, *15*(6), 426-35.

Brolin, K., Halldin, P., & Leijonhufvud, I. (2005). The effect of muscle activation on neck response. *Traffic injury prevention*, *6*(1), 67-76. Taylor & Francis.

Campbell, B., & Cronin, D. S. (2007). High rate characterization of automotive seat foams. In *Proceedings of SEM*.

Carlson, E. J., Tominaga, Y., Ivancic, P. C., & Panjabi, M. M. (2007). Dynamic vertebral artery elongation during frontal and side impacts. *The spine journal*, *7*(2), 222-8.

Cassidy, J. J., Hiltner, A., & Baer, E. (1989). Hierarchical structure of the intervertebral disc. *Connective tissue research*, *23*(1), 75-88.

Cavanaugh, J. M. (2000). Neurophysiology and Neuroanatomy of Neck Pain. In N. Yoganandan & F. A. Pintar, *Frontiers in Whiplash Trauma: Clinical and Biomechanical* (pp. 79-96). Amsterdam: IOS Press.

Chancey, V. C., Nightingale, R. W., Van Ee, C. A., Knaub, K. E., & Myers, B. S. (2003). Improved estimation of human neck tensile tolerance: reducing the range of reported tolerance using anthropometrically correct muscles and optimized physiologic initial conditions. *Stapp car crash journal*, *47*, 135-53.

Chazal, J., Tanguy, A., Bourges, M., Gaurel, G., Escande, G., Guillot, M., et al. (1985). Biomechanical properties of spinal ligaments and a histological study of the supraspinal ligament in traction. *Journal of biomechanics*, *18*(3), 167-76.

Clemens, H. J., & Burow, K. (1972). Experimental investigation on cervical spine injury mechanisms of cervical spine at frontal and rear-front vehicle impacts. *Stapp car crash journal*, 76-104.

Cusick, J. F., Pintar, F. A., & Yoganandan, N. (2001). Whiplash syndrome: kinematic factors influencing pain patterns. *Spine*, *26*(11), 1252-8.

Davidsson, J., Deutscher, C., Hell, W., Linder, A., Lovsund, P., Svensson, M., et al. (1998). Human volunteer kinematics in rear-end sled collisions. In *Proceddings of IRCOBI* (pp. 289-301). Goteborg.

Deans, G. T., Magalliard, J. N., Kerr, M., & Rutherford, W. H. (1987). Neck sprain - a major cause of disability following car accidents. *Injury*, *18*(1), 10-2.

Deng, B. (1999). Kinematics of human cadaver cervical spine during low speed rear end impacts. PhD Thesis, Wayne State University.

Deng, B., Begeman, P. C., Yang, K. H., Tashman, S., & King, A. I. (2000). Kinematics of human cadaver cervical spine during low speed rear-end impacts. *Stapp car crash journal*, *44*, 171-88.

Deng, Y. C. (1999). Modeling of the Human Cervical Spine Using Finite Element Techniques. In *Proceedings of the International Congress & Exposition*. Detroit: SAE International.

DiSilvestro, M. R., & Suh, J. K. (2001). A cross-validation of the biphasic poroviscoelastic model of articular cartilage in unconfined compression, indentation, and confined compression. *Journal of biomechanics*, *34*(4), 519-25.

Dibb, A. T., Nightingale, R. W., Luck, J. F., Chancey, V. C., Fronheiser, L. E., Myers, B. S., et al. (2009). Tension and combined tension-extension structural response and tolerance properties of the human male ligamentous cervical spine. *Journal of biomechanical engineering*, *131*(8), 081008.

Dvorak, J., & Panjabi, M. M. (1987). Functional anatomy of the alar ligaments. *Spine*, *12*(2), 183-9.

Dvorak, J., Valach, L., & Schmid, S. T. (1989). Cervical Spine injuries in Switzerland. *J Manual Med*, *4*, 7-16.

Eichberger, A., Darok, M., Steffan, H., Leinzinger, P. E., Boström, O., Svensson, M. Y., et al. (2000). Pressure measurements in the spinal canal of post-mortem human subjects during rear-end impact and correlation of results to the neck injury criterion. *Accident; analysis and prevention*, *32*(2), 251-60.

Ewing, C. L., Thomas, D. J., Beeler, G., Patrick, L., & Gillis, D. (1968). Dynamic Response of the head and neck of the living human to -Gx impact acceleration. *Stapp Car Crash Journal*.

Ewing, C. L., Thomas, D. J., Patrick, L., Beeler, G., & Smith, M. (1969). Living human dynamic response to -Gx impact acceleration II - accelerations measured on the head and neck. *Stapp Car Crash Journal*.

Falla, D., Bilenkij, G., & Jull, G. (2004). Patients with chronic neck pain demonstrate altered patterns of muscle activation during performance of a functional upper limb task. *Spine*, *29*(13), 1436-40.

Ferguson, S. (2008). Biomechanics of the Spine. In N. Boos & M. Aebi, *Spinal Disorders: Fundamentals of Diagnosis and Treatment* (pp. 41-66). Springer.

Freeman, M. D. (1997). A Study of Chronic Neck Pain Folloing Whiplash Injury. PhD Thesis, Oregon State University.

Fujita, Y., Duncan, N. A., & Lotz, J. C. (1997). Radial tensile properties of the lumbar annulus fibrosus are site and degeneration dependent. *Journal of orthopaedic research*, *15*(6), 814-9.

Fung, Y. C. (1993). *Biomechanics: Mechanical Properties of Living Tissues* (2md.). New York: Springer.

Galasko, C. S., Murray, P. M., Pitcher, M., Chambers, H., Mansfield, S., Madden, M., et al. (1993). Neck sprains after road traffic accidents: a modern epidemic. *Injury*, *24*(3), 155-7.

Garrett, W., Nikolaou, P., Ribbeck, B., Glisson, R., & Seaber, A. (1988). The effect of muscle architecture on the biomechanical failure properties of skeletal muscle under passive extension. *The American Journal of Sports Medicine*, *16*(1), 7.

Garrett, W. E. (1996). Muscle strain injuries. *The American journal of sports medicine*, *24*(6 Suppl), S2-8.

Gilad, I., & Nissan, M. (1986). A study of vertebra and disc geometric relations of the human cervical and lumbar spine. *Spine*, *11*(2), 154-7.

Goel, V. K., Monroe, B. T., Gilbertson, L. G., & Brinckmann, P. (1995). Interlaminar shear stresses and laminae separation in a disc. Finite element analysis of the L3-L4 motion segment subjected to axial compressive loads. *Spine*, *20*(6), 689-98.

Goel, V. K., & Clausen, J. D. (1998). Prediction of load sharing among spinal components of a C5-C6 motion segment using the finite element approach. *Spine*, *23*(6), 684-91.

Grauer, J. N., Panjabi, M. M., Cholewicki, J., Nibu, K., & Dvorak, J. (1997). Whiplash produces an S-shaped curvature of the neck with hyperextension at lower levels. *Spine*, *22*(21), 2489-94. Retrieved from http://www.ncbi.nlm.nih.gov/pubmed/9383854.

Gray, H. (1918). *Anatomy of the Human Body*. Philadelphia: Lea & Febiger. Retrieved from bartleby.com.

Green, D. W., Winandy, J. E., & Kretschmann, D. E. (1999). *Mechanical Properties of Wood*. Madison, WI.

Hallquist, J. O. (2007). LS-Dyna keyword user's manual. Livermore, C.A.

Hedenstierna, S., & Halldin, P. (2008). How does a three-dimensional continuum muscle model affect the kinematics and muscle strains of a finite element neck model compared to a discrete muscle model in rear-end, frontal, and lateral impacts. *Spine*, *33*(8), 236-245.

Heuer, F., Schmidt, H., Klezl, Z., Claes, L., & Wilke, H. (2007). Stepwise reduction of functional spinal structures increase range of motion and change lordosis angle. *Journal of biomechanics*, *40*(2), 271-80.

Hidlingson, C., & Toolanen, G. (1990). Outcome after soft tissue injury of the cervical spine: a prospective study of 93 car-accident victims. *Acta Orthop Scand*, *61*, 357-359.

Holzapfel, G. A., Schulze-Bauer, C. A., Feigl, G., & Regitnig, P. (2005). Single lamellar mechanics of the human lumbar anulus fibrosus. *Biomechanics and modeling in mechanobiology*, *3*(3), 125-40.

Hynd, D., Svensson, M., Trosseille, X., van Ratingen, M., & Davidsson, J. (2007). Dummy requirements and injury criteria for a low-speed rear impact whiplash dummy. *European Enhanced Vehicle-safety Committee*, EEVC WG12 #505A.

Iatridis, J. C., Weidenbaum, M., Setton, L. A., & Mow, V. C. (1996). Is the nucleus pulposus a solid or a fluid? Mechanical behaviors of the nucleus pulposus of the human intervertebral disc. *Spine*, *21*(10), 1174-84.

Iatridis, J. C., Setton, L. A., Foster, R. J., Rawlins, B. A., Weidenbaum, M., Mow, V. C., et al. (1998). Degeneration affects the anisotropic and nonlinear behaviors of human anulus fibrosus in compression. *Journal of biomechanics*, *31*(6), 535-44.

Iatridis, J. C., Kumar, S., Foster, R. J., Weidenbaum, M., & Mow, V. C. (1999). Shear mechanical properties of human lumbar annulus fibrosus. *Journal of orthopaedic research*, *17*(5), 732-7.

Iatridis, J. C., MaClean, J. J., & Ryan, D. A. (2005). Mechanical damage to the intervertebral disc annulus fibrosus subjected to tensile loading. *Journal of biomechanics*, *38*(3), 557-65.

Inami, S., Shiga, T., Tsujino, A., Yabuki, T., Okado, N., Ochiai, N., et al. (2001). Immunohistochemical demonstration of nerve fibers in the synovial fold of the human cervical facel joint. *Journal of Orthopaedic Research*, *19*(4), 593-596.

Ito, S., Ivancic, P. C., Pearson, A. M., Tominaga, Y., Gimenez, S. E., Rubin, W., et al. (2005). Cervical intervertebral disc injury during simulated frontal impact. *European spine journal*, *14*(4), 356-65. doi: 10.1007/s00586-004-0783-4.

Ivancic, P. C., Pearson, A. M., Panjabi, M. M., & Ito, S. (2004). Injury of the anterior longitudinal ligament during whiplash simulation. *European spine journal*, *13*(1), 61-8.

Ivancic, P. C., Panjabi, M. M., Ito, S., Cripton, P. A., & Wang, J. L. (2005). Biofidelic whole cervical spine model with muscle force replication for whiplash simulation. *European spine journal*, *14*(4), 346-55.

Ivancic, P. C., Ito, S., Tominaga, Y., Carlson, E. J., Rubin, W., Panjabi, M. M., et al. (2006). Effect of rotated head posture on dynamic vertebral artery elongation during simulated rear impact. *Clinical biomechanics*, *21*(3), 213-20.

Ivancic, P. C., Ito, S., Tominaga, Y., Rubin, W., Coe, M. P., Ndu, A. B., et al. (2008). Whiplash causes increased laxity of cervical capsular ligament. *Clinical biomechanics*, *23*(2), 159-65.

Jónsson, H., Bring, G., Rauschning, W., & Sahlstedt, B. (1991). Hidden cervical spine injuries in traffic accident victims with skull fractures. *Journal of spinal disorders*, *4*(3), 251-63.

Kaneoka, K., Ono, K., Inami, S., & Hayashi, K. (1999). Motion analysis of cervical vertebrae during whiplash loading. *Spine*, *24*(8), 763-70.

Keinberger, M. (2000). Importance of head restraint position on whiplash injury. In N. Yoganandan & F. A. Pintar, *Frontiers in Whiplash Trauma: Clinical & Biomechanical* (pp. 477-490). Amsterdam: ISO Press.

Kitagawa, Y., Yasuki, T., & Hasegawa, J. (2006). A study of cervical spine kinematics and joint capsule strain in rear impacts using a human FE model. *Stapp car crash journal*, *50*, 545-66.

Kitagawa, Y., Yasuki, T., & Hasegawa, J. (2008). Research study on neck injury lessening with active head restraint using human body FE model. *Traffic injury prevention*, *9*(6), 574-82.

Klinich, K. D., Ebert, S. M., Van Ee, C. A., Flannagan, C. A., Prasad, M., Reed, M. P., et al. (2004). Cervical spine geometry in the automotive seated posture: variations with age, stature, and gender. *Stapp car crash journal*, *48*(November), 301.

Klisch, S. M., & Lotz, J. C. (2000). A special theory of biphasic mixtures and experimental results for human annulus fibrosus tested in confined compression. *Journal of biomechanical engineering*, *122*(2), 180-8.

Knaub, K. E., & Myers, B. S. (1998). Project F.2(c) Cervical Spine Muscle. *National Highway Traffic Safety Administration*, NHTSA-98-3588-133.

Koelbaek Johansen, M., Graven-Nielsen, T., Schou Olesen, A., & Arendt-Nielsen, L. (1999). Generalised muscular hyperalgesia in chronic whiplash syndrome. *Pain*, *83*(2), 229-34.

Kotani, Y., McNulty, P. S., Abumi, K., Cunningham, B. W., Kaneda, K., McAfee, P. C., et al. (1998). The role of anteromedial foraminotomy and the uncovertebral joints in the stability of the cervical spine. A biomechanical study. *Spine*, *23*(14), 1559-65.

Krafft, M., Kullgren, A., Tingvallb, C., Boströmc, O., & Fredrikssonc, R. (2000). How crash severity in rear impacts influences short and long term consequences to the neck. *Accident Analysis & Prevention*, *32*(2), 187-195.

Krafft, M., Kullgren, A., Ydenius, A., & Tingvall, C. (2002). Influence of crash pulse characteristics on whiplash associated disorders in rear impacts - crash recording in real life crashes. *Traffic Injury Prevention*, *3*(2), 141-149.

Krakenes, J., & Kaale, B. R. (2006). Magnetic resonance imaging assessment of craniovertebral ligaments and membranes after whiplash trauma. *Spine*, *31*(24), 2820-6.

Kumaresan, S., Yoganandan, N., & Pintar, F. A. (1998). Finite element modeling approaches of human cervical spine facet joint capsule. *Journal of biomechanics*, *31*(4), 371-6.

Lee, I. H., Choi, H. Y., Lee, J. H., & Han, D. C. (2004a). Development of finite element human neck model for vehicle safety simulation. *International Journal of Automotive Technology*, *5*(1), 33-46.

Lee, K. E., Thinnes, J. H., Gokhin, D. S., & Winkelstein, B. A. (2004b). A novel rodent neck pain model of facet-mediated behavioral hypersensitivity: implications for persistent pain and whiplash injury. *Journal of neuroscience methods*, *137*(2), 151-9.

Lee, K. E., Franklin, A. N., Davis, M. B., & Winkelstein, B. A. (2006). Tensile cervical facet capsule ligament mechanics: failure and subfailure responses in the rat. *Journal of biomechanics*, *39*(7), 1256-64.

Loeser, J. D. (2006). Pain as a disease. In F. Cervero & T. S. Jensen, *Handbook of Clinical Neurology v81 - Pain* (3 ed., pp. 11-20). Amsterdam: Elsevier.

Lord, S. M., Barnsley, L., Wallis, B. J., & Bogduk, N. (1996). Chronic cervical zygapophysial joint pain after whiplash. A placebo-controlled prevalence study. *Spine*, *21*(15), 1737-45.

Lu, Y., Chen, C., Kallakuri, S., Patwardhan, A., & Cavanaugh, J. M. (2005). Neurophysiological and biomechanical characterization of goat cervical facet joint capsules. *Journal of orthopaedic research*, *23*(4), 779-87.

Macpherson, P. C., Schork, M. A., & Faulkner, J. A. (1996). Contraction-induced injury to single fiber segments from fast and slow muscles of rats by single stretches. *The American journal of physiology*, *271*(5 Pt 1), C1438-46.

Maimaris, C., Barnes, M. R., & Allen, M. J. (1988). 'Whiplash injuries' of the neck: a retrospective study. *Injury*, *19*(6), 393-6.

Manchikanti, L., Singh, V., Rivera, J., & Pampati, V. (2002). Prevalence of cervical facet joint pain in chronic neck pain. *Pain physician*, *5*(3), 243-9.

Marchand, F., & Ahmed, A. M. (1990). Investigation of the laminate structure of lumbar disc anulus fibrosus. *Spine*, *15*(5), 402-10.

McConnell, W. E., Howard, R. P., Poppel, J. V., Krause, R., Guzman, H. M., Bomar, J. B., et al. (1995). Human head and neck kinematics after low velocity rear-end impacts understanding whiplash. *Stapp Car Crash Journal*.

McCully, K. K., & Faulkner, J. A. (1985). Injury to skeletal muscle fibers of mice following lengthening contractions. *Journal of applied physiology*, *59*(1), 119-26.

Myklebust, J. B., Pintar, F., Yoganandan, N., Cusick, J. F., Maiman, D., Myers, T. J., et al. (1988). Tensile strength of spinal ligaments. *Spine*, *13*(5), 526-31.

Nachemson, A. L., & Evans, J. H. (1968). Some mechanical properties of the third human lumbar interlaminar ligament (ligamentum flavum). *Journal of Biomechanics*, *1*(3), 211-220.

Nashner, L. M. (1985). Strategies for organization of human posture. In M. Igarashi & F. Black, *Vestibular and Visual Control of Posture and Locomotor Equilibrium* (pp. 1-8). Houston, TX: Karger, Basel.

Nederhand, M. J., Hermens, H. J., IJzerman, M. J., Turk, D. C., & Zilvold, G. (2002). Cervical muscle dysfunction in chronic whiplash-associated disorder grade 2: the relevance of the trauma. *Spine*, *27*(10), 1056-61.

Niv, D., & Devor, M. (2007). Position paper of the European Federation of IASP Chapters (EFIC) on the subject of pain management. *European journal of pain*, *11*(5), 487-9.

Norris, S. H., & Watt, I. (1983). The prognosis of neck injuries resulting from rear-end vehicle collisions. *The Journal of bone and joint surgery. British volume*, *65*(5), 608-11.

Ono, K., Kaneoka, K., Wittek, A., & Kajzer, J. (1997). Cervical injury mechanism based on the analysis of human cervical vertebral motion and head-neck-torso kinematics during low-speed rear impacts. *Stapp Car Crash Journal*, *41*, 339-356.

Ono, K., & Kaneoka, K. (1999). Motion Analysis of Human Cervical Vertebrae During Low-Speed Rear Impacts by the Simulated Sled. *Traffic Injury Prevention*, *1*(2), 87-99. Taylor & Francis.

Ovadia, D., Steinberg, E. L., Nissan, M. N., & Dekel, S. (2002). Whiplash injury--a retrospective study on patients seeking compensation. *Injury*, *33*(7), 569-73.

Pal, G. P., Routal, R. V., & Saggu, S. K. (2001). The orientation of the articular facets of the zygapophyseal joints at the cervical and upper thoracic region. *Journal of anatomy*, *198*(4), 431-41.

Panjabi, M. M., Oxland, T. R., & Parks, E. H. (1991). Quantitative anatomy of cervical spine ligaments. Part I. Upper cervical spine. *Journal of spinal disorders*, *4*(3), 270-6.

Panjabi, M. M., Oxland, T., Takata, K., Goel, V., Duranceau, J., Krag, M., et al. (1993). Articular facets of the human spine. Quantitative three-dimensional anatomy. *Spine*, *18*(10), 1298-310.

Panjabi, M. M., Crisco, J. J., Lydon, C., & Dvorak, J. (1998a). The mechanical properties of human alar and transverse ligaments at slow and fast extension rates. *Clinical biomechanics (Bristol, Avon)*, *13*(2), 112-120.

Panjabi, M. M., Cholewicki, J., Nibu, K., Grauer, J., & Vahldiek, M. (1998b). Capsular ligament stretches during in vitro whiplash simulations. *Journal of spinal disorders*, *11*(3), 227-32.

Panjabi, M. M., Chen, N. C., Shin, E. K., & Wang, J. L. (2001). The cortical shell architecture of human cervical vertebral bodies. *Spine*, *26*(22), 2478-84.

Panjabi, M. M., Pearson, A. M., Ito, S., Ivancic, P. C., Gimenez, S. E., Tominaga, Y., et al. (2004a). Cervical spine ligament injury during simulated frontal impact. *Spine*, *29*(21), 2395-403.

Panjabi, M. M., Ito, S., Pearson, A. M., & Ivancic, P. C. (2004b). Injury mechanisms of the cervical intervertebral disc during simulated whiplash. *Spine*, *29*(11), 1217-25.

Panjabi, M. M., Maak, T. G., Ivancic, P. C., & Ito, S. (2006). Dynamic intervertebral foramen narrowing during simulated rear impact. *Spine*, *31*(5), 128-34.

Panzer, M. B. (2006). Numerical modelling of the human cervical spine in frontal impact. M.A.Sc Thesis, University of Waterloo.

Panzer, M. B., & Cronin, D. S. (2009). C4-C5 segment finite element model development, validation, and load-sharing investigation. *Journal of biomechanics*, *42*(4), 480-90.

Pearson, A. M., Ivancic, P. C., Ito, S., & Panjabi, M. M. (2004). Facet joint kinematics and injury mechanisms during simulated whiplash. *Spine*, *29*(4), 390-7.

Pearson, A. M., Panjabi, M. M., Ivancic, P. C., Ito, S., Cunningham, B. W., Rubin, W., et al. (2005). Frontal impact causes ligamentous cervical spine injury. *Spine*, *30*(16), 1852-8.

Pettersson, K., Hildingsson, C., Toolanen, G., Fagerlund, M., & Björnebrink, J. (1997). Disc pathology after whiplash injury. A prospective magnetic resonance imaging and clinical investigation. *Spine*, *22*(3), 283-8.

Pfirrmann, C. W., Binkert, C. A., Zanetti, M., Boos, N., & Hodler, J. (2001). MR morphology of alar ligaments and occipitoatlantoaxial joints: study in 50 asymptomatic subjects. *Radiology*, *218*(1), 133-7.

Pooni, J. S., Hukins, D. W., Harris, P. F., Hilton, R. C., & Davies, K. E. (1986). Comparison of the structure of human intervertebral discs in the cervical, thoracic and lumbar regions of the spine. *Surgical and radiologic anatomy*, *8*(3), 175-82.

Przybylski, G. J., Patel, P. R., Carlin, G. J., & Woo, S. L. (1998). Quantitative anthropometry of the subatlantal cervical longitudinal ligaments. *Spine*, *23*(8), 893-8.

Quinlan, K. P., Annest, J. L., Myers, B., Ryan, G., & Hill, H. (2004). Neck strains and sprains among motor vehicle occupants-United States, 2000. *Accident analysis and prevention*, *36*(1), 21-7.

Quinn, K. P., & Winkelstein, B. A. (2007). Cervical facet capsular ligament yield defines the threshold for injury and persistent joint-mediated neck pain. *Journal of biomechanics*, *40*(10), 2299-306.

Radanov, B. P., Sturengger, M., & Di Stefano, G. (1995). Long-Term Outcome after Whiplash Injury: A 2-Year Follow-Up Considering Features of Injury Mechanism and Somatic, Radiologic, and Psychosocial Findings. *Medicine*, *74*(5), 281-297.

Ren, K., & Dubner, R. (1999). Central nervous system plasticity and persistent pain. *Journal of orofacial pain*, *13*(3), 155-71.

Robbins, D. H. (1983). *Anthropometric Specifications for Mid-Sized Male Dummy, Volume 2*. University of Michigan Transportation Research Institute, UMTRI-83-53-2.

Roberts, A. K., Hynd, D., Dixon, P. R., Murphy, O., Magnusson, M., Pope, M. H. (2002). Kinematics of the human spine in rear impact and the biofidelity of current dummies. In *IMechE conference proceedings* (pp. 227-246).

Roy, S., Hol, P. K., Laerum, L. T., & Tillung, T. (2004). Pitfalls of magnetic resonance imaging of alar ligament. *Neuroradiology*, *46*(5), 392-8.

Schmitt, K., Muser, M., Niederer, P., & Walz, F. (2003). Pressure aberrations inside the spinal canal during rear-end impact. *Pain research & management*, *8*(2), 86-92.

Scott, S., & Sanderson, P. L. (2002). Whiplash: a biochemical study of muscle injury. *European spine journal*, *11*(4), 389-92.

Siegmund, G. P., Myers, B. S., Davis, M. B., Bohnet, H. F., & Winkelstein, B. A. (2001). Mechanical evidence of cervical facet capsule injury during whiplash: a cadaveric study using combined shear, compression, and extension loading. *Spine*, *26*(19), 2095-101.

Siegmund, G. P., Sanderson, D. J., Myers, B. S., & Inglis, J. T. (2003). Rapid neck muscle adaptation alters the head kinematics of aware and unaware subjects undergoing multiple whiplash-like perturbations. *Journal of biomechanics*, *36*(4), 473-82.

Siegmund, G. P., Winkelstein, B. A., Ivancic, P. C., Svensson, M. Y., & Vasavada, A. (2009). The anatomy and biomechanics of acute and chronic whiplash injury. *Traffic injury prevention*, *10*(2), 101-12.

Stemper, B. D., Yoganandan, N., & Pintar, F. A. (2004). Validation of a head-neck computer model for whiplash simulation. *Medical & biological engineering & computing*, *42*(3), 333-8.

Stemper, B. D., Yoganandan, N., & Pintar, F. A. (2005). Effects of abnormal posture on capsular ligament elongations in a computational model subjected to whiplash loading. *Journal of biomechanics*, *38*(6), 1313-23.

Stemper, B. D., Yoganandan, N., Pintar, F. A., & Rao, R. D. (2006). Anterior longitudinal ligament injuries in whiplash may lead to cervical instability. *Medical engineering & physics*, *28*(6), 515-24.

Sterling, M., Treleaven, J., Edwards, S., & Jull, G. (2002). Pressure pain thresholds in chronic whiplash associated disorder: further evidence of altered central pain processing. *Journal of Musculoskeletal Pain*, *10*(3), 69-81.

Sturzenegger, M., DiStefano, G., Radanov, B. P., & Schnidrig, A. (1994). Presenting symptoms and signs after whiplash injury: the influence of accident mechanisms. *Neurology*, *44*(4), 688-93.

Svensson, M. Y., Boström, O., Davidsson, J., Hansson, H. A., Håland, Y., Lövsund, P., et al. (2000). Neck injuries in car collisions--a review covering a possible injury mechanism and the development of a new rear-impact dummy. *Accident; analysis and prevention*, *32*(2), 167-75.

Szabo, T. J., & Welcher, J. B. (1996). Subject kinematics and electromyographic activity during low speed rear impacts. *Stapp Car Crash Journal*, *40*, 295-315.

Taylor, J. R., Twomey, L. T., & Kakulas, B. A. (1998). Dorsal root ganglion injuries in 109 blunt trauma fatalities. *Injury*, *29*(5), 335-9.

Thunnissen, J. G., Wismans, J. S., Ewing, C. L., & Thomas, D. J. (1995). Human volunteer head-neck response in frontal flexion: a new analysis. *Stapp car crash journal*.

Tominaga, Y., Ndu, A. B., Coe, M. P., Valenson, A. J., Ivancic, P. C., Ito, S., et al. (2006a). Neck ligament strength is decreased following whiplash trauma. *BMC musculoskeletal disorders*, *7*, 103.

Tominaga, Y., Maak, T. G., Ivancic, P. C., Panjabi, M. M., & Cunningham, B. W. (2006b). Head-turned rear impact causing dynamic cervical intervertebral foramen narrowing: implications for ganglion and nerve root injury. *Journal of neurosurgery. Spine*, *4*(5), 380-7.

Tropiano, P., Thollon, L., Arnoux, P. J., Huang, R. C., Kayvantash, K., Poitout, D. G., et al. (2004). Using a finite element model to evaluate human injuries application to the HUMOS model in whiplash situation. *Spine*, *29*(16), 1709-16.

Vasavada, A. N., Brault, J. R., & Siegmund, G. P. (2007). Musculotendon and fascicle strains in anterior and posterior neck muscles during whiplash injury. *Spine*, *32*(7), 756-65.

Viejo-Fuertes, D., Liguoro, D., Rivel, J., Midy, D., & Guerin, J. (1998). Morphologic and histologic study of the ligamentum flavum in the thoraco-lumbar region. *Surgical and Radiologic Anatomy*, *20*(3), 171-176.

Vilkman, E., & Karma, P. (1989). Vertical hyoid bone displacement and fundamental frequency of phonation. *Acta oto-laryngologica*, *108*(1-2), 142-51.

Wagner, D. R., & Lotz, J. C. (2004). Theoretical model and experimental results for the nonlinear elastic behavior of human annulus fibrosus. *Journal of orthopaedic research*, *22*(4), 901-9.

Walker, L., Harris, E., & Pontius, U. (1973). Mass, volume, center of mass, and mass moment of inertia of head and head and neck of human body. *Stapp car crash journal*. SAE International.

Ward, S. R., & Lieber, R. L. (2005). Density and hydration of fresh and fixed human skeletal muscle. *Journal of biomechanics*, *38*(11), 2317-20.

White, A. A., & Panjabi, M. M. (1990). *Clinical Biomechanics of the Spine* (2nd.). Philadelphia: Lippincott Williams & Wilkins.

Willauschus, W. G., Kladny, B., Beyer, W. F., Glückert, K., Arnold, H., Scheithauer, R., et al. (1995). Lesions of the alar ligaments. In vivo and in vitro studies with magnetic resonance imaging. *Spine*, *20*(23), 2493-8.

Wilmink, J. T., & Patijn, J. (2001). MR imaging of alar ligament in whiplash-associated disorders: an observer study. *Neuroradiology*, *43*(10), 859-63.

Winkelstein, B. A., Nightingale, R. W., Richardson, W. J., & Myers, B. S. (2000). The cervical facet capsule and its role in whiplash injury: a biomechanical investigation. *Spine*, *25*(10), 1238-46.

Winters, J. (1995). How detailed should muscle models be to understand multi-joint movement coordination? *Human Movement Science*, *14*(4-5), 401-442.

Winters, J. M., & Stark, L. (1985). Analysis of fundamental human movement patterns through the use of in-depth antagonistic muscle models. *IEEE transactions on bio-medical engineering*, *32*(10), 826-39.

Winters, J. M., & Stark, L. (1988). Estimated mechanical properties of synergistic muscles involved in movements of a variety of human joints. *Journal of biomechanics*, *21*(12), 1027-41.

Winters, J. M., & Woo, S. L. (1990). *Multiple Muscle Systems: Biomechanics and Movement Organization*. New York: Springer.

Womack, W., Woldtvedt, D., & Puttlitz, C. M. (2008). Lower cervical spine facet cartilage thickness mapping. *Osteoarthritis and cartilage*, *16*(9), 1018-23.

Yoganandan, N., Pintar, F., Butler, J., Reinartz, J., Sances, A., Larson, S. J., et al. (1989). Dynamic response of human cervical spine ligaments. *Spine*, *14*(10), 1102-10.

Yoganandan, N., Kumaresan, S., & Pintar, F. A. (2001). Biomechanics of the cervical spine Part 2. Cervical spine soft tissue responses and biomechanical modeling. *Clinical biomechanics (Bristol, Avon)*, *16*(1), 1-27.

Yoganandan, N., Pintar, F. A., & Cusick, J. F. (2002). Biomechanical analyses of whiplash injuries using an experimental model. *Accident; analysis and prevention*, *34*(5), 663-71.

Yoganandan, N., Knowles, S. A., Maiman, D. J., & Pintar, F. A. (2003). Anatomic study of the morphology of human cervical facet joint. *Spine*, *28*(20), 2317-23.